Short-Duration Gamma-Ray Bursts

Edo Berger

Harvard-Smithsonian Center for Astrophysics, 60 Garden Street, Cambridge, Massachusetts 02139; email: eberger@cfa.harvard.edu

Key Words

gamma rays: observations, theory; gravitational waves; radiation mechanisms: non-thermal; relativistic processes; stars: neutron

Abstract

Gamma-ray bursts (GRBs) display a bimodal duration distribution, with a separation between the short- and long-duration bursts at about 2 sec. The progenitors of long GRBs have been identified as massive stars based on their association with Type Ic core-collapse supernovae, their exclusive location in star-forming galaxies, and their strong correlation with bright ultraviolet regions within their host galaxies. Short GRBs have long been suspected on theoretical grounds to arise from compact object binary mergers (NS-NS or NS-BH). The discovery of short GRB afterglows in 2005, provided the first insight into their energy scale and environments, established a cosmological origin, a mix of host galaxy types, and an absence of associated supernovae. In this review I summarize nearly a decade of short GRB afterglow and host galaxy observations, and use this information to shed light on the nature and properties of their progenitors, the energy scale and collimation of the relativistic outflow, and the properties of the circumburst environments. The preponderance of the evidence points to compact object binary progenitors, although some open questions remain. Based on this association, observations of short GRBs and their afterglows can shed light on the on- and off-axis electromagnetic counterparts of gravitational wave sources from the Advanced LIGO/Virgo experiments.

Contents

1 Introduction

Gamma-ray bursts (GRBs) are short, intense, and non-repeating flashes of $\sim$ MeV γ-rays with a wide range of spectral and temporal properties. GRBs were discovered serendipitously by the *Vela* satellites starting in 1967 (Klebesadel, Strong & Olson 1973), leading to an intense investigation of their origin, energy source, and progenitor systems that is still on-going at the present. Despite the broad diversity in their γ-ray emission properties (peak energy, spectral shape, variability timescale, duration), it was recognized primarily based on data from the Burst and Transient Source Experiment (BATSE) on-board the Compton Gamma-Ray Observatory that GRBs can be generally divided into two groups based on their duration and spectral hardness: the short-hard and long-soft bursts, with a separation at about 2 sec (Norris et al. 1984, Dezalay et al. 1992, Kouveliotou et al. 1993).

For both GRB classes, the uniform projected distribution of the bursts on the sky and the fluence distribution (the so-called $\log N - \log S$ or $V/V_{\rm max}$ distributions) pointed to a cosmological origin (e.g., van den Bergh 1983; Goodman 1986; Paczynski 1986; Schmidt, Higdon & Hueter 1988; Meegan et al. 1992; Piran 1992; Schmidt 2001; Guetta & Piran 2005). Despite these statistical tests, the distance scale of GRBs continued to be debated at least into the mid-1990s (Lamb 1995, Paczynski 1995). On the other hand, the non-repeating nature of GRBs, their harder non-thermal spectra, and non-Euclidean space distribution separated them from the soft γ-ray repeaters (SGRs; e.g., Kouveliotou et al. 1987, Laros et al. 1987, Norris et al. 1991), which originate from magnetars in the Milky Way and nearby galaxies (Kouveliotou et al. 1998); it is important to note, however, that some events classified as short GRBs may represent extragalactic giant SGR flares with a long recurrence timescale (Abbott et al. 2008, Ofek et al. 2008, Hurley et al. 2010, Abadie et al. 2012b).

In the framework of a cosmological origin, the large energy release (up to an isotropic-equivalent value of $\sim 10^{54}$ erg), short variability timescale (down to milliseconds), and observed non-thermal γ-ray spectra led to the "compactness problem"; namely, the observed properties result in an enormous optical depth to pair-production, and hence an expected thermal emission (Ruderman 1975). A key result in GRB research was the realization that this problem can be resolved by invoking relativistic expansion with a large bulk Lorentz factor of $\Gamma \gtrsim 10^2$ (e.g., Paczynski 1986; Krolik & Pier 1991; Fenimore, Epstein & Ho 1993; Baring & Harding 1997). The large Lorentz factor in turn requires exceedingly clean explosions with ejecta masses of $\lesssim 10^{-5}$ $M_\odot$, the so-called baryon loading problem (Shemi & Piran 1990). In addition, it was recognized that the interaction of the relativistic outflow with the surrounding medium will generate synchrotron emission ranging from radio to X-rays, with a longer duration than the prompt γ-ray emission – the "afterglow" (Rees & Meszaros 1992; Meszaros & Rees 1993; Paczynski & Rhoads 1993; Meszaros & Rees 1997; Sari, Piran & Narayan 1998). The detection of such afterglow emission became an intense pursuit since it held the key to precise positions and hence a distance scale to the bursts.

Motivated in part by the ~ 0.1 Gyr merger timescale of the Hulse-Taylor binary (Hulse & Taylor 1975), seminal studies by Paczynski (1986) and Eichler et al. (1989) pointed out that neutron star binary mergers may lead to γ-ray emission with an energy scale of $\gtrsim 10^{50}$ erg, typical of a cosmological GRB. Such mergers are also expected to result in an outflow with a low baryon load due to the absence of a dense surrounding environment, and can therefore drive relativistic outflows. A more detailed investigation of the neutron star binary merger model was carried out by Narayan, Paczynski & Piran (1992), who pointed out that testable predictions include significant offsets from the host galaxies due to natal kicks imparted to the binaries at birth, and gravitational wave emission in the frequency range of the Laser Interferometer Gravitational Wave Observatory (LIGO). Lattimer et al. (1977) and Eichler et al. (1989) also proposed these mergers as a potential site for r-process nucleosynthesis. Subsequent to these initial studies, a wide range of investigations of neutron star binary (NS-NS) and neutron star black hole binary (NS-BH) mergers were carried out with the aim of exploring their gravitational wave emission, the production of r-process enriched ejecta, and the possible production of GRBs. In parallel, an alternative model of GRBs from core-collapse supernovae (the collapsar model) was developed (MacFadyen & Woosley 1999), with clear predictions about the resulting population that included an exclusive origin in star-forming galaxies and association with core-collapse supernovae.

The major breakthrough in the study of GRBs, their distance and energy scale, environments, and progenitors came from the eventual discovery of afterglows from long GRBs starting in 1997 (Costa et al. 1997, Frail et al. 1997, van Paradijs et al. 1997). The localization of the bursts to arcminute scale (in X-rays) and to sub-arcsecond scale (in optical and radio), led to redshift measurements from optical spectroscopy of the afterglows and host galaxies, which directly demonstrated a cosmological origin (Metzger et al. 1997, Kulkarni et al. 1999). The afterglow emission also provided observational evidence for relativistic expan-

sion (Waxman, Kulkarni & Frail 1998; Taylor et al. 2004), jet collimation with typical opening angles of $\sim 3 - 10^{\circ}$ (Harrison et al. 1999, Stanek et al. 1999, Frail et al. 2001), a beaming-corrected energy scale of $\sim 10^{51}$ erg (Frail et al. 2001; Bloom, Frail & Sari 2001; Berger, Kulkarni & Frail 2003), and a typical circumburst density of $\sim 1 - 10$ cm^{-3} with evidence for mass loss from the massive progenitor stars in some cases (Chevalier & Li 2000, Panaitescu & Kumar 2002, Yost et al. 2003). In addition, follow-up studies of the hosts demonstrated an exclusive location in star-forming galaxies (Bloom et al. 1998; Djorgovski et al. 1998; Christensen, Hjorth & Gorosabel 2004; Wainwright, Berger & Penprase 2007), while high resolution imaging with the *Hubble Space Telescope* (*HST*) showed that long GRBs follow the radial distribution expected for star formation in disk galaxies (Bloom, Kulkarni & Djorgovski 2002), and are spatially correlated with bright star-forming regions in their hosts (Fruchter et al. 2006). Moreover, long GRBs were shown to be associated with Type Ic supernovae, based on both photometric and spectroscopic observations (Galama et al. 1998, Hjorth et al. 2003, Stanek et al. 2003, Woosley & Bloom 2006, Hjorth & Bloom 2012). Taken together, the environments and supernova associations indicated that long GRBs arise from the death of massive stars, and not from compact object binary mergers.

Despite the impressive pace of discovery for long GRBs, the study of short GRBs proved much more challenging, although compact object binary mergers remained an attractive progenitor model. Kehoe et al. (2001) carried out rapid but shallow optical follow-up of three short GRBs, with non-detections to a limit of $\sim 13 - 15$ mag. Hurley et al. (2002) presented deeper optical follow-up (to limits of $16 - 20$ mag with a delay of ~ 2 d) and the first radio follow-up (to limits of about $0.5 - 1.5$ mJy with a similar delay) for four short GRBs, but none were detected. In light of the existing afterglow detections summarized in this review, these early searches were woefully inadequate. At the same time, Panaitescu, Kumar & Narayan (2001) argued that a lower energy scale, and potentially lower circumburst densities, will result in dimmer afterglows than for long GRBs, by at least an order of magnitude (e.g., typical optical brightness of ~ 23 mag at 10 hours post-burst). Similarly, Perna & Belczynski (2002) argued based on compact object binary population synthesis models that due to kicks such mergers will tend to occur in lower density environments than long GRBs (~ 0.1 cm^{-3}), and hence lead to fainter afterglows, if they indeed produced short GRBs.

As in the case of long GRBs, the watershed moment in the study of short GRBs came with the discovery of the first afterglows in May–July 2005, following bursts from the *Swift* (Gehrels et al. 2004) and HETE-2 (Ricker et al. 2003) satellites. Rapid *Swift* X-ray Telescope follow-up of GRB 050509b led to the discovery of the first X-ray counterpart, with a localization of about 9″ radius (Gehrels et al. 2005). Deep follow-up optical observations revealed no afterglow emission, but instead uncovered a massive elliptical galaxy at $z = 0.225$ near the X-ray error circle, with a chance coincidence probability of $\sim 10^{-3}$ (Castro-Tirado et al. 2005, Gehrels et al. 2005, Bloom et al. 2006). Assuming that the association with the galaxy (and hence the redshift) was correct, it was also shown that the burst lacked a supernova (Hjorth et al. 2005a). Shortly thereafter, HETE-2 discovered the short GRB 050709 (Villasenor et al. 2005), and follow-up observations with the *Chandra X-ray Observatory* precisely localized the X-ray afterglow (Fox et al. 2005), with subsequent observations revealing the first short GRB optical afterglow (Hjorth et al. 2005b). The resulting sub-arcsecond position pinpointed the origin of the burst to the outer regions of a star-forming galaxy at $z = 0.160$ (Fox et al. 2005), while optical follow-up ruled out the presence of an associated supernova (Hjorth et al. 2005b). Finally, the detection of the short GRB 050724 by *Swift* (Barthelmy et al. 2005) led to the discovery of X-ray, optical/near-IR, and the first radio afterglow, and a definitive localization in an elliptical galaxy at $z = 0.257$ (Figure 1; Berger et al. 2005b). The combination of radio to X-ray afterglow emission also demonstrated that both the energy and density scale were lower than for long GRBs (Berger et al. 2005b). Taken together, these three early events demonstrated that short GRBs are cosmological in origin, that they produce afterglow emission similar to that of long GRBs but with a lower energy and density scale, and that their progenitors are not massive stars.

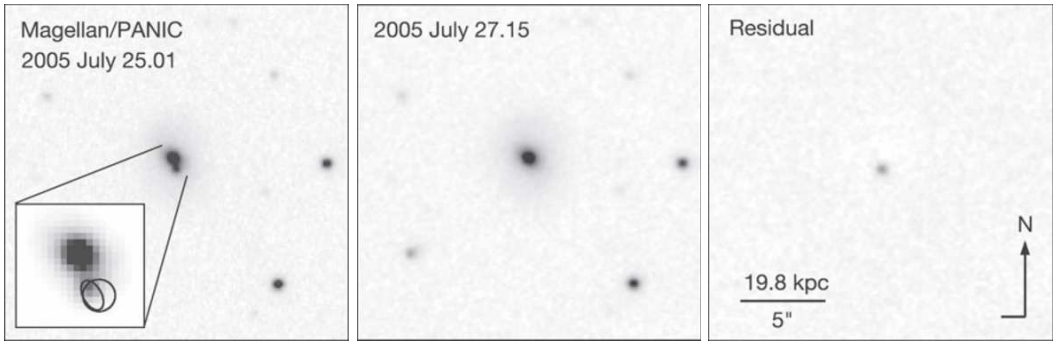

Figure 1:

Near-infrared images of the afterglow and host galaxy of the short GRB 050724, obtained 0.49 d (left) and 2.63 d (middle) post-burst, reveal a fading afterglow (right) on the outskirts of an elliptical galaxy. The inset in the left panel shows the locations of the X-ray afterglow detected with *Chandra* (circle) and the radio afterglow detected with the VLA (ellipse). This was the first short GRB with a definitive association to an elliptical galaxy, and a broad-band afterglow spanning radio to X-rays. From Berger et al. (2005b).

In the decade following the initial discovery of short GRB afterglows, over 70 short GRBs have been discovered by *Swift* and other γ-ray satellites, with a substantial detection fraction of X-ray and optical afterglows, and a few radio afterglow detections. The resulting localizations have also led to the identification of nearly 40 host galaxies, and have enabled studies of the sub-galactic locations of short GRBs. This is the first substantial sample of short GRBs with extensive afterglow and host galaxy data. The primary goal of this review is to utilize and synthesize the information from short GRB afterglows and environments for the first time in order to: (i) delineate the basic observational properties of short GRBs and their environments (from parsec to galactic scales); (ii) use this information to confront theoretical progenitor models; (iii) determine some of the basic properties of the progenitors and the resulting explosions; and (iv) explore the expected electromagnetic counterparts of Advanced LIGO/Virgo gravitational wave sources in the context of compact object binary progenitors.

In this vein, the outline of the paper is as follows. In §2 I summarize the basic properties of the prompt γ-ray emission, compare these with the γ-ray properties of long GRBs, and discuss the issue of short versus long GRB classification. In §3 I describe current short GRB progenitor models. In §4 I define the existing sample of short GRBs, including the completeness for afterglow and host galaxy detections. In §5 I summarize basic observational arguments for a distinct origin from the massive star explosion that produce long GRBs. In §6 I provide a detailed analysis of short GRB host galaxy properties, and use this information to shed light on the age distribution of the progenitors. In §7 I zoom in on the sub-galactic locations of short GRBs in terms of their radial offset distribution and their spatial relation to the underlying ultraviolet and optical light distribution of their hosts, and compare these results with the location of long GRBs and supernovae, and with predictions from compact object binary population synthesis models. In §8 I turn to the afterglow properties in X-rays, optical, and radio, and use a comparison to both long GRB afterglows and afterglow theory to provide insight on the energy scale of short GRBs, their collimation, and their circumburst environments. In §9 I discuss the expected production and optical/near-IR emission from *r*-process ejecta in compact object binary mergers, and compare these predictions to observations of the short GRB 130603B, the first burst to show evidence for such emission. In §10 I use the inferred properties of short GRBs and their afterglows to explore on- and off-axis electromagnetic emission from gravitational wave sources detected by the upcoming Advanced LIGO/Virgo detectors. I conclude with the key results

and a discussion of future directions in §11.

In addition to the comprehensive review of short GRBs presented here, I also refer the reader to several previous reviews that provide additional insight on GRB theory and observations. These include a review of GRBs in the BATSE era (Fishman & Meegan 1995); an early review of long GRB afterglow discoveries, the emerging GRB-supernova connection, and afterglow theory (van Paradijs, Kouveliotou & Wijers 2000); comprehensive reviews of the prompt emission and afterglow theory (Mészáros 2002, Piran 2004); a detailed review of the long GRB-supernova connection (Woosley & Bloom 2006); a preliminary review of short GRBs, focused primarily on theoretical issues, and including data from the first few well-localized events in 2005 (Nakar 2007); a comprehensive review of short GRB progenitor models, primarily compact object mergers and collisions (Lee & Ramirez-Ruiz 2007); a review of the primary early results from the *Swift* satellite, including in part the detections of short GRBs (Gehrels, Ramirez-Ruiz & Fox 2009); and finally, an initial review of short GRB galactic and sub-galactic environments (Berger 2011).

2 The Prompt Emission and the Short-Long Divide

The defining feature of GRBs among the wide variety of known astrophysical transients is their dominant, non-repeating, and non-periodic prompt γ-ray emission, which displays a rich phenomenology in terms of duration, variability, spectral parameters, fluence, peak flux, temporal and spectral evolution, and various correlations between these parameters. Within this broad range of properties, the clearest sub-classes are the short-hard and long-soft bursts. It is important to note that generally the short end of the short GRB duration distribution is affected by detector trigger times (tens of ms), while at the long end there is some overlap with the duration distribution of long GRBs, such that some events belonging to the short burst progenitor population will have durations of $\gtrsim 2$ s, while some events with duration of $\lesssim 2$ s will have long GRB progenitors (e.g., Bromberg et al. 2013). In addition, since various instruments measure durations in different energy bands, it is possible that the value of T_{90} separating short and long GRBs varies for each sample; for example, Bromberg et al. (2013) suggest that for *Swift* the division is at $T_{90} \approx 0.8$ s. The effect of cosmological time dilation adds another potential complication, as indicated for example by the high-redshift GRBs 080913 ($z = 6.7$) and 090423 ($z = 8.3$) whose observed durations place them in the long GRB category, while their rest-frame durations of ≈ 1 s are nominally in the short GRB range (Zhang et al. 2009, Belczynski et al. 2010).

Such effects can be potentially mitigated by the use of auxiliary information, motivated in part by our knowledge of long GRBs (e.g., their association with Type Ic SNe, their exclusive location in star-forming galaxies), and partly by expectations for short GRB progenitors. In this vein, Zhang et al. (2007) and Zhang et al. (2009) advocate a new classification scheme into Type I GRBs (compact object mergers) and Type II GRBs (massive star progenitors), motivated by the nomenclature for supernovae. To determine the type of each burst, they argue for the use of information such as redshift, supernova association, host galaxy type and star formation rate, burst offset relative to the host galaxy, the density profile of the circumburst medium, the γ-ray and afterglow energy scale, and a combination of prompt emission properties (see Figure 8 of Zhang et al. 2009). Lü et al. (2010) instead advocate the use of a new prompt emission empirical parameter, $E_{\gamma,\rm iso}/E_p^{5/3}$, with a value of $\lesssim 0.03$ coupled with a rest-frame $T_{90} \lesssim 5$ s separating Type I and II events; here $E_{\gamma,\rm iso}$ is the isotropic-equivalent γ-ray energy and E_p is the spectral peak of the prompt emission. Bloom, Butler & Perley (2008) propose a classification scheme based on physical properties of the progenitor systems, for example destructive (Type I) versus non-destructive (Type II) events, with further separation into sub-classes based on the presence or absence of a degenerate object (and whether it is a neutron star or black hole), and membership in a binary system.

While such classification schemes are potentially more powerful than relying on duration and hardness

alone, and in the long run may be essential for a complete mapping of GRB progenitors, they also carry the risk of biasing the results. For example, the requirement of elliptical hosts for Type I GRBs will obscure the fact that their presumed compact object binary progenitors occur in both star-forming and elliptical galaxies, and may therefore impede the ability to determine properties such as the delay time distribution from the host galaxy demographics (e.g., Zheng & Ramirez-Ruiz 2007, Berger 2009, Leibler & Berger 2010, Fong et al. 2013). Similarly, the requirement of a lower energy scale or larger physical offsets for Type I GRBs will restrict our understanding of the full range of properties spanned by the progenitors and explosions. In the case of a progenitor-based classification scheme, it is currently unclear either from observations or from theory how different systems manifest in terms of unique observables, particularly in the context of the prompt γ-ray emission for which even the radiation mechanism has not been conclusively identified. Finally, since complete knowledge of the prompt emission, distance scale, afterglow parameters, and host galaxy properties is only available for a small subset of events, it is currently more profitable to begin the investigation of short GRBs with a broad sample that may guide future classification schemes and observational follow-up efforts. Ultimately, it is important to recognize that while the analogy with the supernova classification scheme is tempting, that classification is based on spectroscopic signatures that already provide critical (though not always definitive) physical insight into the nature of the explosions (e.g., Filippenko 1997). For GRBs, on the other hand, the starting point for any classification scheme is the prompt emission, which exhibits many similarities between long and short GRBs (as I discuss below), and even after four decades of investigation is not fully understood.

Thus, in this review I pursue the simplest approach of studying a sample of short GRBs based on a duration cut of $T_{90} \lesssim 2$ s. It is possible that some events in the sample are produced by long GRB progenitors, and that some events with $T_{90} \gtrsim 2$ s that belong to the short GRB progenitor population are not included in the sample. However, as I discuss in detail in subsequent sections, the overall differences in the resulting short and long GRB populations in terms of afterglow and host galaxy properties are sufficiently clear that they both shed light on the nature of short GRB progenitors (despite any marginal contamination), and can serve as the basis for future classification schemes by revealing the most relevant and critical differences.

2.1 Comparative Studies of the Prompt Emission

Within the context of a duration-based classification scheme, there have been multiple comparative studies of the prompt emission properties of short and long GRBs, based on the samples from various instruments, primarily BATSE, *Swift*, and most recently *Fermi*. These studies have uncovered both differences and commonalities in the prompt emission of short and long GRBs. Below I provide a short overview of these results, and I refer the reader to Nakar (2007) and Gehrels, Ramirez-Ruiz & Fox (2009) for a more detailed discussion.

In the framework of the phenomenological Band function which was constructed to fit the spectrum of the prompt emission (Band et al. 1993), a key finding is that short GRBs generally have harder spectra than long GRBs due to a combination of a shallower low-energy spectral slope, $\alpha \approx -0.4$ versus ≈ -0.9, and a higher spectral peak, $E_p \approx 400$ versus ≈ 200 keV (e.g., Paciesas et al. 2003; Ghirlanda et al. 2009; Ghirlanda, Ghisellini & Nava 2011). However, these differences are less evident when the sample is restricted to short GRBs with the highest peak fluxes (Paciesas et al. 2003, Kaneko et al. 2006), or when considering only the first ~ 2 s of long GRB light curves (Ghirlanda, Ghisellini & Celotti 2004). Similarly, the variability timescales of short GRBs are comparable to those in the first ~ 2 s of long GRBs (Nakar & Piran 2002).

Another difference between short and long GRBs is evident in the distribution of spectral lags, which are generally $\gtrsim 0$ s for long GRBs (i.e., they exhibit a hard to soft evolution), while they are ~ 0 s (± 20 ms) for short GRBs (Norris & Bonnell 2006; Norris, Gehrels & Scargle 2011). Some long GRBs also exhibit

negligible lags, but those are events with the highest peak luminosities, which are distinct from the zero lag, low peak luminosity short GRBs (Norris & Bonnell 2006). The difference in spectral lags between short and long GRBs may ultimately provide another useful prompt emission discriminator in the context of classification schemes (e.g., Gehrels et al. 2006).

Finally, it has been noted that short GRBs occupy a distinct region in the $E_p - E_{\gamma,\rm iso}$ phase-space than long GRBs, namely they have lower $E_{\gamma,\rm iso}$ values for a given E_p than long GRBs (Amati et al. 2002, Ghirlanda et al. 2009, Qin & Chen 2013, Tsutsui et al. 2013). It remains to be seen, however, whether both sub-classes follow a similar relation if only the first ~ 2 s of long GRBs are considered when determining their E_p and $E_{\gamma,\rm iso}$ values.

On the other hand, an overall similarity between short and long GRBs has been found in terms of a common inverse correlation between the duration and intensity for individual pulses (Hakkila & Preece 2011; Norris, Gehrels & Scargle 2011). In addition, short and long GRBs appear to follow the same relation between E_p and $L_{\rm peak}$ (Yonetoku et al. 2004, Ghirlanda et al. 2009).

To date only two short GRBs have been detected at $\sim$ GeV energies with the *Fermi* Large Area Telescope. GRB 081024B was detected at $\sim 0.1 - 3$ GeV with a slight delay and a duration of about 3 s, compared to $T_{90} \approx 0.8$ s at MeV energies (Abdo et al. 2010). Even more extreme GeV emission (up to ~ 30 GeV) was observed in GRB 090510, with a delay of about 0.6 s and extending to ~ 200 s (Abdo et al. 2009, Ackermann et al. 2010). The delayed onset and longer duration of the GeV emission in both long and short GRBs have been interpreted as evidence for a hadronic origin (Asano, Guiriec & Mészáros 2009), a synchrotron self-Compton origin (Ackermann et al. 2010), or an afterglow origin (Ackermann et al. 2010; Ghirlanda, Ghisellini & Nava 2010; Kumar & Barniol Duran 2010).

2.2 Extended Emission

An interesting feature of some short GRBs is the presence of extended γ-ray emission that is softer than the prompt spike, lasts $\sim 10 - 100$ s, and sometimes exhibits a delayed onset. The presence of such an emission component was first noted in a stacking analysis of BATSE short GRBs by Lazzati, Ramirez-Ruiz & Ghisellini (2001) who demonstrated that the emission was softer than both the prompt spike and long GRBs of similar durations. These authors interpreted the soft extended component as the onset of the X-ray afterglow. Subsequent studies confirmed the presence of extended emission in at least some BATSE and Konus short bursts (Connaughton 2002, Frederiks et al. 2004).

The presence of soft extended emission in individual bursts garnered attention with the discovery of the first short GRB afterglows. GRB 050709 exhibited an initial spike with $T_{90} \approx 0.07$ s in the $30 - 400$ keV band, followed by a pronounced bump in the $2 - 25$ keV range with a duration of about 130 s, and a larger fluence by about a factor of 2.5 compared to the initial spike (Villasenor et al. 2005). A similar component was observed in the GRB 050724, with emission in the $15 - 25$ keV band lasting about 100 s, but accounting for only 10% of the fluence of the initial spike (Barthelmy et al. 2005). A particularly extreme example is GRB 080503, in which the extended emission dominated over the fluence of the prompt spike by a factor of 32 (Perley et al. 2009).

A study by Norris & Bonnell (2006) identified eight BATSE short bursts with individual detections of extended emission, with a counts ratio relative to the initial spike ranging up to ~ 40, and an estimated overall dynamic range of this ratio of $\sim 10^4$. These authors also noted that short GRBs with and without extended emission share a negligible spectral lag in the initial spike. A follow-up study of extended emission in *Swift* short bursts by Norris, Gehrels & Scargle (2010) indicated that about one-quarter of the events clearly exhibit extended emission, while the bulk of the remaining events lack such a component. However, I note that not all of the bursts in their sample have a genuine initial short spike, and the incidence rate of extended

emission may be closer to $\sim 15\%$. Building on this sample, Norris, Gehrels & Scargle (2011) argued that bursts with extended emission have durations and pulse profiles in the prompt spike that are $\sim 2-3$ times longer than events lacking extended emission, potentially indicative of differences in the central engine.

Two other note-worthy events in the context of extended emission and the T_{90} divide between long and short bursts are GRBs 060505 and 060614, with durations of 4 and 102 s, respectively, low redshifts of 0.089 and 0.125, and yet no supernova associations to limits of about $6-7$ mag fainter than typical long GRB-SNe (Della Valle et al. 2006, Fynbo et al. 2006, Gal-Yam et al. 2006, Gehrels et al. 2006). The prompt emission of GRB 060505 exhibited a significant spectral lag, typical of long GRBs, and the burst coincided with a low metallicity and young star-forming region of its late-type host galaxy (Ofek et al. 2007, Thöne et al. 2008), matching the properties of long GRB environments. The γ-ray emission of GRB 060614 exhibited an initial 5-sec spike with negligible spectral lag, typical of short GRBs, followed by extended emission with significant variability, somewhat softer spectrum, and a larger fluence than the prompt spike by about a factor of 5 (Gehrels et al. 2006). The host galaxy of GRB 060614 has a low luminosity typical of long GRB hosts, but a lower than average specific star formation rate (Gal-Yam et al. 2006). Moreover, the burst itself was located at a significant offset from the host in a region with little evidence for underlying ultraviolet emission (Gal-Yam et al. 2006). Thus, GRBs 060505 and 060614 present a challenge to any GRB classification scheme, with their prompt emission sharing properties typical of both long and short GRBs, their host environments similarly spanning locations typical of long and short GRBs, and the lack of supernova association suggesting a non-massive star progenitor.

There have been attempts to discern other differences between the population of short GRBs with and without extended emission. Norris, Gehrels & Scargle (2011) claim that short bursts with extended emission have larger X-ray fluxes at ~ 100 s post-burst and longer lasting X-ray afterglows. However, it is not obvious that the X-ray emission at such early times is not directly related to the soft extended emission itself. Troja et al. (2008) used a sample of short GRBs up to mid-2007 to argue that events with extended emission have systematically smaller spatial offsets from their hosts, and hence distinct progenitors. However, subsequent studies of the offset distribution indicate that short GRBs with extended emission span as wide an offset range as events with no extended emission (Fong, Berger & Fox 2010; Fong & Berger 2013); a Kolmogorov-Smirnov (K-S) test comparing the two offset distributions leads to a p-value of 0.9, indicating that there is no evidence for two distinct populations (Fong & Berger 2013). In addition, Fong et al. (2013) find that the distributions of host galaxy types for short GRBs with and without extended emission are currently indistinguishable.

Motivated by the discovery of extended emission, several attempts have been made to provide a theoretical explanation. Metzger, Quataert & Thompson (2008) propose that short GRBs with extended emission are produced by the formation of a rapidly rotating proto-magnetar through accretion-induced collapse of a white dwarf, the merger of a white dwarf binary, or the merger of a neutron star binary. In this framework, the prompt spike is due to the standard picture of accretion onto the central object, while the extended emission is powered by a relativistic wind that extracts the proto-magnetar's rotational energy. Bucciantini et al. (2012) discuss a slight variation of the magnetar model, in which the delay in the onset of extended emission is due to a breakout of the relativistic outflow through a baryon-loaded wind from the proto-magnetar. Metzger et al. (2010a) suggest instead that the gap between the prompt spike and extended emission may be due to heating from r-process nucleosynthesis, which momentarily halts fall-back accretion onto the central object. In this scenario, events lacking extended emission are due to a timescale for the r-process heating of $\gtrsim 1$ s, which leads to a complete cut-off in fallback accretion, while those with extended emission resume fall-back accretion after a delay. MacFadyen, Ramirez-Ruiz & Zhang (2005) propose a model in which the short GRBs with extended emission are due to the accretion-induced collapse of a neutron star (generating the prompt spike) followed by interaction of the relativistic outflow with the non-degenerate

stellar companion (leading to a delay followed by soft extended emission).

2.3 X-ray Flares

The discovery of early X-ray flares following the prompt γ-ray emission was enabled by the rapid follow-up capabilities of *Swift* (Burrows et al. 2005, Nousek et al. 2006, Chincarini et al. 2007, Falcone et al. 2007). The X-ray flares generally follow a fast rise exponential decay profile with $\Delta t/t \ll 1$, and share spectral and temporal properties with the prompt emission, pointing to a common origin in activity from the central engine (Chincarini et al. 2010, Margutti et al. 2010); here, Δt is the flare duration and t is the time since the onset of the burst. In the case of short GRBs, Margutti et al. (2011) carried out a systematic search for flares, and found eight *Swift* events that exhibit flaring activity. The sample includes bursts with and without extended emission, and in both early- and late-type host galaxies. The resulting flares follow some of the relations of long GRB flares, for example a positive correlation between the flare width and time since the burst. On the other hand, the short GRB flares are generally weaker in terms of flux contrast relative to the underlying X-ray emission (with $\Delta F/F \lesssim 2$), have about 1% of the peak luminosity and isotropic-equivalent energy of long GRB flares, and like the prompt emission, do not follow the lag-luminosity relation of long GRB flares. The lower peak luminosity compared to long GRB flares remains true even when scaled by the peak luminosity of the prompt emission, but short and long GRB flares track the same negative correlation between the ratio of peak flare to prompt luminosity as a function of the ratio of flare peak time to burst duration. Potentially related to this point, the ratio of flare to prompt isotropic-equivalent energy is similar for both short and long GRBs. Given these results, Margutti et al. (2011) conclude that flares in both short and long GRBs are related to the prompt emission.

Flares and re-brightenings at late time ($\sim$ hours) have also been detected in some short GRBs, with distinct properties from the early flares described above. GRB 050724 exhibited a significant X-ray flare centered at $\approx$ 14 hr with $\Delta F/F \approx 40$ and $\Delta t/t \approx 1$, with apparent associated emission in the optical/near-IR (Campana et al. 2006, Grupe et al. 2006, Malesani et al. 2007). The fact that the flare is superposed on an underlying single power law decline suggests a distinct, though currently not understood origin from the afterglow. A delayed peak was found in the optical (and potentially X-ray) emission from GRB 080503 at $\sim$ 1 day, although the subsequent evolution matched typical afterglow emission rather than a distinct flare (Perley et al. 2009). Finally, excess X-ray emission at $\gtrsim$ 1 d was found in GRB 130603B, with no corresponding emission in the optical or radio bands, and an apparent single power law behavior compared to the early X-ray emission (Fong et al. 2013). Thus, the late flares and re-brightenings are likely to have a distinct origin from the early rapid X-ray flares.

Several ideas have been proposed to explain flares in short (and long) GRBs. Perna, Armitage & Zhang (2006) suggest that fragmentation in the outer accretion disk, caused by gravitational instabilities, could lead to large amplitude variations of the central engine. Rosswog (2007) propose that the flares can be caused by fall-back accretion of material launched into eccentric orbits during a compact object merger (see also Lee, Ramirez-Ruiz & López-Cámara 2009). Proga & Zhang (2006) suggest that the accretion can be episodically stopped and re-started through variations in the accumulated magnetic flux around the accreting central engine. Finally, Giannios (2006) propose that the flares can be produced by delayed magnetic reconnection as a strongly magnetized outflow decelerates through interaction with the circumburst medium; unlike the other proposed models, this scenario does not require a re-activation of the central engine.

2.4 Precursors

Precursor γ-ray emission, preceding the main event by tens of seconds, has been found in $\sim 20\%$ of long GRBs (Lazzati 2005), and has been attributed to either the transition of the expanding fireball to the optically thin regime, or to the breakout of the relativistic jet from the surface of the progenitor star (e.g., Lazzati & Begelman 2005). If the former scenario is correct, precursors should also be present in short GRBs. In addition, precursors in short GRBs may be produced by other mechanisms, for example magnetospheric interaction between the compact objects (Hansen & Lyutikov 2001) or resonant shattering of the neutron star crusts (Tsang et al. 2012) prior to the merger. Troja, Rosswog & Gehrels (2010) conducted a search for precursors in 49 *Swift* short GRBs with and without extended emission, and uncovered 5 potential candidates (with $2-5.5\sigma$ significance), of which 3 candidates (GRBs 081024A, 090510, and 091117) had likely independent detections in other satellite data. In those 3 cases, the precursor candidates occurred 0.5 – 2.7 s prior to the main spike, and it is therefore not clear if these emission episodes are indeed distinct precursors, or a part of the prompt emission complex.

3 Short GRB Progenitor Models

The bimodality of GRB durations is highly suggestive of two dominant progenitor populations. The short durations of short GRBs, down to tens of milliseconds, point to compact progenitor systems with a dynamical timescale of milliseconds. In this context, the most popular progenitor model is the merger of compact object binaries comprised of two neutron stars or a neutron star and a black hole (NS-NS/NS-BH; Eichler et al. 1989; Narayan, Paczynski & Piran 1992). The merger occurs due to angular momentum and energy losses by gravitational wave radiation. In the binary neutron star case, the expected remnant is a black hole surrounded by a hyper-accreting disk of debris, while a NS-BH merger can lead to the same configuration if the neutron star is tidally disrupted outside of the black hole's horizon. The resulting interplay of high accretion rate and rapid rotation can lead to energy extraction via neutrino-antineutrino annihilation or magnetohydrodynamic processes (e.g., Blandford & Znajek 1977, Rosswog & Ramirez-Ruiz 2002, Lee & Ramirez-Ruiz 2007), which in turn drive a collimated relativistic outflow. As discussed in §1, NS-NS/NS-BH mergers were proposed as GRB progenitors prior to the discovery of the duration bimodality since they provided a known source population with roughly the correct event rate, the requisite rapid release of a large energy reservoir, and a clean environment to avoid significant baryon loading.

The compact object merger model leads to several testable observational predictions. First, the delay time between the binary formation and eventual merger is expected to span a wide range that depends on the initial separation and consituent masses, $\tau_{\rm GW} \propto a^4/(\mu M^2)$, where a is the initial binary separation, $M \equiv M_1 + M_2$ is the total binary mass and $\mu \equiv M_1 M_2/M$ is the reduced mass. As a result of the wide delay time distribution, the resulting short bursts will occur in both early- and late-type galaxies (e.g., Belczynski et al. 2006, Zheng & Ramirez-Ruiz 2007). This is indeed the case for the small observed population of Galactic NS-NS binaries, which have coalescence timescales of tens of Myr to much longer than a Hubble time (e.g., Burgay et al. 2003, Champion et al. 2004). Second, natal kicks imparted to the binary system during the supernova explosions that gave rise to the neutron stars and/or black hole, coupled with the broad range of merger timescales, should lead to some mergers at large offsets from their birth sites and host galaxies (tens to hundreds of kpc; Narayan, Paczynski & Piran 1992; Bloom, Sigurdsson & Pols 1999; Fryer, Woosley & Hartmann 1999; Perna & Belczynski 2002; Belczynski et al. 2006). A broad spatial distribution is also expected if some short GRBs result from dynamically-formed binaries in globular clusters (Grindlay, Portegies Zwart & McMillan 2006; Lee, Ramirez-Ruiz & van de Ven 2010). Third, the mergers will be accompanied by strong gravitational wave emission, detectable with the Advanced

LIGO/Virgo detectors to about 200 Mpc for NS-NS mergers (Abramovici et al. 1992, Harry & LIGO Scientific Collaboration 2010, Accadia et al. 2011). Fourth, the mergers will produce neutron-rich ejecta, which will in turn lead to *r*-process nucleosynthesis; the decay of the resulting radioactive elements may be detectable at optical/near-IR wavelengths (Lattimer & Schramm 1976, Li & Paczyński 1998, Metzger et al. 2010b, Barnes & Kasen 2013). Finally, the mergers will not be accompanied by supernova explosions. Most of these predictions can now be tested with existing observations of short GRBs, as delineated in subsequent sections of this review.

In principle, some of these properties may differ between NS-NS and NS-BH mergers. For example, numerical simulations suggest that mergers with a larger mass ratio (i.e., NS-BH) may produce larger ejecta masses, with more pronounced asymmetry that may lead to brighter optical/near-IR counterparts (Piran, Nakar & Rosswog 2013). Similarly, since neutron star disruption outside the horizon of a typical black hole with ~ 10 $M_\odot$ requires significant black hole spin, the resulting accretion disk will undergo significant Lense-Thirring precession that may imprint detectable variability on the prompt emission light curve (Stone, Loeb & Berger 2013). Finally, it is possible that the larger masses of NS-BH systems may lead to systematically smaller effective kicks, and hence smaller offsets than for NS-NS mergers (e.g., Belczynski et al. 2006, Dhawan et al. 2007). However, it is important to keep in mind that to date no NS-BH binaries have been identified in nature, and it is therefore not clear if they contribute to the short GRB population at all, whether any of the predicted differences match the actual properties of NS-BH binaries, and if the differences relative to NS-NS binaries are significant enough to be discernible in the existing short GRB sample. These questions may be resolved with joint gravitational wave and short GRB detections (§10).

In the NS-NS merger model it is generally assumed that a black hole is rapidly formed, with the resulting accretion powering the short GRB and its afterglow. However, the recent discovery of neutron stars with masses of about 2 $M_\odot$ (Demorest et al. 2010, Antoniadis et al. 2013), suggest that some mergers may lead instead to a transitory or stable rapidly-spinning and highly-magnetized neutron star (a magnetar; Duncan & Thompson 1992; Metzger, Quataert & Thompson 2008). The magnetar can in turn power a short GRB through its spin-down energy. In the transitory case, as the magnetar spins down it will eventually collapse to a black hole when differential rotation can no longer support its large mass. This transition could in principle lead to an observable signature; for example, it has been recently claimed that short-lived X-ray plateaus in some short GRBs are due to magnetar spin-down energy injection and the subsequent collapse to a black hole (Rowlinson et al. 2013). However, fall-back accretion may also explain the plateaus (Rosswog 2007). Similarly, it is not clear if a stable magnetar can be distinguished from an accreting black hole engine in terms of the resulting prompt and afterglow emission.

Given the potential ability of magnetars to provide the required energy source, it has also been proposed that such objects can form, and power short GRBs or soft γ-ray repeaters, following the accretion-induced collapse of a white dwarf or white dwarf binary mergers (Levan et al. 2006b; Metzger, Quataert & Thompson 2008). Unlike formation through core-collapse, such delayed magnetar formation will lead to events in both early- and late-type galaxies, similar to the prediction for NS-NS/NS-BH mergers. However, such systems are not expected to experience significant natal kicks, to be accompanied by gravitational wave emission in the Advanced LIGO/Virgo band, or to produce *r*-process radioactive elements.

Another proposed progenitor model is accretion-induced collapse of a neutron star to a black hole (Qin et al. 1998; MacFadyen, Ramirez-Ruiz & Zhang 2005), although this model has not been explored in detail. Finally, Lazzati, Morsony & Begelman (2010) suggested that short GRBs with extended emission may be produced from the same massive star progenitors as long GRBs, but with a wide off-axis viewing angle that leads to predominant emission from the cocoon surrounding the jet. In this model, short GRBs with extended emission will occur only in star-forming galaxies and will be accompanied by Type Ic supernovae.

These requirements are violated in several events (e.g., Berger et al. 2005b, Hjorth et al. 2005b).

4 Defining the Sample

In this review I address the properties of short GRBs, their afterglows, and environments, by focusing on a sample of 70 events discovered primarily by the *Swift* satellite (Gehrels et al. 2004) in the eight-year period spanning January 2005 to January 2013, supplemented by the recent well-studied benchmark event GRB 130603B (Berger, Fong & Chornock 2013; Cucchiara et al. 2013; de Ugarte Postigo et al. 2013; Tanvir et al. 2013). The sample includes three short bursts discovered by HETE-2 (GRBs 050709 and 060121; Fox et al. 2005, Hjorth et al. 2005b, Villasenor et al. 2005, de Ugarte Postigo et al. 2006, Levan et al. 2006a) and INTEGRAL (GRB 070707; McGlynn et al. 2008, Piranomonte et al. 2008) for which afterglows and host galaxies have been identified. This is the first sample of short GRBs with a substantial fraction of afterglow detections, enabling studies of both the burst properties and the host galaxies. A basic summary of the prompt and afterglow emission of these GRBs is provided in Table 1.

The most detailed information, both in terms of explosion properties and host galaxy and sub-galactic environments, comes from events localized to sub-arcsecond precision through an optical afterglow detections or a *Chandra* detection of the X-ray afterglow (e.g., Fox et al. 2005, Hjorth et al. 2005b, Berger et al. 2005b, Fong et al. 2012, Margutti et al. 2012); radio detections are also a route to sub-arcsecond positions (Berger et al. 2005b), but to date all short GRBs detected in the radio have also been detected in the optical. *Swift*/XRT positions alone, generally with a precision of $\sim 1.5-5''$, are also useful for host identifications (Bloom et al. 2007, Berger et al. 2007a, Fong et al. 2013). However, for these bursts the availability of only X-ray data limits the extraction of afterglow properties, and the positions are not precise enough to locate the bursts within their hosts.

In this vein, of the 67 *Swift* short GRBs considered here, 53 events were rapidly followed up with the on-board X-ray Telescope (XRT) on a timescale of $\lesssim 100$ s, leading to 47 detections (89%). This is only slightly lower than the detection rate for long GRBs. It is important to note that the 6 undetected events had a lower than average γ-ray fluence of $\langle F_\gamma \rangle \approx 2.5\times10^{-8}$ erg cm^{-2} and may therefore simply be fainter events. Two of the three non-*Swift* events (GRBs 060121 and 070707) were also followed up with the XRT and both were detected, enabling the subsequent identification of optical afterglows. The third non-*Swift* event (GRB 050709) was detected in the X-rays with *Chandra* (Fox et al. 2005). Of the 50 total X-ray detections, 28 events (56%) exhibit long-term X-ray emission beyond $\sim 10^3$ s, while the remaining 22 events rapidly fade below the *Swift*/XRT detection threshold at $\lesssim 10^3$ s. The *Swift*/XRT positions span a range of $1.4-5.5''$ radius, with a median value of $1.8''$ (90% confidence[1]). These positions are generally sufficient for a robust identification of host galaxies with a probability of chance coincidence of $\sim 1-10\%$ (Bloom et al. 2007, Berger et al. 2007a, Fong et al. 2013). Finally, the 14 bursts lacking rapid XRT follow-up include 8 events with *Swift* observing constraints, and 6 events with delayed follow-up ($\gtrsim 1$ hr post-burst). Thus, the lack of X-ray detections for these events is not expected to bias the sample considered here.

Deep optical follow-up observations were obtained for 37 of the 47 *Swift* bursts with XRT positions, leading to 21 detections (57%) with a range of about $21-26$ mag at $\delta t \approx 0.4-30$ hr. It is remarkable that the optical afterglow detection fraction is comparable to that for long GRBs despite the relative faintness of short GRB afterglows. This is a testament to the concerted follow-up effort undertaken by the community over the past decade, utilizing the largest ground-based telescopes. The three non-*Swift* events were also detected in the optical. Of the 10 events lacking deep optical follow-up, 6 events were located along constrained Galactic sight-lines with large extinction and/or contaminating bright stars, while the other 4 events lack deep afterglow and host galaxy searches at the present. Thus, as in the case of missing X-

[1] http://www.swift.ac.uk/xrt_positions/

ray follow-up, these events are not expected to bias the sample considered here. The 16 bursts with deep follow-up and no detected optical afterglows typically have limits of ~ 23 mag at $\sim 1-20$ hr, comparable to the median brightness of the detected afterglows (e.g., Berger 2010). As I demonstrate in §8 these events do not appear to be distinct from those with detected afterglows, suggesting that the searches were likely too shallow. In addition, 2 of the 16 events with optical non-detections (GRBs 111020A and 111117A) were subsequently detected with *Chandra* leading to sub-arcsecond positions (Fong et al. 2012, Margutti et al. 2012).

Finally, radio observations have been obtained for 28 short GRBs (including some non-*Swift* bursts and *Swift* bursts with only γ-ray positions) leading to only three detections to date (11%; GRBs 050724A, 051221A, and 130603B: Berger et al. 2005b, Soderberg et al. 2006a, Fong et al. 2013). This is a low detection fraction compared to long GRBs (with $\sim 30\%$; Chandra & Frail 2012), but it is not surprising considering that radio follow-up is generally sensitivity-limited even for long GRBs. As I discuss in §8, despite the low detection fraction, the radio limits are generally useful for placing constraints on the circumburst densities of short GRBs.

In addition to afterglow follow-up observations, there has been an intensive effort to characterize the environments of short GRBs from sub-galactic to galaxy cluster scales (e.g., Berger et al. 2007b; Berger 2009; D'Avanzo et al. 2009; Fong, Berger & Fox 2010; Berger 2011; Fong et al. 2013; Fong & Berger 2013). The sample presented in this paper includes nearly 40 identified host galaxies, with about 30 redshift measurements. A subset of these galaxies have detailed measurements that include morphologies, stellar masses, stellar population ages, star formation rates, and metallicities (see Table 2). In addition, for about 20 events (those with sub-arcsecond afterglow localizations) there are precise measurements of the sub-galactic environments based on *HST* observations, including projected offsets and the brightness at the GRB location relative to the underlying light distribution of the host galaxy (Berger 2010; Fong, Berger & Fox 2010; Fong & Berger 2013).

5 A Non-Massive Star Origin

Two key observations helped to establish the connection between long GRBs and the deaths of massive stars (the collapsar model; MacFadyen & Woosley 1999): (i) the association of long GRBs with Type Ic core-collapse supernovae (Galama et al. 1998, Hjorth et al. 2003, Stanek et al. 2003, Woosley & Bloom 2006); and (ii) the exclusive locations of long GRBs in star-forming galaxies (Bloom et al. 1998; Djorgovski et al. 1998; Christensen, Hjorth & Gorosabel 2004; Wainwright, Berger & Penprase 2007), as well as their spatial offsets relative to their hosts' overall light distribution and their coincidence with bright star-forming regions within their hosts (Bloom, Kulkarni & Djorgovski 2002; Fruchter et al. 2006). The SN associations are based on spectroscopic observations, mainly at $z \lesssim 0.5$ where the spectroscopic signatures can be discerned with sufficient significance (e.g., Hjorth et al. 2003, Stanek et al. 2003, Pian et al. 2006, Berger et al. 2011), and on photometric re-brightenings on a timescale of $\sim 15-20$ d post-burst that match Type Ic SN light curves in both brightness and color (to $z \sim 1$; e.g., Bloom et al. 1999, 2002, Woosley & Bloom 2006). The observed distribution of long GRB-SN peak magnitudes is relatively narrow, spanning only about 1 mag for the bulk of the sample (Woosley & Bloom 2006, Hjorth & Bloom 2012). Moreover, long GRB-SNe are generally more luminous than normal Type Ib/c SNe (Drout et al. 2011), although there is some overlap in the distributions. These results are summarized in Figure 2 in which I plot the peak absolute magnitudes of GRB-SNe and Type Ib/c SNe relative to the canonical SN 1998bw associated with GRB 980425. In terms of spatial locations within their hosts, long GRBs radially track an exponential light distribution, typical of star formation in disk galaxies, with a median offset of about one half-light radius (Bloom, Kulkarni & Djorgovski 2002). Moreover, long GRBs are spatially correlated with bright

star-forming regions, even in comparison to normal core-collapse SNe (Fruchter et al. 2006, Svensson et al. 2010).

5.1 Lack of Supernova Associations

In the short GRB sample defined in §4 there are several events at sufficiently low redshifts to allow clear detections of associated SNe, yet none have been found to date (Fox et al. 2005; Hjorth et al. 2005a,b; Soderberg et al. 2006a; D'Avanzo et al. 2009; Kocevski et al. 2010; Rowlinson et al. 2010; Berger, Fong & Chornock 2013). In Figure 2 I plot all existing upper limits for associated SNe (for 7 short bursts), measured relative to the peak absolute magnitude of the canonical long GRB-SN 1998bw. I also plot the limits for the peculiar events GRBs 060505 and 060614. As can be seen from the figure, SNe associated with long GRBs span a narrow peak brightness range, with a median and standard deviation relative to SN 1998bw of $+0.18 \pm 0.45$ mag. On the other hand, the upper limits on SN associations for short GRBs range from 0.6 to 7.4 mag fainter than SN 1998bw; GRBs 060505 and 060614 have limits of 6.9 and 6.4 mag fainter than SN 1998bw, respectively. Thus, in all cases an associations with SNe that are drawn from the same distribution as long GRB-SNe can be ruled out. This demonstrates that short and long GRBs do not share a common progenitor system, and that at least the short GRBs with deep SN limits are not produced by massive star explosions. It is also important to note that of the 7 short bursts with limits on associated SNe, 6 events are located in star-forming galaxies, indicating that while the hosts exhibit on-going star formation activity, the short GRB progenitors themselves do not belong to a young population of massive stars. I return to this point in §7 when discussing the locations of short GRB within and around their host galaxies.

The dominance of star-forming hosts in the sample of short GRBs lacking SN associations indicates that the use of galaxy type as an indicator of progenitor type (as advocated for example by Zhang et al. 2007, 2009) can severely bias the resulting GRB classification. In particular, a star-forming host does not indicate a young massive star progenitor. In a similar vein, I note that two of the short bursts with SN non-detections (GRBs 051221A and 070724A) are claimed to be likely collapsars according to the duration-hardness analysis of Bromberg et al. (2013), and a third event (GRB 080905A) has a duration that is longer than their nominal divide between short and long GRBs (see inset of Figure 2). The fact that these events lack associated SNe casts doubt on the claimed statistical significance of a collapsar origin assigned to individual events in their analysis.

5.2 A Mix of Ellipticals and Spirals

The second clear distinction between the short and long GRB populations is the occurrence of some short GRBs in elliptical galaxies (Figure 3). The current short GRB sample includes two secure cases of elliptical host galaxies based on sub-arcsecond afterglow positions and spatially coincident hosts (GRBs 050724A and 100117A; Berger et al. 2005b, Fong et al. 2011), two additional cases with sub-arcsecond afterglow positions and likely elliptical hosts with large projected offsets (GRBs 070809 and 090515; Berger 2010), and four additional likely cases (probabilities of about $1 - 5\%$) based on *Swift*/XRT positions alone (GRBs 050509b, 060502b, 070729, 100625A; Gehrels et al. 2005, Bloom et al. 2006, 2007, Fong et al. 2013). Overall, about 20% of short GRBs are associated with early-type host galaxies (Fong et al. 2013). In nearly all cases, the identification of the hosts as early-type galaxies is based on spectroscopic observations that reveal no star formation activity (to $\lesssim 0.1$ $M_\odot$ yr^{-1}), optical/near-IR spectral energy distributions that are matched by a single stellar population with an age of $\gtrsim 1$ Gyr, and/or morphological information based on *HST* observations. I explore the host galaxy demographics distribution, and its implications for the progenitor population, in the next section, but it is clear from the occurrence of at least some short GRBs

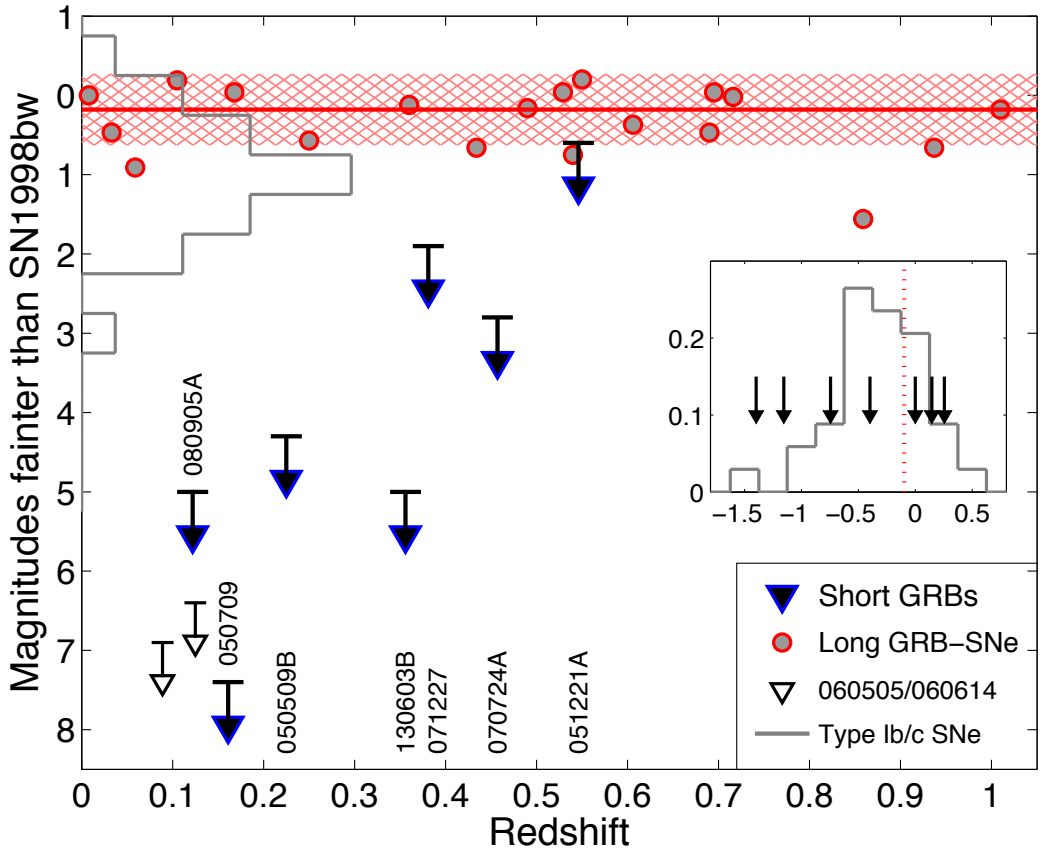

Figure 2:

Limits on supernovae associated with short GRBs (filled triangles) relative to the peak absolute magnitude of the canonical long GRB-SN 1998bw. Also shown are the distribution of SN peak magnitudes for long GRBs (filled circles; hatched region marks the median and standard deviation for the population; Hjorth & Bloom 2012), local Type Ib/c SNe (histogram; Drout et al. 2011), and two unusual long GRBs that lacked associated SNe (060505 and 060614; Della Valle et al. 2006, Fynbo et al. 2006, Gal-Yam et al. 2006, Gehrels et al. 2006). The latter may represent a long duration or extended emission tail of the short GRB population. With the exception of GRB 050509b, all short bursts with limits on associated SNe occurred in star-forming galaxies, indicating that despite the overall star formation activity, the short GRB progenitors were not massive stars. The inset shows the overall duration distribution of the short GRBs considered in this review (histogram), with the durations of the 7 short GRBs with SN limits marked by arrows. The dotted vertical line marks the claimed duration separating *Swift* non-collapsar and collapsar progenitors according to the analysis of Bromberg et al. (2013), and yet three of the short GRBs lacking SN associations have longer durations.

in elliptical galaxies that he progenitors belong to an old stellar population.

6 Short GRB Galaxy-Scale Environments

Having established that the progenitors of short GRBs are generally distinct from those of long GRBs based on the lack of SN associations and their occurrence in elliptical galaxies, I now turn to the question of what

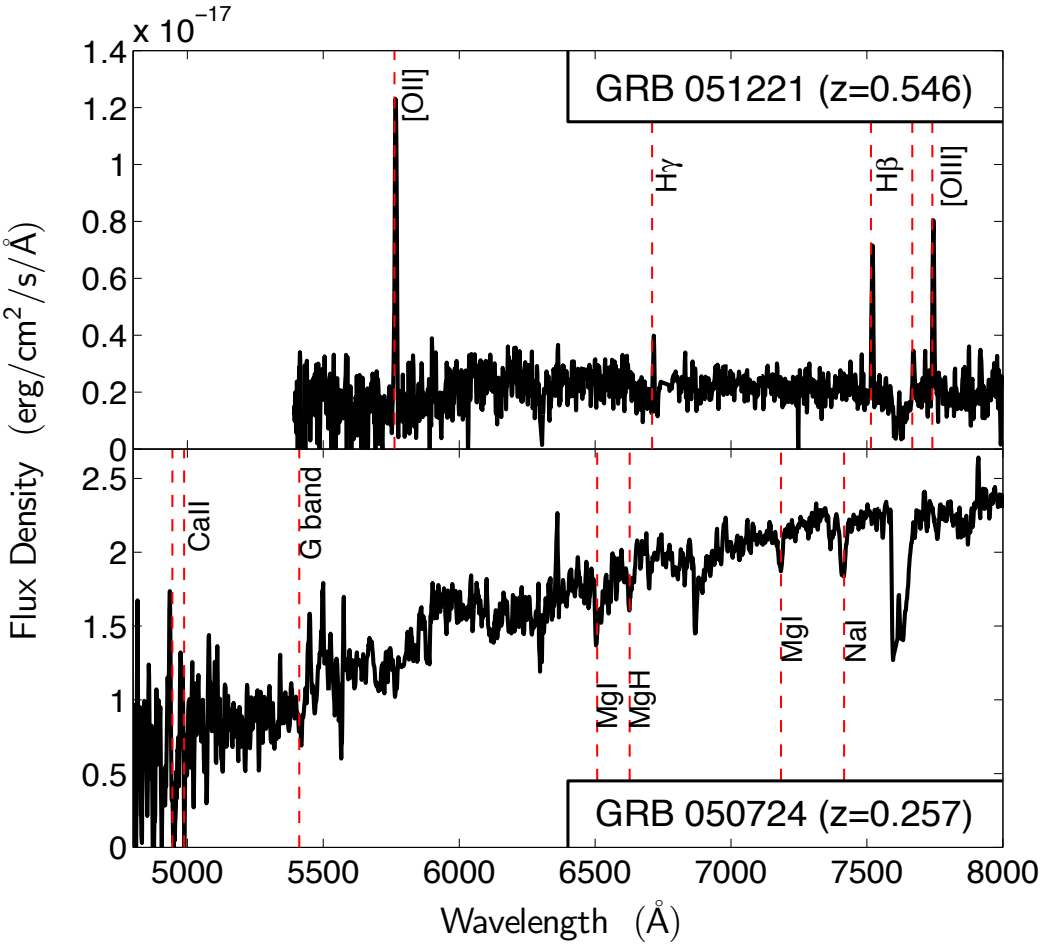

Figure 3:

Representative optical spectra of a late-type short GRB host galaxy exhibiting emission lines typical of star-forming galaxies (top: GRB 051221 at $z = 0.546$) and an early-type short GRB host galaxy with no evidence for on-going star formation activity (bottom: GRB 050724 at $z = 0.257$). Primary absorption and emission lines seen in the spectra are marked. The spectra are from Soderberg et al. (2006a) and Berger et al. (2005b), respectively.

the progenitors are, and what we can infer about their nature from the properties of the host galaxies. In general, the galaxy-scale and local environments of astrophysical transients provide critical insight into the nature of their progenitors, and this has been used to establish the progenitor properties of various supernova types and long GRBs (e.g., van den Bergh & Tammann 1991; Bloom, Kulkarni & Djorgovski 2002; Fruchter et al. 2006; Li et al. 2011). In this section I contrast the environments of short and long GRBs to further demonstrate their distinct origins, and compare the short GRB environments to field galaxy populations to establish some of the basic properties of their progenitors. I also provide a comparison with the hosts of Type Ia supernovae since these white dwarf thermonuclear explosions are known to arise from an evolved stellar population, with a broad range of delay times (Mannucci, Della Valle & Panagia 2006; Sullivan et al. 2006; Maoz et al. 2011), potentially similar to compact object binary mergers.

A summary of the key properties of short GRB host galaxies is provided in Table 2. The data are primarily drawn from Berger (2009), Leibler & Berger (2010), Berger (2010), Fong et al. (2013) and references therein.

6.1 The Redshift Distribution

At the most basic level, host galaxy associations are critical since essentially all short GRB redshifts to date (spectroscopic or photometric) have been obtained from the associated hosts (Figure 3; e.g., Fox et al. 2005, Berger et al. 2005b, Bloom et al. 2006, Berger 2009, 2011). The sole exceptions are GRB 090426 at $z = 2.609$ (Antonelli et al. 2009, Levesque et al. 2010a) and GRB 130603B at $z = 0.356$ (Cucchiara et al. 2013, de Ugarte Postigo et al. 2013) for which redshifts have been determined from afterglow absorption spectra. The bulk of the measured redshifts span $z \approx 0.1 - 1.3$, but it is likely that at least some of the faintest host galaxies (with optical magnitudes of $\approx 24 - 27$), which lack redshift measurements are located at $z \gtrsim 1$ (Berger et al. 2007a). The redshift distributions of short and long GRBs are shown in Figure 4. The median redshift of the short GRB population with established redshifts is $\langle z \rangle \approx 0.48$, while the addition of faint hosts that are presumably located at $z \gtrsim 1$ increases the median to $\langle z \rangle \approx 0.63$; the use of redshift upper limits from afterglow and/or host galaxy detections in optical bands (i.e., the lack of a Lyman break) leads to an upper bound on the median redshift of $\langle z \rangle \lesssim 0.83$. Since only 6 short bursts lack XRT positions despite rapid follow-up (§4), and hence the ability to identify hosts, the observed redshift distribution robustly represents the redshifts of *Swift* short GRBs. Assuming that the median redshift is $\langle z \rangle \sim 0.5 - 0.8$, and that it is not affected by the sensitivity threshold of *Swift* the resulting median progenitor age relative to the peak of the cosmic star formation history ($z \sim 3$) is $\tau \sim 5$ Gyr. Since the observed sample is almost certainly limited by the detector sensitivity, this inferred age can be used as an upper bound.

There is no clear trend between redshift and host galaxy type, with both early- and late-type hosts spanning the same redshift range with similar median values (Figure 4; Fong et al. 2013). Since the progenitors are expected to be systematically older in early-type galaxies and hence to occur at lower redshifts (e.g., Zheng & Ramirez-Ruiz 2007), the similar redshift distributions for early- and late-type galaxies suggest that the *Swift* sensitivity threshold indeed plays a role in the redshift distribution. The short GRB population is substantially more local than *Swift* long GRBs, which extend to $z \sim 9.4$ (Cucchiara et al. 2011) with a median value of $\langle z \rangle \approx 2$ (Berger et al. 2005a, Jakobsson et al. 2006). This is partly a reflection of the lower energy scale of short GRBs, but also a result of longer delay times between star formation activity and the occurrence of short GRBs.

6.2 Demographics

An additional constraint on the progenitors and their age distribution is provided by the demographics of the host galaxy sample. While long GRBs only occur in star-forming galaxies (Bloom, Kulkarni & Djorgovski 2002; Fruchter et al. 2006; Wainwright, Berger & Penprase 2007), as expected for young massive star progenitors, short GRBs occur in a mixed population of early-type and star-forming galaxies (Berger et al. 2005b, Fox et al. 2005, Bloom et al. 2006, Fong et al. 2011, 2013) indicating that their progenitors span a wide range of ages. More broadly, since at $z \sim 0 - 1$, the redshift range relevant for the existing short GRB population, a roughly equal fraction of the cosmic stellar mass density is in early-type and star-forming galaxies (Bell et al. 2003, Ilbert et al. 2010), an exclusively old progenitor population (i.e., tracking stellar mass alone) will also exhibit an equal fraction of early- and late-type hosts. On the other hand, a progenitor population skewed to relatively short delay times relative to star formation activity (tens to hundreds of Myr) will exhibit an over-abundance of late-type hosts due to their recent star formation (Zheng & Ramirez-Ruiz

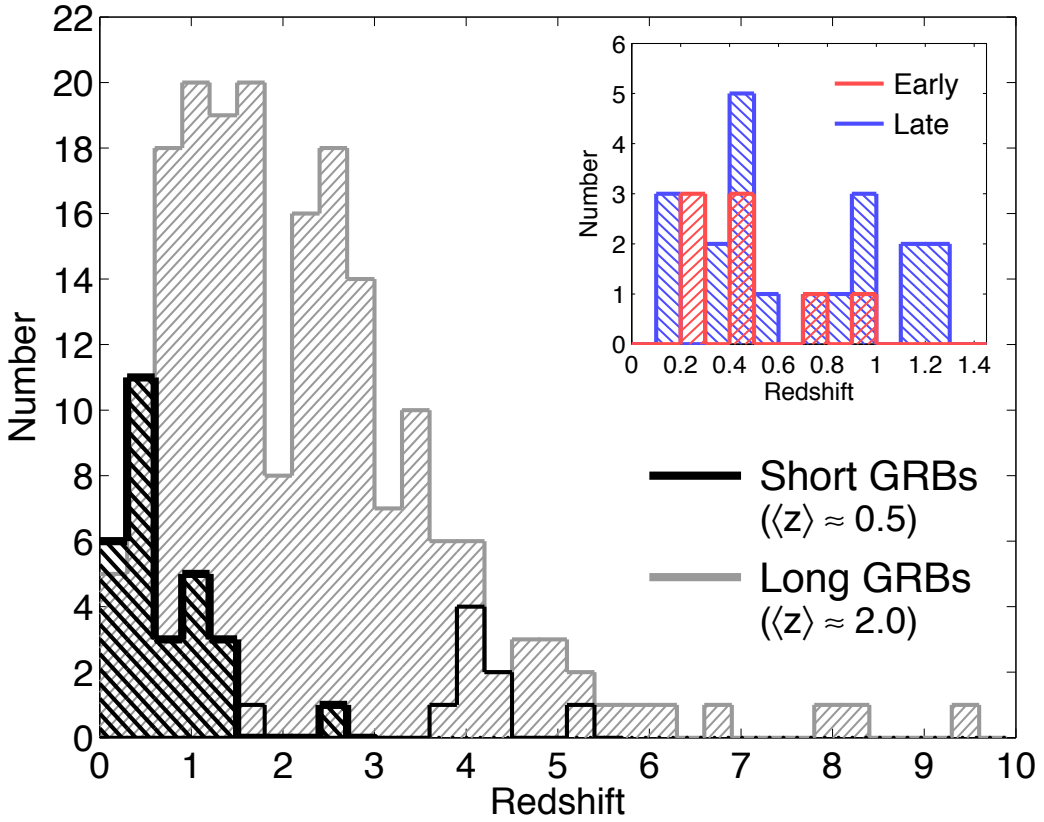

Figure 4:

The redshift distribution of short GRBs (black) and long GRBs (gray). The open histogram marks redshift upper limits based on the lack of a Lyman-α break in afterglow and/or host galaxy optical detections. The inset shows the redshift distribution of short GRBs separated by host galaxy type, which exhibits no discernible difference between early-type (red) and late-type (blue) hosts.

2007; O'Shaughnessy, Belczynski & Kalogera 2008). Studies of the first few short GRB host galaxies from 2005, led several groups to conclude that early-type galaxies dominate the sample at a ratio of about 2:1, and that the progenitors are therefore exceedingly old, with a characterstic age of $\sim 5 - 10$ Gyr (Prochaska et al. 2006, Nakar 2007, Gal-Yam et al. 2008).

A different conclusion is reached by Fong et al. (2013) in a study of the short GRB host galaxy demographics using a much larger sample of 36 events. These authors find that regardless of various cuts on the sample, only $\sim$ 20% of the hosts are early-type galaxies (Figure 5; see also Leibler & Berger 2010). This result is robust when considering only events with sub-arcsecond positions, when including those with XRT positions, or when restricting the sample according to the duration-hardness analysis of Bromberg et al. (2013). The dominance of late-type galaxies indicates that the short GRB rate does not depend on stellar mass alone, and is instead influenced by recent star formation activity. Comparing the observed relative fraction of early- and late-type hosts to the theoretical predictions of Zheng & Ramirez-Ruiz (2007) leads to a power law delay time distribution of $P(\tau) \propto \tau^{-1}$.

An additional clue to the role of star formation in the short GRB rate is the identification of two short GRB hosts as luminous and ultra-luminous infrared galaxies (U/LIRG). GRB 100206A is associated with

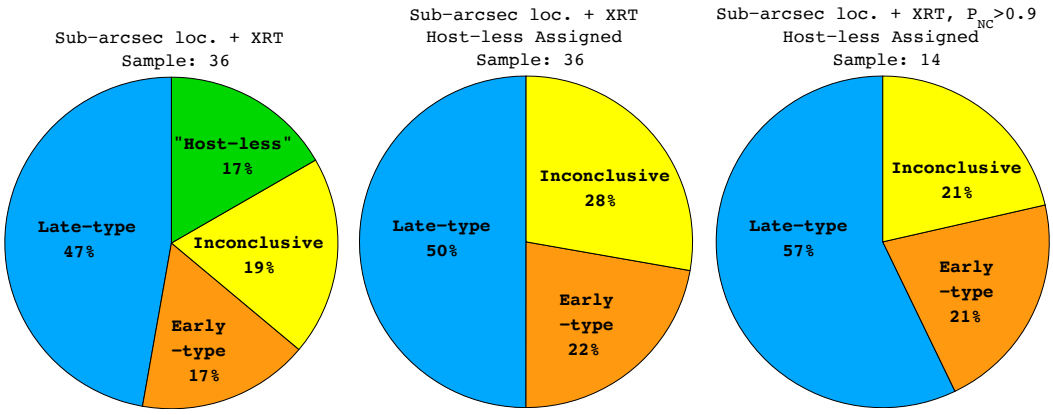

Figure 5:

Demographics of the galaxies hosting short GRBs. *Left:* A breakdown into late-type (blue), early-type (orange), host-less (green), and inconclusive (yellow) for all identified hosts based on sub-arcsecond positions and *Swift*/XRT positions (Table 2). *Middle:* Same as the left panel, but with the host-less events assigned to the other categories based on the galaxies with the lowest probability of chance coincidence in each case (Berger 2010, Fong & Berger 2013). *Right:* Same as the middle panel, but for short GRBs with a probability of a non-collapsar origin of $P_{\rm NC} \gtrsim 0.9$ based on the analysis of Bromberg et al. (2013). Regardless of the sample selection, late-type galaxies dominate the host sample. This indicates that star formation activity plays a role in the short GRB rate. Adapted from Fong et al. (2013).

a dusty LIRG at $z = 0.407$ (Perley et al. 2012), while GRB 120804A is associated with a dusty ULIRG at a photometric redshift of $z \approx 1.3$ (Berger et al. 2013). The expected U/LIRG fraction for a progenitor population that tracks stellar mass alone is $\sim 1\%$ (Caputi et al. 2006), while for progenitors that track only star formation it is $\sim 25\%$ (Le Floc'h et al. 2005, Caputi et al. 2007). Since the observed fraction in the short GRB sample is $\sim 5 - 10\%$ percent, it suggests that the progenitor population is influenced by both stellar mass and star formation activity, indicative of a broad age distribution.

6.3 Stellar Masses and Stellar Population Ages

The distribution of host galaxy stellar masses and stellar population ages can also shed light on the progenitor age distribution. The stellar masses inferred from modeling of the host optical/near-IR spectral energy distributions with single stellar population models span $M_* \approx 10^{8.5-11.8}$ M$_\odot$. The median for the full sample is $\langle M_* \rangle \approx 10^{10.0}$ M$_\odot$, while for the star-forming hosts alone it is $\langle M_* \rangle \approx 10^{9.7}$ M$_\odot$ (Figure 6; Leibler & Berger 2010). The stellar masses of long GRB hosts are substantially lower, with a median value of about $10^{9.2}$ M$_\odot$ (Savaglio, Glazebrook & Le Borgne 2009; Leibler & Berger 2010). This indicates that even the star-forming hosts of short GRBs are typically more massive than the hosts of long GRBs, pointing to a more dominant role of stellar mass in determining the rate of short GRBs.

A comparison to the mass function of field galaxies is even more illuminating. In Figure 6 I compare the cumulative distributions of stellar masses for the early- and late-type hosts of short GRBs with the expected distributions for mass-selection from the field galaxy mass function (Bell et al. 2003, Ilbert et al. 2010). For a progenitor population that tracks stellar mass alone, we expect that the observed stellar mass distribution of short GRB hosts will closely track the mass-weighted mass distribution of field galaxies. While this is indeed the case for the early-type mass function, the late-type hosts of short GRBs have systematically lower stellar masses than expected from mass-selection alone (Leibler & Berger 2010). This indicates that

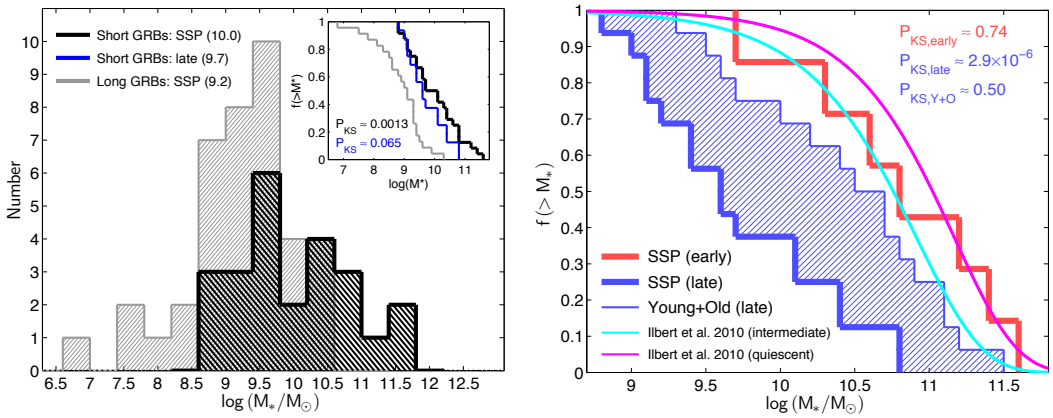

Figure 6:

Left: Histogram of host galaxy stellar masses for short GRBs (black) and long GRBs (gray). Median values for each population (and separately for short GRB late-type hosts) are quoted in parentheses. The inset shows the cumulative distributions along with K-S probabilities that the short and long GRB hosts are drawn from the same parent population. *Right:* Comparison of the cumulative distributions of stellar masses for late-type (blue) and early-type (red) short GRB hosts to the expected distributions for a mass-weighted selection from the field galaxy mass function (cyan and magenta lines, respectively). The resulting K-S probabilities indicate that the early-type hosts are consistent with pure mass selection, while the late-type hosts have lower than expected stellar masses. This indicates that star formation activity plays a role in the short GRB rate. Adapted from Leibler & Berger (2010).

in late-type galaxies the short GRB rate per unit stellar mass is higher than in early-type galaxies, due to the presence of star formation activity. This agrees with the observed over-abundance of late-type galaxies in the short GRB host population. Quantitatively, for a range of host stellar mass determinations, the short GRB rate per unit stellar mass in late-type galaxies is about 2 – 9 times higher than in early-type galaxies (Leibler & Berger 2010).

The difference between short and long GRB hosts is also evident in the distribution of stellar population ages. The distribution for short GRB hosts spans a wide range, from a few tens of Myr to about 4 Gyr, with a median value of $\langle \tau_* \rangle \approx 0.25$ Gyr, while the long GRB hosts have a median stellar population age of $\langle \tau_* \rangle \approx 60$ Myr (Figure 7; Leibler & Berger 2010). Coupled with the stellar mass distribution discussed above, this indicates that the short GRB rate per 10^{10} $M_\odot$ in late-type hosts (with $\langle \tau_* \rangle \approx 0.15$ Gyr) and early-type hosts (with $\langle \tau_* \rangle \approx 1.6$ Gyr) is 0.7 and 0.075, respectively, leading to a power law delay time distribution of $P(\tau) \propto \tau^{-0.9}$, in good agreement with the distribution inferred from the early- to late-type fraction. Similarly, separating the sample into galaxies with stellar population ages younger and older than ~ 0.3 Gyr I find that the typical ages are about 0.1 and 1 Gyr, respectively, with a resulting rate per 10^{10} $M_\odot$ of 0.8 and 0.12, respectively, leading to a delay time distribution of $P(\tau) \propto \tau^{-0.8}$. The inferred delay time distribution is in good agreement with that of Galactic neutron star binaries with a power law index of $n \sim -1$ (e.g., Piran 1992).

6.4 Specific Star Formation Rates

The interplay of stellar mass and star formation activity in short GRB hosts is also evident in the distribution of specific star formation rates (SSFR), relative to both long GRB hosts and field star-forming galaxies. In

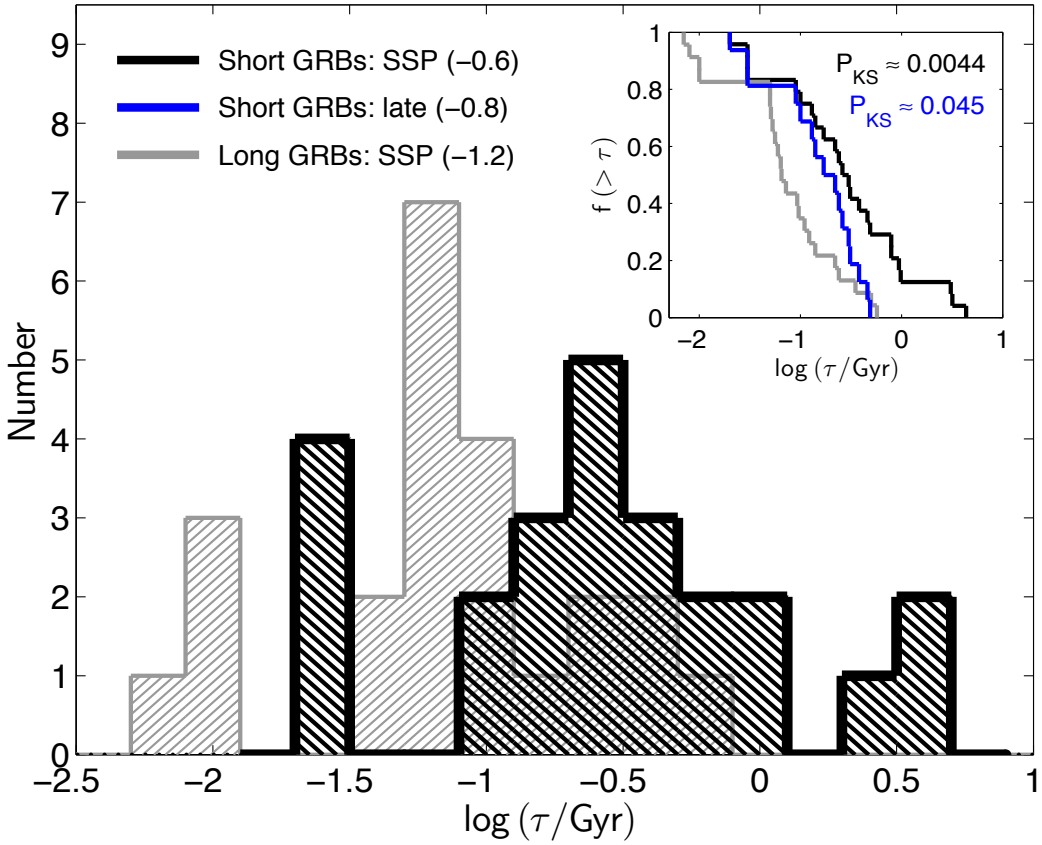

Figure 7:

Histogram of host galaxy stellar population ages for short GRBs (black) and long GRBs (gray). Median values for each population (and separately for short GRB late-type hosts) are quoted in parentheses. The inset shows the cumulative distributions along with K-S probabilities that the short and long GRB hosts are drawn from the same parent population. The results indicate that short GRB hosts, even the late-type galaxies, have systematically older stellar population than long GRB hosts. Adapted from Leibler & Berger (2010).

Figure 8 I plot the star formation rates (SFR) as a function of rest-frame optical B-band luminosity (L_B) for short and long GRB hosts. For the short GRB hosts the luminosities span $L_B \approx 0.1 - 5\ L_B^*$, and the star formation rates span $\lesssim 0.1$ to ≈ 5 M$_\odot$ yr^{-1}, with the upper limits corresponding to the early-type hosts; here L_B^* is the characteristic luminosity in the Schechter function. However, while both short and long GRB hosts exhibit a clear trend between SFR and L_B (at least for the star-forming short GRB hosts), the overall normalization (i.e., the SSFR) is lower for the short GRB hosts by about a factor of 5, with $\langle \mathrm{SFR}/L_B \rangle \approx 2$ M$_\odot$ yr^{-1} L_B^*. The K-S test gives a p-value of 0.003 for the null hypothesis that the short and long GRB hosts are drawn from a galaxy population with the same underlying distribution of SSFR.

Since the specific star formation rate is the inverse of the characteristic timescale to build up a galaxy's stellar mass, the lower values for short GRB hosts indicates that while the majority are star-forming galaxies, their star formation activity is more moderate, and has a longer characteristic timescale than in long GRB hosts. Thus, the massive star progenitors of long GRBs track recent star formation (tens of Myr), while the progenitors of short GRBs track star formation with a delay of hundreds of Myr to several Gyr.

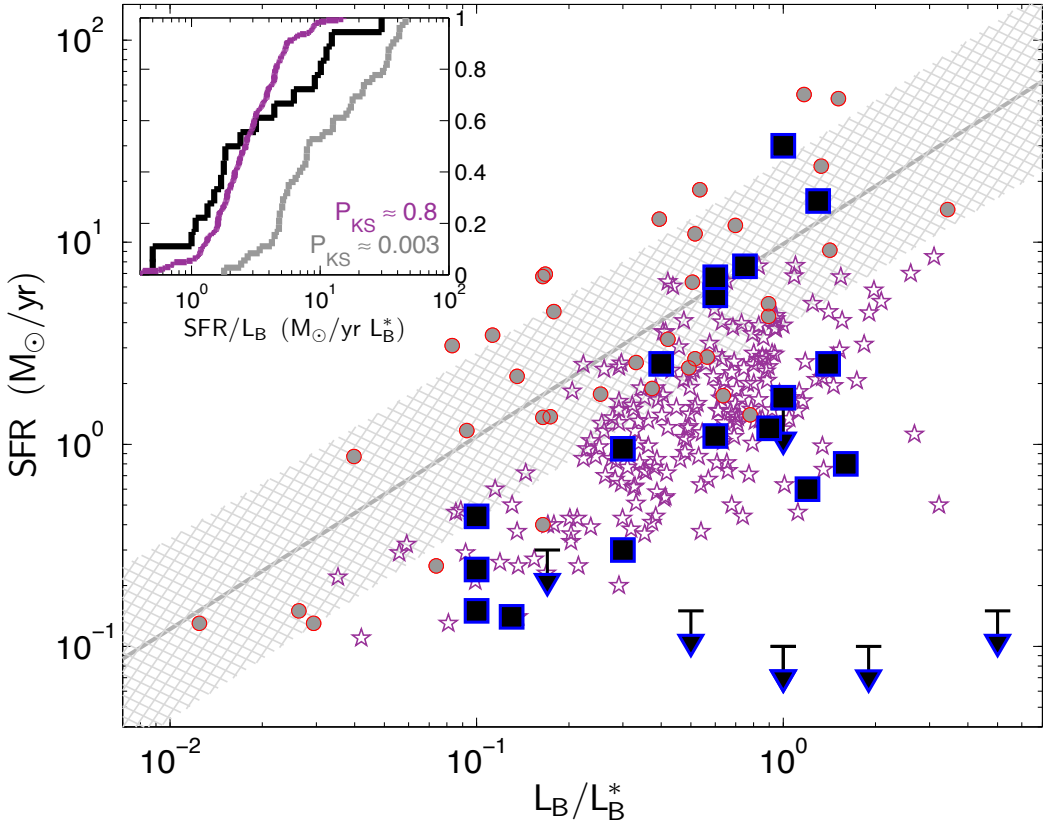

Figure 8:

Star formation rate as a function of rest-frame *B*-band luminosity for the host galaxies of short GRBs (squares), long GRBs (circles), and field star-forming galaxies at similar redshifts to short GRB hosts (pentagrams; Kobulnicky & Kewley 2004). The gray line and hatched region delineate the correlation (and standard deviation) for long GRB host galaxies. Short GRB host galaxies have substantially lower star formation rates as a function of luminosity than long GRBs hosts (i.e., they have lower specific star formation rates), but they closely track the field galaxy population (inset).

Moreover, the short GRB hosts clearly track the distribution of specific star formation rates in field galaxies of similar luminosities (Kobulnicky & Kewley 2004), with a K-S *p*-value of 0.8, indicating that short GRBs select galaxies from the general field sample.

6.5 Metallicities

Short GRB hosts span a wide range of metallicities, with $12 + \log(\mathrm{O/H}) \approx 8.5 - 9.2$, and a median value of $\langle 12 + \log(\mathrm{O/H}) \rangle \approx 8.8 \approx 1\ \mathrm{Z}_{\odot}$ (Figure 9; Berger 2009, D'Avanzo et al. 2009). In addition, the measured metallicities track a positive trend with host galaxy luminosity, as generally observed for field galaxies (Tremonti et al. 2004). The metallicities of short GRB hosts are significantly higher than those of long GRB hosts, for which the median value is $\langle 12+\log(\mathrm{O/H}) \rangle \approx 8.3$ (Stanek et al. 2006, Modjaz et al. 2008, Levesque et al. 2010b). On the other hand, short GRB hosts track the metallicity distribution of field star-forming galaxies at similar redshifts and with similar luminosities (Kobulnicky & Kewley 2004). Combining the

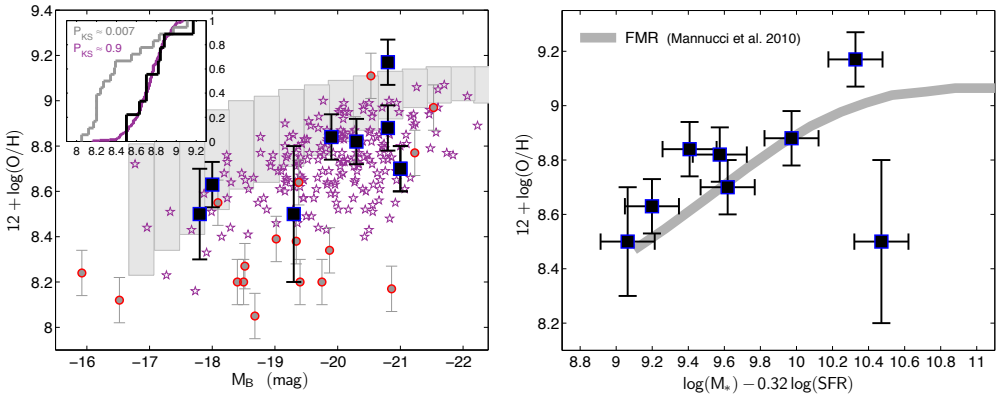

Figure 9:

Left: Metallicity as a function of host galaxy rest-frame B-band luminosity for short GRBs (squares), long GRBs (circles), field galaxies at similar redshifts to short GRB hosts (pentagrams; Kobulnicky & Kewley 2004), and the Sloan Digital Sky Survey luminosity-metallicity relation (Tremonti et al. 2004). Short GRB host galaxies have higher metallicities than long GRBs hosts, but closely track the luminosity-metallicity relation for the field galaxy population (inset). Adapted from Berger (2009). *Right:* Comparison of short GRB hosts to the fundamental metallicity relation of star-forming galaxies (grey line; Mannucci et al. 2010), which uses a combination of stellar mass and star formation rate, $\log(M_*) - 0.32\log(\mathrm{SFR})$. The short GRB hosts follow the relation along a wide span of the combined stellar mass and star formation parameter.

host stellar masses and star formation rates according to the fundamental metallicity relation of Mannucci et al. (2010), $\mu = \log(M_*) - 0.32\log(\mathrm{SFR})$, I find that short GRB hosts track the relation for field galaxies (Figure 9). Thus, while the sample of short GRB hosts with metallicities is still small, it demonstrates that the hosts follow the relations for field galaxies, but are clearly distinct from long GRB hosts. Based on this result, it does not appear that short GRB progenitors are directly affected by metallicity.

6.6 Galaxy Clusters

The first short GRB with an afterglow detection, GRB 050509b, was most likely associated with a galaxy cluster at $z = 0.225$ (Gehrels et al. 2005, Pedersen et al. 2005, Bloom et al. 2006, Dahle et al. 2013). This association led to several investigations of galaxy clusters hosting short GRBs. Ghirlanda et al. (2006) cross-correlated BATSE short GRBs with catalogs of X-ray selected clusters to $z \sim 0.45$ and claim an association at a 2σ confidence level on an angular scale of $\lesssim 3^\circ$. Berger et al. (2007b) searched for galaxy clusters in association with 4 *Swift* short GRBs using multi-object optical spectroscopy, and in association with 15 *Swift* short GRBs using stacked X-ray observations from *Swift*/XRT. The search yielded a galaxy cluster at $z = 0.165$, based on redshift clustering and diffuse X-ray emission, in the field of the short GRB 050911 (BAT-only position) with a probability of chance coincidence of 0.1 – 1%. The limit on galaxy clusters in the fields of the remaining bursts is $M \lesssim 5 \times 10^{13}$ M$_\odot$ based on the lack of diffuse X-ray emission (Berger et al. 2007b).

Since the stellar populations in galaxy clusters are systematically older than in field galaxies, the fraction of short GRBs in clusters can be used as an indicator of the age distribution (Shin & Berger 2007). At present, the fraction of short GRBs in clusters appears to be $\sim$ 10% (Berger et al. 2007b), at the low end of the fraction of cosmic stellar mass in clusters of about 10 – 20% (Fukugita, Hogan & Peebles 1998; Eke et al. 2005). There is therefore no indication from galaxy cluster associations for an exceedingly old

progenitor population.

6.7 Comparison to the Host Galaxies and Delay Time Distribution of Type Ia Supernovae

Type Ia SNe result from the thermonuclear explosions of CO white dwarfs that approach the Chandrasekhar mass in single- or double-degenerate binary systems. Unlike core-collapse SNe, Type Ia events are found in both early- and late-type galaxies (e.g., van den Bergh 1990, van den Bergh & Tammann 1991, Li et al. 2011), reflecting the wide range of timescales for the accretion or merger process that eventually leads to a supernova. As a result, the environments and delay time distribution of Type Ia SNe provide a useful comparison to short GRBs, particularly in the context of compact object merger progenitors. Mannucci et al. (2005) found that for nearby Type Ia SNe, about 30% occur in E/S0 galaxies, while the remaining events occur in spirals (63%) and irregular galaxies (7%). This distribution is similar to the short GRB demographics (Figure 5; Fong et al. 2013). The Type Ia SNe also exhibit a clear increase in the rate per unit stellar mass from early- to late-type galaxies, ranging from about 0.044 (E/SO) to 0.065 (Sa/b) to 0.17 (Sc/d) per 10^{10} $M_\odot$ per century (Mannucci et al. 2005), similar to the inference for short GRBs (§6.3; Leibler & Berger 2010).

The Type Ia SN rate as a function of galaxy type and properties (stellar mass, star formation rate) led Mannucci, Della Valle & Panagia (2006) and Sullivan et al. (2006) to propose a bimodal or two-component delay time distribution with a prompt population ($\sim 0.1 - 0.3$ Gyr) whose rate depends primarily on the host galaxy star formation rate, and a delayed population (~ 3 Gyr with a broad range) whose rate depends on the host galaxy stellar mass (see also Maoz & Badenes 2010, Maoz et al. 2011). Indeed, Sullivan et al. (2006) find that the Type Ia SN rate per unit stellar mass increases by at least an order of magnitude with higher SSFR (over the range of $0.02 - 1$ Gyr^{-1}). They conclude that the Type Ia SN rate per year is about $5 \times 10^{-4}\,(10^{10}\,M_\odot)^{-1} + 4 \times 10^{-4}\,(M_\odot/\mathrm{yr})^{-1}$. More recent work on the delay time distribution point instead to a continuous, rather than bimodal distribution, following a power law of about $\tau^{-1.1}$ (Maoz, Mannucci & Brandt 2012). Thus, the results for short GRBs and Type Ia SNe exhibit close similarities, in terms of both the distribution of host galaxy types, and the enhanced rate in late-type galaxies, with a typical delay of $\sim 0.1 - 0.3$ Gyr. This indicates that short GRBs and Type Ia SN progenitors share a similar delay time distribution.

7 The Locations of Short GRBs in and Around Their Host Galaxies

As demonstrated in the previous section, the properties of short GRB hosts help to reveal the short GRB redshift distribution, to shed light on the progenitor age distribution, and to establish the differences between long and short GRB progenitors. Studies of short GRB sub-galactic environments can further this insight by providing information on their spatial association (or lack thereof) with star formation or stellar mass. Similar studies of long GRBs have established that their projected spatial offsets relative to the host galaxy centers follow the expected distribution for star formation in exponential disk galaxies, with a median value of $\approx 1\ r_e$ (Bloom, Kulkarni & Djorgovski 2002), where r_e is the host galaxy half-light radius. Moreover, studies of the rest-frame UV brightness at the locations of long GRBs relative to the overall UV light distribution of the hosts have shown that long GRBs tend to occur in unusually bright star-forming regions, significantly more so than core-collapse SNe (Fruchter et al. 2006, Svensson et al. 2010).

What is the expectation for the locations of short GRBs? As I already demonstrated from the lack of SN associations, the occurrence of some short GRBs in elliptical galaxies, and the systematically older stellar population of short GRB hosts compared to long GRB hosts, short GRBs are not expected to coincide with young star-forming environments. On the other hand, based on the distribution of host galaxy stellar

masses, and the host galaxy demographics I concluded that short GRB progenitors have a broad delay time distribution and that their rate is influenced in part by star formation activity (i.e., some systems have delays of only $\sim$ 0.1 Gyr). In addition, one of the key predictions of the compact object merger model is systemic natal kicks that may lead to substantial offsets between the birth and explosion sites of these systems. Indeed, offset distributions predicted from population synthesis models indicate a typical median projected offset of 5 – 7 kpc, with about 10 – 25% of events occurring at offsets of $\gtrsim$ 20 kpc, and up to $\sim$ 10% extending beyond 100 kpc (Bloom, Sigurdsson & Pols 1999; Fryer, Woosley & Hartmann 1999; Perna & Belczynski 2002; Belczynski et al. 2006). Observationally, short GRBs at such large offsets will appear to be "host-less" since their projected locations will extend much beyond the visible extent of typical galaxies. A progenitor population of young magnetars, on the other hand, will exhibit a spatial coincidence with star-forming regions and offsets that track an exponential disk distribution. Delayed magnetars will not track young star-forming regions, but will track the overall light distribution of their hosts due to the lack of natal kicks. Finally, a dominant population of dynamically formed NS-NS binaries in globular clusters will track the overall globular cluster distribution around galaxies, extending to tens of kpc (Salvaterra et al. 2010).

7.1 The Offset Distribution

To determine the locations of short GRBs relative to their host centers (offsets) and relative to the underlying light distribution in the rest-frame optical (stellar mass) and UV (star formation) requires the high angular resolution and superior depth of the *HST*. A comprehensive study based on *HST* observations of 32 short GRB host galaxies was carried out by Fong, Berger & Fox (2010) and Fong & Berger (2013); see also Church et al. (2011). The *HST* data, combined with ground-based optical afterglow observations (and in two cases, *Chandra* observations), provide accurate offsets at the sub-pixel level, and reveal the broad distribution shown in Figure 10. The projected offsets span 0.5 – 75 kpc with a median of about 5 kpc. This is about 4 times larger than the median offset for long GRBs (Bloom, Kulkarni & Djorgovski 2002), and about 1.5 times larger than the median offsets of core-collapse and Type Ia supernovae (Prieto, Stanek & Beacom 2008). In addition, while no long GRBs, and only $\sim$ 10% of SNe have offsets of $\gtrsim$ 10 kpc, the fraction of short GRBs with such offsets is about 25%. For offsets of $\gtrsim$ 20 kpc, the fraction of short GRBs is about 10%, but essentially no SNe exhibit such large offsets.

Equally important, the observed offset distribution is in remarkable agreement with the population synthesis predictions for compact object mergers, particularly the fraction of events with large offsets. I note that the observed distribution is mainly based on short GRBs with optical afterglows, which may be skewed on average to higher circumburst densities, and hence to smaller offsets. It is therefore conceivable that events with only XRT or BAT positions (14 and 6 *Swift* short GRBs, respectively; §4), whose precise offsets cannot be ascertained, in reality have systematically larger offsets than a few kpc.

The subset of short GRBs with offsets of $\gtrsim$ 20 kpc require specific mention since these offsets are larger than the typical visible extent of galaxies. These bursts lack coincident host galaxies at angular separations of $\lesssim 1''$ in deep optical and near-IR *HST* observations, and have been termed "host-less". Systematic studies of the host-less bursts, their afterglows, and environments was carried out by Berger (2010) and Fong & Berger (2013), although individual cases were noted previously (Bloom et al. 2007, Stratta et al. 2007, Perley et al. 2009). A few examples based on deep *HST* near-IR observations are shown in Figure 11. In all cases there is a clear absence of coincident galaxies to optical limits of $\gtrsim$ 27 mag and near-IR limits of $\gtrsim$ 26 mag (Berger 2010, Fong & Berger 2013). Any undetected coincident host galaxies with properties similar to the known host galaxy sample (Figure 8) will have to reside at $z \gtrsim 3$ to evade detection, leading to an unexpected bimodal redshift distribution (Figure 4; Berger 2010, Fong & Berger 2013). Similarly, if we

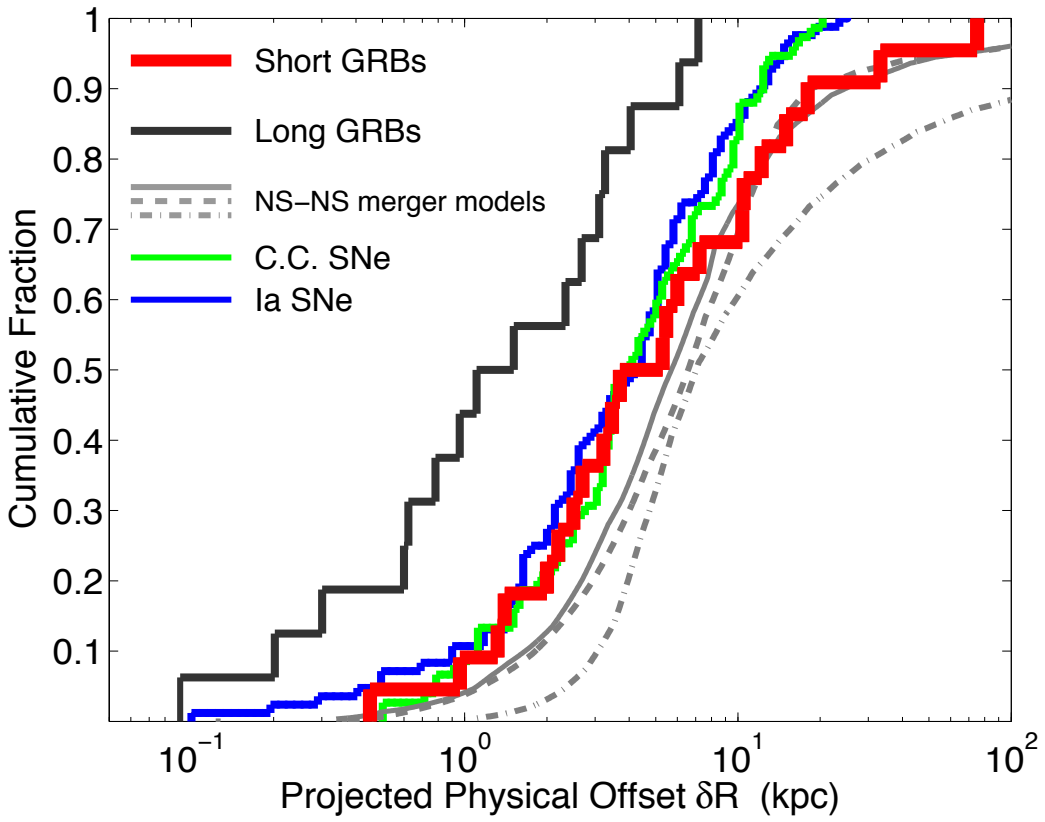

Figure 10:

Cumulative distribution of projected physical offsets for short GRBs with sub-arcsecond positions (red; Fong, Berger & Fox 2010; Fong & Berger 2013), compared to the distributions for long GRBs (black; Bloom, Kulkarni & Djorgovski 2002), core-collapse SNe (green; Prieto, Stanek & Beacom 2008), Type Ia SNe (blue; Prieto, Stanek & Beacom 2008), and predicted offsets for NS-NS binaries from population synthesis models (grey; Bloom, Sigurdsson & Pols 1999; Fryer, Woosley & Hartmann 1999; Belczynski et al. 2006). Short GRBs have substantially larger offsets than long GRBs, and match the predictions for compact object binary mergers. From Fong & Berger (2013).

impose a similar redshift range for any undetected hosts, then the resulting host luminosities will be $\lesssim 0.01$ L^*, at least an order of magnitude below the known host population (Figure 8), making this explanation equally unlikely.

A more likely alternative is that these bursts are associated with nearby galaxies in their field, with resulting projected offsets of tens of kpc, as expected for a subset of compact object mergers. This possibility can be assessed by analyzing the probabilities of chance coincidence for field galaxies in the *HST* images. The probability for a given galaxy of brightness m to be located at a separation δR from a short GRB position is given by (Bloom, Kulkarni & Djorgovski 2002; Berger 2010):

$$P_{\rm cc} = 1 - e^{-\pi(\delta R)^2 \Sigma(\leq m)}, \quad (1)$$

where the galaxy number counts are given by $\Sigma(\leq m) = 1.3 \times 10^{0.33(m-24)-2.44}$ arcsec^{-2} (Hogg et al. 1997, Beckwith et al. 2006). Applying this approach, Berger (2010) and Fong & Berger (2013) find that the host-less short GRBs exhibit nearby field galaxies with low chance-coincidence probabilities of $P_{\rm cc} \approx$ few

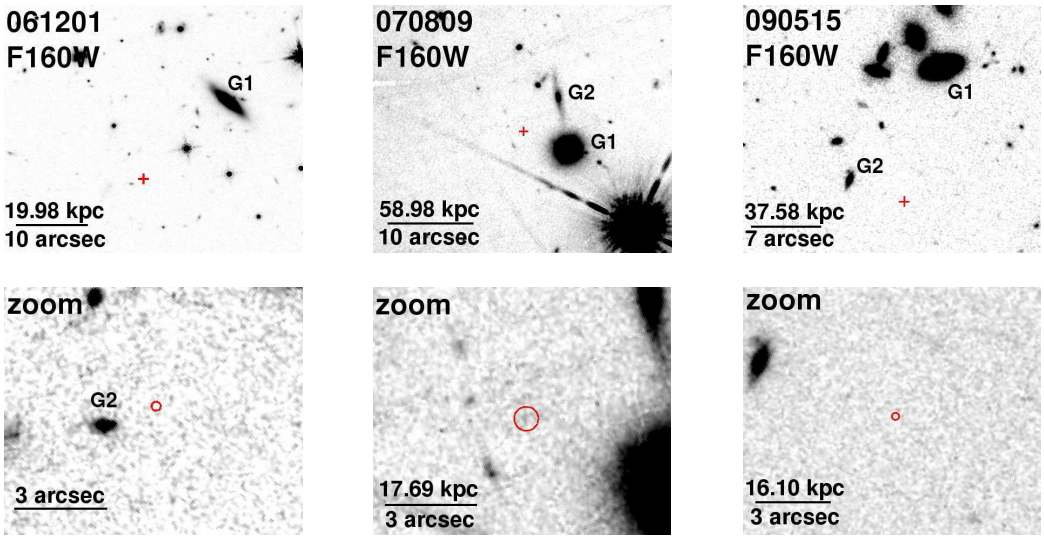

Figure 11:

Hubble Space Telescope Wide-Field Camera 3 images of the locations of three short GRBs with sub-arcsecond positions and no coincident host galaxies (host-less bursts). In each case the top panel shows a wide field and the bottom panel is zoomed on the GRB location (red circle). The galaxies marked "G1" and "G2" in represent the objects with the lowest and second lowest probabilities of chance coincidence in each field. The magnitude limits at the GRB positions are $m_{\rm F160W} \gtrsim 26$ mag, ruling out the presence of galaxies typical of short GRB hosts at $z \lesssim 3$. Adapted from Fong & Berger (2013).

percent, indicating a likely association with resulting projected separations of $\sim 10''$. A similar analysis for short GRBs with coincident host galaxies does not reveal a similar effect (Berger 2010), demonstrating that the offset galaxies with a low probability of chance coincidence in the fields of host-less short GRBs are indeed the hosts. While a definitive association will benefit from independent redshift measurements for the afterglow and galaxy, the observed excess of galaxies at moderate separations is highly indicative of a progenitor population capable of occurring at large offsets. The redshifts and properties of these likely host galaxies reveal that they are similar to the known population of short GRB hosts, and the resulting projected physical offsets are tens of kpc (Berger 2010).

While the projected physical offsets are already indicative of compact object mergers, it is important to account for the range of host galaxy sizes, and any systematic trends in these sizes between the various GRB and SN populations. This can be accomplished by normalizing the projected offsets in units of host galaxy effective radii. Short GRB hosts tend to be larger than long GRB hosts, commensurate with their larger luminosities and stellar masses (Fong, Berger & Fox 2010; Fong & Berger 2013). The cumulative distributions of host-normalized offsets for short GRBs, long GRBs, core-collapse SNe, and Type Ia SNe is shown in Figure 12. The median host-normalized offsets for long GRBs and for both Type Ia and core-collapse SNe is $\delta R/r_e \approx 1$ (Fong & Berger 2013), as expected from the definition of the half-light radius and the fact that long GRB and SN progenitors do not migrate from their birth-sites. Short GRBs, on the other hand, have a median offset of $\delta R/r_e \approx 1.5$, with 20% of the population occurring at $\delta R/r_e \gtrsim 5$ (compared to only a few percent of stellar light) , and only 20% of the bursts located at $\delta R/r_e \lesssim 1$. A K-S test relative to the Type Ia SN population yields a p-value of about 10^{-3} for the null hypothesis that both populations are drawn from the same underlying distribution of host-normalized offset (Fong & Berger 2013). Thus, the offset distribution of short GRBs indicates that they are located at larger distances than expected for a

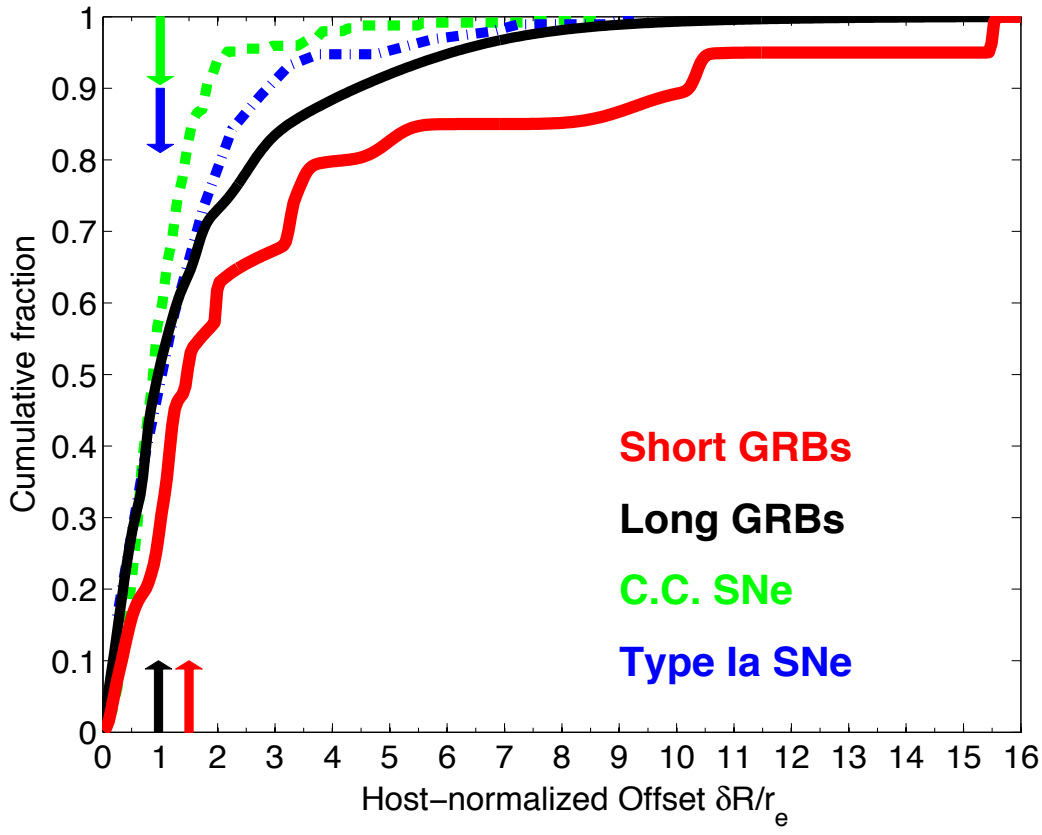

Figure 12:

Cumulative host-normalized offset distributions for short GRBs, long GRBs, core-collapse SNe, and Type Ia SNe (colors are as in Figure 10). The host-normalized offsets are determined relative to the effective radius of each host, and the cumulative distributions take into account the uncertainty in each offset measurement. The distributions for core-collapse SNe are from Kelly & Kirshner (2012), while those for Type Ia SNe are from Galbany et al. (2012). The arrows mark the median host-normalized offset for each type of transient, with long GRBs and SNe matching the expected value of about 1 r_e. Short GRBs, on the other hand, have a median offset of about 1.5 r_e and only 20% of events occur within 1 r_e. From Fong & Berger (2013).

progenitor population that radially tracks stellar light, particularly when accounting for their host galaxy sizes. The offsets are larger than even those of Type Ia SNe, but are in good agreement with compact object population synthesis predictions that include kicks.

7.2 Relation to the Underlying Ultraviolet and Optical Light Distribution

Independent of the offset distribution, an additional test of the progenitor population is the spatial correlation (or lack thereof) between short GRBs and the underlying light distribution of their hosts. In particular, for progenitors that track star formation activity with a short delay (i.e., massive stars) we expect direct spatial correlation with the underlying rest-frame UV light (as found for long GRBs and core-collapse SNe; Fruchter et al. 2006; Kelly, Kirshner & Pahre 2008; Svensson et al. 2010; Kelly & Kirshner 2012).

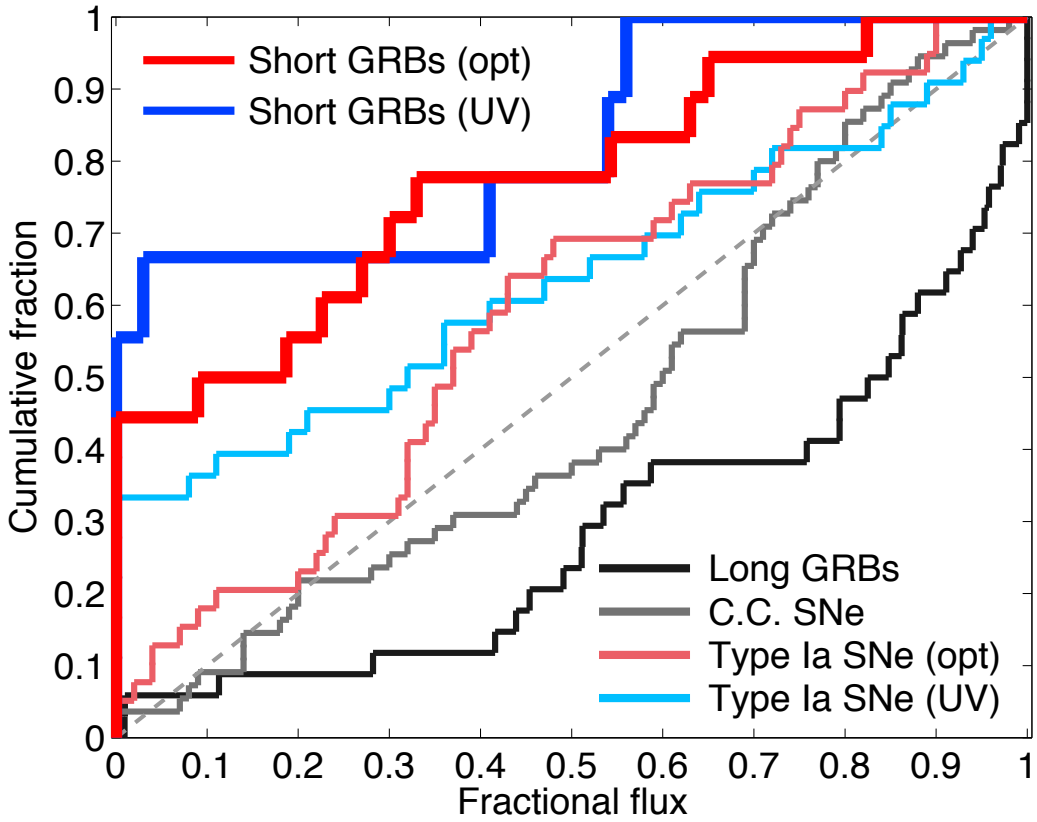

Figure 13:

Cumulative distribution of the fractional flux at short GRB locations relative to the underlying light distributions of their hosts. Shown are the distributions for rest-frame optical (red) and rest-frame UV (blue) from *HST* observations of short GRBs with sub-pixel positions (Fong, Berger & Fox 2010; Fong & Berger 2013). Also shown are the distributions for long GRBs (UV: black; Fruchter et al. 2006, Svensson et al. 2010), Type Ia SNe (UV: light blue; optical: pink; Wang et al. 2013), and core-collapse SNe (UV: grey; Svensson et al. 2010). The diagonal dashed line marks the expected distribution for a population that linearly tracks the underlying stellar light. Long GRBs and core-collapse SNe strongly track UV light (star formation), while Type Ia SNe track optical light (stellar mass). Short GRBs, on the other hand, exhibit a poor correlation with UV or optical light, indicating that the progenitors migrate from their birth-sites to the eventual explosion sites. From Fong & Berger (2013).

On the other hand, an old progenitor population without a kick mechanism will spatially track rest-frame optical light (as is the case for Type Ia SNe; Wang et al. 2013). Finally, compact object mergers with significant kicks will result in a distribution that is only weakly correlated with the underlying rest-frame optical light.

Fong, Berger & Fox (2010) and Fong & Berger (2013) determined the light fraction at the sub-pixel locations of 20 short GRBs relative to the overall light distribution of each host galaxy (following the methodology of Fruchter et al. 2006). These measurements are available only for bursts with sub-arcsecond positions and *HST* follow-up, but as I discussed above, the requirement of an optical afterglow detection might only bias the resulting distribution to locations with higher ambient densities, and hence to brighter

regions within the hosts. The cumulative distributions of the light fraction at short GRB locations relative to the underlying rest-frame UV and optical light are shown in Figure 13. The results are striking; namely, about half of the short GRBs are located in regions of their hosts that are fainter in both the UV and optical than any other location within these galaxies (i.e., they have a fractional flux value of zero). This essentially means that even with the superior depth of *HST*, no stellar light is detected at the short GRB locations. This result remains true even if the short GRBs at projected offsets of tens of kpc (the host-less events) are ignored (Fong & Berger 2013).

A K-S test relative to the null hypothesis that the progenitors track the underlying UV or optical light results in p-values of 0.01 and 0.04, respectively (Fong & Berger 2013). Similarly, a comparison to long GRBs in terms of UV light leads to $p \approx 2\times10^{-3}$, while a comparison to Type Ia SNe in terms of optical light indicates $p \approx 0.02$. This indicates that short GRBs occur in distinct environments from other explosive transients whose progenitors are not expected to experience kicks (massive stars, single- or double-degenerate white dwarf systems), and are overall weakly correlated with the underlying distribution of star formation and even stellar mass in their hosts (Fong & Berger 2013). Given this clear discrepancy, the implication is that short GRB explosion sites are not representative of the progenitor birth-sites, and therefore require significant migration (kicks). This is a strong line of argument in favor of compact object mergers.

7.3 Kick Velocities

The offset distribution, and the locations of short GRBs relative to the stellar light of their hosts, are indicative of systemic kicks. The required kick velocities can be inferred from a comparison of the projected physical offsets and the host galaxy stellar population ages, taking into account the host masses. While projection effects and uncertainty about the age of any specific short GRB progenitor relative to the host mean stellar population age prevent the extraction of a detailed distribution, it is still possible to determine characteristic kick velocities. Making the assumption (Bloom et al. 2007) that the required kick velocities are roughly the geometric mean between the minimum required velocity ($v_{\rm kick,min} = \delta R/\tau_*$) and the host velocity dispersion ($v_{\rm disp} \approx 120$ km s^{-1} for late-type hosts and ≈ 250 km s^{-1} for the more massive early-type hosts; Battaglia et al. 2005, Xue et al. 2008), the resulting projected kick velocities span $v_{\rm kick} \sim 20 - 140$ km s^{-1} with a median value of about 60 km s^{-1} (Fong & Berger 2013). This range is consistent with the kick velocities derived for Galactic NS-NS binaries based on population synthesis models, $v_{\rm kick} \approx 5 - 500$ km s^{-1} (Fryer & Kalogera 1997; Fryer, Burrows & Benz 1998; Wang, Lai & Han 2006; Wong, Willems & Kalogera 2010). It is important to note that the inferred distribution of kicks for short GRBs is consistent with some progenitors having negligible kicks, and it does not strictly require velocities that will unbind the progenitors from their hosts.

7.4 Globular Clusters

An alternative explanation for the broad offset distribution and weak correlation with stellar light is that some short GRB progenitors originate in globular clusters, due to dynamically-formed compact object binaries, or to the tidal capture and collisions of compact objects (e.g., Bhattacharya & van den Heuvel 1991; Grindlay, Portegies Zwart & McMillan 2006; Lee, Ramirez-Ruiz & van de Ven 2010; Salvaterra et al. 2010). Estimates of the event rate for these processes compared to primordial binaries is $\lesssim 10\%$ (Grindlay, Portegies Zwart & McMillan 2006; Lee, Ramirez-Ruiz & van de Ven 2010). This is roughly similar to the $\sim 10\%$ of short GRBs with inferred offsets of $\gtrsim 20$ kpc, but it is not sufficient to explain the weak correlation with stellar light, i.e., $\sim 50\%$ of short GRBs with fractional flux values of zero.

A substantial fraction of short GRBs originating in globular clusters will also lead to the prediction of a

dominant population of early-type hosts since the globular cluster specific frequency is several times higher in early-type than in late-type galaxies (Harris 1991, Brodie & Strader 2006). This is in contrast to the observed low fraction of early-type hosts in the short GRB sample, which is already deficient relative to the cosmic stellar mass budget (§6). In addition, formation of binaries in globular clusters generally requires core-collapsed clusters, thereby leading to a significant time delay relative to the cluster formation epoch (Grindlay, Portegies Zwart & McMillan 2006; Lee, Ramirez-Ruiz & van de Ven 2010; Salvaterra et al. 2010). As a result, a dominant globular cluster population will lead to systematically lower redshifts; for example, Lee, Ramirez-Ruiz & van de Ven (2010) predict a median redshift of $z \approx 0.5$, and essentially no short GRBs at $z \gtrsim 1.5$. This result is not in strong conflict with the current redshift distribution, although the median redshift of short GRBs is probably somewhat higher than $z \sim 0.5$ (§6). Thus, while it is unlikely that most short GRBs originate in globular clusters, it is possible that $\sim 10\%$ of the events originate in these environments.

8 The Afterglows and Explosion Properties of Short GRBs

Having explored the galactic and sub-galactic environments of short GRBs, and the implications for the nature of their progenitors, I now turn to an investigation of the short GRB explosion properties and their parsec-scale circumburst environments. The key parameters of interest that can be extracted from the prompt and afterglow emission are the energy scale in γ-rays (E_γ) and in the blastwave powering the afterglow (E_K), the geometry of the outflow (characterized by a jet half opening angle, θ_j), and the density of the ambient medium (n). The standard formulation of the afterglow synchrotron emission includes additional free parameters related to the relativistic shock microphysics: the fraction of post-shock energy in the magnetic fields (ϵ_B) and in the radiating relativistic electrons (ϵ_e), which are assumed to follow a power law distribution, $N(\gamma) \propto \gamma^{-p}$, above a minimum Lorentz factor, γ_m (Sari, Piran & Narayan 1998). To determine the values of the various parameters requires multi-wavelength, multi-epoch afterglow observations spanning radio to X-rays.

The synchrotron emission spectrum resulting from the interaction of the relativistic outflow with the circumburst medium is characterized by three break frequencies, corresponding to self-absorption (ν_a), the minimum Lorentz factor (ν_m), and synchrotron cooling (ν_c), as well as an overall flux normalization (Sari, Piran & Narayan 1998). The instantaneous values of these four parameters and the slope of the spectrum at $\nu > \nu_m$ can be converted to $E_{\rm K,iso}$, n, ϵ_e, ϵ_B, and p; here $E_{\rm K,iso}$ is the isotropic-equivalent blastwave kinetic energy. In addition, the time evolution of the spectrum can be used to extract θ_j and p. This simple formulation has been confirmed with observations of multiple long GRBs (e.g., Panaitescu & Kumar 2002, Yost et al. 2003), although some deviations from the standard model are apparent at $\lesssim 10^3$ s, particularly in the X-ray band (e.g., initial steep decline, flares, plateaus; Nousek et al. 2006, Chincarini et al. 2007). Using the formulation of the afterglow model in Granot & Sari (2002) I employ the following relations to determine the locations of the break frequencies (relevant for the dominant slow-cooling regime, with $\nu_a < \nu_m < \nu_c$):

$$\nu_a = 1.24 \times 10^9 \, {\rm Hz} \, \frac{(p-1)^{3/5}}{(3p+2)^{3/5}} (1+z)^{-1} \bar{\epsilon}_e^{\,-1} \epsilon_B^{1/5} n_0^{3/5} E_{52}^{1/5} \quad (2)$$

$$\nu_m = 3.73 \times 10^{15} \, {\rm Hz} \, (p-0.67) (1+z)^{1/2} \bar{\epsilon}_e^{\,2} \epsilon_B^{1/2} E_{52}^{1/2} t_d^{-3/2} \quad (3)$$

$$\nu_c = 6.37 \times 10^{13} \, {\rm Hz} \, (p-0.46) e^{-1.16p} (1+z)^{-1/2} \epsilon_B^{-3/2} n_0^{-1} E_{52}^{-1/2} t_d^{-1/2} \quad (4)$$

$$F_{\nu_a} = 0.65 \, {\rm mJy} \, \frac{(p-1)^{6/5}}{(3p-1)(3p+2)^{1/5}} (1+z)^{1/2} \bar{\epsilon}_e^{\,-1} \epsilon_B^{2/5} n_0^{7/10} E_{52}^{9/10} t_d^{1/2} d_{L,28}^{-2} \quad (5)$$

where $\bar{\epsilon}_e \equiv \epsilon_e (p-2)/(p-1)$, E_{52} is the isotropic-equivalent blastwave kinetic energy in units of 10^{52}

erg, t_d is the observer-frame time in days, and $d_{L,28}$ is the luminosity distance in units of 10^{28} cm. For fiducial parameters relevant to short GRBs ($z \sim 0.5$, $E_{52} \sim E_{\gamma,\rm iso,52} \sim 0.1$, $n_0 \sim 0.1$), and assuming the typical microphysical parameters from long GRB afterglow data ($\epsilon_e \sim 0.1$, $\epsilon_B \sim 0.01$, $p \sim 2.4$; Panaitescu & Kumar 2002, Yost et al. 2003), the typical values of the synchrotron parameters are: $\nu_a \sim 1$ GHz, $\nu_m \sim 200\, t_d^{-1.5}$ GHz, $\nu_c \sim 2 \times 10^{17}\, t_d^{-0.5}$ Hz, and $F_{\nu_a} \sim 20\ \mu$Jy. These values confirm that observations from radio to X-rays are required to probe the full set of synchrotron parameters. They also indicate that the typical brightness level in the radio band ($\sim 1 - 10$ GHz) is quite challenging for detection, even with the upgraded Karl G. Jansky Very Large Array. Similarly, these parameters predict a faint optical afterglow brightness level of ~ 23 AB mag at ~ 7 hr, the mean timescale for existing searches (see also Panaitescu, Kumar & Narayan 2001).

In reality, the afterglow data for short GRBs are much sparser than for long GRBs, and the complete set of physical parameters for most individual events cannot be determined uniquely. For example, only three short GRBs to date have been detected in the radio (Berger et al. 2005b, Soderberg et al. 2006a, Fong et al. 2013), providing meaningful constraints on the location of the self-absorption frequency. Still, using basic constraints, including expectations for the values of the microphysical parameters, and a combination of detections and upper limits in the radio, optical, and X-rays, it is possible to determine the distributions of some key short GRB properties.

Of particular interest for our understanding of the central engine and energy extraction mechanism is the beaming-corrected energy, which requires the determination of jet opening angles (see §8.4). The jet collimation also influences the true short GRB event rate, which in turn provides an additional constraint on the progenitor model, and potentially useful information on the rate of gravitational wave detections in the specific context of compact object merger progenitors. Finally, the circumburst density provides insight on the progenitors, through constraints on their parsec-scale environments. Beyond the direct properties of short GRBs, the energy scale and circumburst densities can also be used to shed light on the expected brightness of electromagnetic counterparts to gravitational wave sources, both on- and off-axis; I discuss this point in detail in §10.

To date there have been only a few studies of short GRB afterglows. Berger et al. (2005b) determined the properties of GRB 050724 from radio, optical/near-IR, and X-ray observations, while Grupe et al. (2006) placed lower bounds on its collimation. Soderberg et al. (2006a) determined the explosion properties of GRB 051221A, and along with Burrows et al. (2006) measured its opening angle. Fong et al. (2013) presented the radio, optical, and X-ray afterglow of GRB 130603B and determined its properties and jet collimation angle. Berger (2007) presented an analysis of the γ-ray and X-ray observations of 16 short GRBs that revealed a clear correlation between $E_{\gamma,\rm iso}$ and $L_{\rm X,iso}$ (a rough proxy for $E_{\rm K,iso}$), as well as a broad range of isotropic-equivalent energies in the prompt emission and afterglows (see also Nakar 2007, Gehrels et al. 2008). Similarly, Nysewander, Fruchter & Pe'er (2009) investigated correlations between the γ-ray, X-ray, and optical emission.

8.1 X-ray Afterglow Emission

The most extensive afterglow data set for short GRBs is in the X-ray band from *Swift*/XRT (Table 1). As shown in §4, of the 50 short GRBs with X-ray detections, 28 events exhibit detectable long-term X-ray emission beyond $\sim 10^3$ s, as expected for afterglow emission, while the remaining events rapidly fade below the XRT detection threshold at $\lesssim 10^3$ s, and therefore yield only upper limits on the timescale dominated by the afterglow. The initial rapid decline phase is generally attributed to high latitude emission associated with the prompt phase (e.g., Nousek et al. 2006), and therefore cannot be reliably used to constrain the afterglow properties. In Figure 14, I plot the isotropic-equivalent X-ray luminosity of short and long GRBs

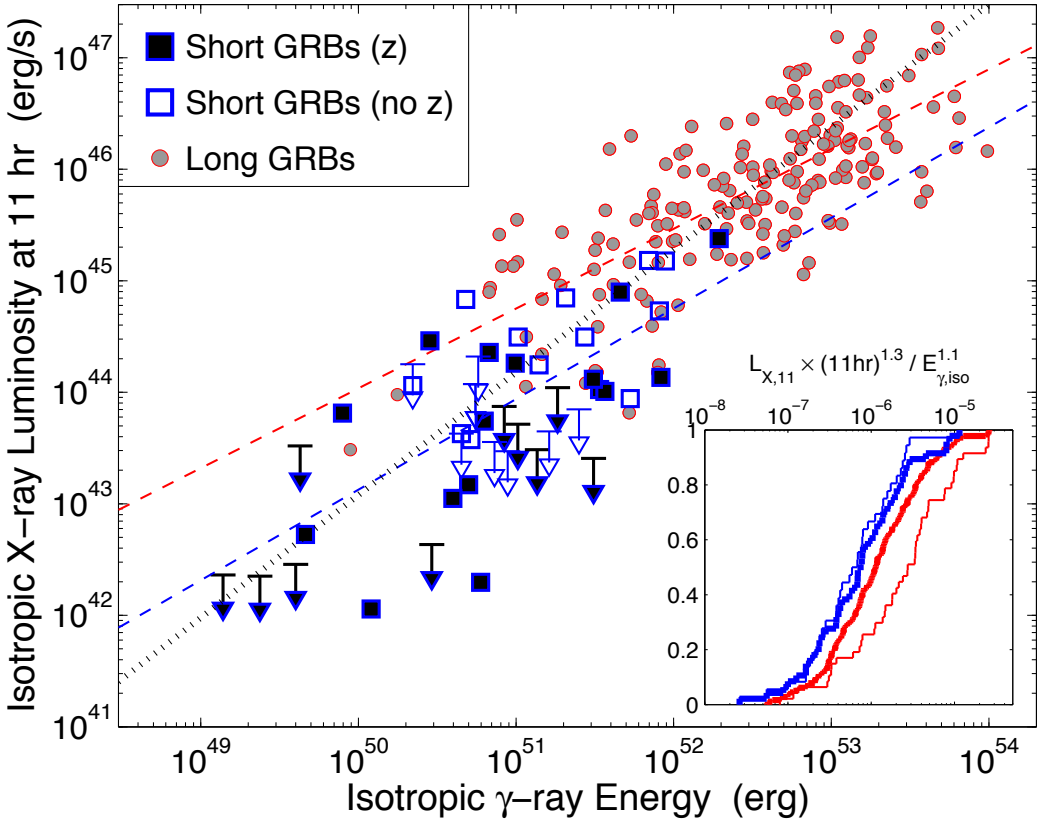

Figure 14:

Isotropic-equivalent afterglow X-ray luminosity at a rest-frame time of 11 hr ($L_{X,11}$) versus the isotropic-equivalent γ-ray energy ($E_{\gamma,\rm iso}$) for short GRBs (blue) and long GRBs (gray). Open symbols for short GRBs indicate events without a known redshift, for which a fiducial value of $z = 0.75$ is assumed. The dashed blue and red lines are the best-fit power law relations to the trends for short and long GRBs, respectively, while the dotted black line is the expected correlation based on the afterglow synchrotron model with $\nu_X > \nu_c$ and $p = 2.4$ ($L_{X,11} \propto E^{1.1}_{\rm K,iso}$). The inset shows the distribution of the ratio $L_{X,11} \times (11\,{\rm hr})^{1.3}/E^{1.1}_{\gamma,\rm iso}$, for the full samples (thick lines) and for bursts in the region of $E_{\gamma,\rm iso}$ overlap (thin lines). The lower level of $L_{X,11}$ relative to $E_{\gamma,\rm iso}$ for short GRBs is evident from these various comparisons.

at a fiducial rest-frame time of 11 hr in a rest-frame band of 0.3 – 10 keV ($L_{X,11}$) as a function of the isotropic-equivalent γ-ray energy ($E_{\gamma,\rm iso}$). I use $E_{\gamma,\rm iso}$ as a proxy for the more directly relevant, but generally unknown $E_{\rm K,iso}$. This is a reasonable approach for each GRB sample individually since variations in the radiative γ-ray efficiency, $\epsilon_\gamma \equiv E_{\gamma,\rm iso}/(E_{\gamma,\rm iso} + E_{\rm K,iso}$, will increase the scatter, but should not introduce systematic trends. On the other hand, any systematic trends in ϵ_γ between short and long GRBs may lead to systematic effects when using $E_{\gamma,\rm iso}$ as a proxy for $E_{\rm K,iso}$. I return to this point in §8.5.

As expected, both the short and long GRB samples exhibit a clear correlation between $L_{X,11}$ and $E_{\gamma,\rm iso}$ (Figure 14; Berger 2007; Gehrels et al. 2008; Nysewander, Fruchter & Pe'er 2009). For long GRBs the best-fit power law relation is $L_{X,11} \approx 5.6 \times 10^{44}\, E^{0.72}_{\gamma,\rm iso,51}$ erg s^{-1}, while for short GRBs it is systematically lower, with $L_{X,11} \approx 8.5 \times 10^{43}\, E^{0.83}_{\gamma,\rm iso,51}$ erg s^{-1}. In the region of overlap between the two GRB populations ($E_{\gamma,\rm iso} \approx 3 \times 10^{50} - 10^{52}$ erg), the short GRB isotropic X-ray afterglow luminosity is on average about 7

times lower than for long GRBs.

Comparing the short GRBs with afterglow detections to those with only a rapid decline phase and no X-ray detections beyond $\sim 10^3$ s, I find no clear difference in the ratio $L_{X,11}/E_{\gamma,\rm iso}$. In particular, short GRBs with X-ray afterglow detections span $L_{X,11}/E_{\gamma,\rm iso} \approx 10^{-8} - 10^{-6}$, with 40% of these events having $L_{X,11}/E_{\gamma,\rm iso} \lesssim 10^{-7}$. The upper limits are generally $L_{X,11}/E_{\gamma,\rm iso} \lesssim 10^{-7}$ (although some shallower limits exist as well). Thus, it appears that events without detected X-ray emission beyond $\sim 10^3$ s are generally due to inadequate searches, rather than to intrinsically weaker X-ray afterglows.

In the context of the standard afterglow synchrotron model, the X-ray band is expected to be located near or above the synchrotron cooling frequency ($\nu_X > \nu_c$; see discussion following Equation 5). In this spectral regime the afterglow X-ray flux is given by $F_{\nu,X} \propto E_{\rm K,iso}^{(p+2)/4}\, \epsilon_e^{p-1}\, \epsilon_B^{(p-2)/4} \approx \epsilon_e\, E_{\rm K,iso}$ (Granot & Sari 2002). Assuming that $E_{\gamma,\rm iso}$ is a close proxy for $E_{\rm K,iso}$, it is evident that the observed correlations for short and long GRBs are flatter than the theoretical expectation. At the same time, the observed dispersion around this relation is at least a factor of few, suggestive of dispersion in the values of p, ϵ_e, and ϵ_B, as well as cases with $\nu_X < \nu_c$ for which the density also influences the observed flux.

In Figure 14 I also plot the distribution of the ratio $L_{X,11} \times (11\,{\rm hr})^{1.3}/E_{\gamma,\rm iso}^{1.1}$, which is the expected relation for $p = 2.4$ and $E_{\gamma,\rm iso} = E_{\rm K,iso}$ based on the afterglow model. For the full samples of short and long GRBs I find that the distributions of this ratio are similar, although with a systematically lower value for short GRBs; a K-S test yields a p-value of about 0.23, indicating that the two samples are compatible with the null hypothesis of being drawn from the same underlying distribution. On the other hand, using only events in the overlap region of $E_{\gamma,\rm iso} \approx 3 \times 10^{50} - 10^{52}$ erg yields a substantial difference (K-S test value of $p \approx 1.1 \times 10^{-4}$). I therefore conclude that short GRBs have systematically weaker X-ray afterglow emission compared to long GRBs, relative to both the observed correlation between $L_{X,11}$ and $E_{\gamma,\rm iso}$, and the relation expected from afterglow theory.

8.2 Optical Afterglow Emission

I next turn to the optical afterglow emission, which has been detected in 24 short GRBs, with upper limits for an additional 16 bursts (§4). Most detections and limits have been obtained on a timescale of about 1 hr to 1 day after the burst, with a magnitude range of about 21 – 26 AB mag (Table 1). The median r-band brightness level at a fiducial time of 7 hr is $\langle m_r(7\,{\rm hr})\rangle \approx 23.2$ AB mag, in excellent agreement with the expectation for the fiducial set of parameters discussed in relation to Equations 5, and with the prediction of Panaitescu, Kumar & Narayan (2001). For comparison, long GRB afterglows are generally an order of magnitude brighter, with $\langle m_r(7\,{\rm hr})\rangle \approx 20.8$ AB mag (e.g., Kann et al. 2011), despite their significantly larger redshifts (Figure 4).

Converting to rest-frame properties, in Figure 15 I plot the isotropic-equivalent optical luminosity in the rest-frame r-band at a fiducial rest-frame time of 7 hours ($L_{\rm opt,7}$) as a function of $E_{\gamma,\rm iso}$. As in the case of the isotropic X-ray luminosity, there is a clear correlation between the optical luminosity and γ-ray energy. For short GRBs, the best-fit power law relation is $L_{\rm opt,7} \approx 6.9 \times 10^{42}\, E_{\gamma,\rm iso,51}^{0.74}$ erg s^{-1}, while for long GRBs the relation is systematically higher, $L_{\rm opt,7} \approx 5.0 \times 10^{43}\, E_{\gamma,\rm iso,51}^{0.73}$ erg s^{-1}. Thus, in the range of $E_{\gamma,\rm iso}$ in which the short and long GRB populations overlap, the optical afterglow luminosity of short GRBs is on average about 7 times fainter than for long GRBs, just as in the case of the X-ray luminosity.

The expected trend based on the afterglow synchrotron model (for the case of $\nu_m < \nu_{\rm opt} < \nu_c$) is $F_{\nu,\rm opt} \propto E_{\rm K,iso}^{(p+3)/4}\, n_0^{1/2}\, \epsilon_e^{p-1}\, \epsilon_B^{(p+1)/4}$. For a typical value of $p = 2.4$, this indicates a steeper slope than inferred from the data, with $F_{\nu,\rm opt} \propto E_{\rm K,iso}^{1.35}$. This trend is shown in Figure 15 with a dotted line, and indeed seems to be a reasonable representation of the full range of $E_{\gamma,\rm iso}$ spanned by short and long GRBs. This is also borne out in the nearly identical cumulative distributions of the ratio $L_{\rm opt,7} \times (7\,{\rm hr})^{1.05}/E_{\gamma,\rm iso}^{1.35}$ for both short and long

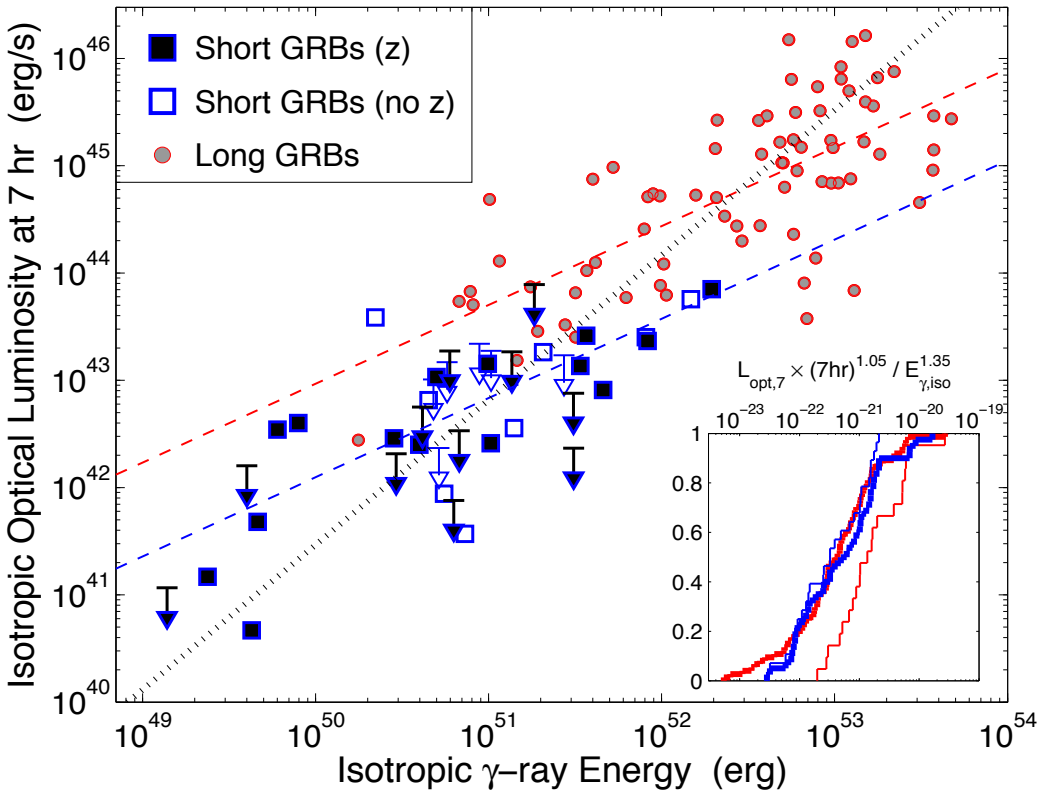

Figure 15:

Same as Figure 14 but for the Isotropic-equivalent afterglow optical luminosity at a rest-frame time of 7 hr ($L_{\rm opt,7}$). The dotted black line is the expected correlation based on the afterglow model for $\nu_m < \nu_{\rm opt} < \nu_c$ and $p = 2.4$ ($L_{\rm opt,7} \propto E^{1.35}_{\rm K,iso}$). The inset shows the distribution of the ratio $L_{\rm opt,7} \times (7\,{\rm hr})^{1.05}/E^{1.35}_{\gamma,\rm iso}$, for the full samples (thick lines) and for bursts in the region of $E_{\gamma,\rm iso}$ overlap (thin lines). The lower level of $L_{\rm opt,7}$ relative to $E_{\gamma,\rm iso}$ for short GRBs is evident from these various comparisons.

GRBs (Figure 15). However, despite the overall similarity, the short GRBs have systematically lower values of this ratio in the overlap range of $E_{\gamma,\rm iso} \approx 3 \times 10^{50} - 10^{52}$ erg. A K-S test yields a p-value of about 0.016, indicating that the two samples are not likely to be drawn from the same underlying distribution. Thus, despite the larger scatter in the optical band compared to the X-ray band, it appears that short GRBs have systematically weaker optical afterglow emission compared to long GRBs, relative to both the observed correlation between $L_{\rm opt,7}$ and $E_{\gamma,\rm iso}$, and to the relation expected from afterglow theory.

8.2.1 X-ray / Optical Comparison The X-ray and optical luminosities of short GRB afterglows appear to be fainter relative to $E_{\gamma,\rm iso}$ than for long GRBs, by a similar factor of about 7. This indicates that the ratio $L_{\rm opt,7}/L_{X,11}$ should have a similar distribution for both GRB samples. In Figure 16 I plot $L_{\rm opt,7}$ versus $L_{X,11}$ for short and long GRBs, and indeed find that both populations follow a similar trend, consistent with a linear correlation (see also Nysewander, Fruchter & Pe'er 2009). The median value for both the short and long GRB samples is $\langle L_{\rm opt,7}/L_{X,11}\rangle \approx 0.08$, and nearly all events have $L_{\rm opt,7}/L_{X,11} \lesssim 1$. In the context of the synchrotron model, the expected ratio for the case in which both the optical and X-ray bands are located below ν_c is $L_{\rm opt,7}/L_{X,11} \approx 0.2$ (for $p = 2.4$). On the other hand, for the case when ν_c is intermediate

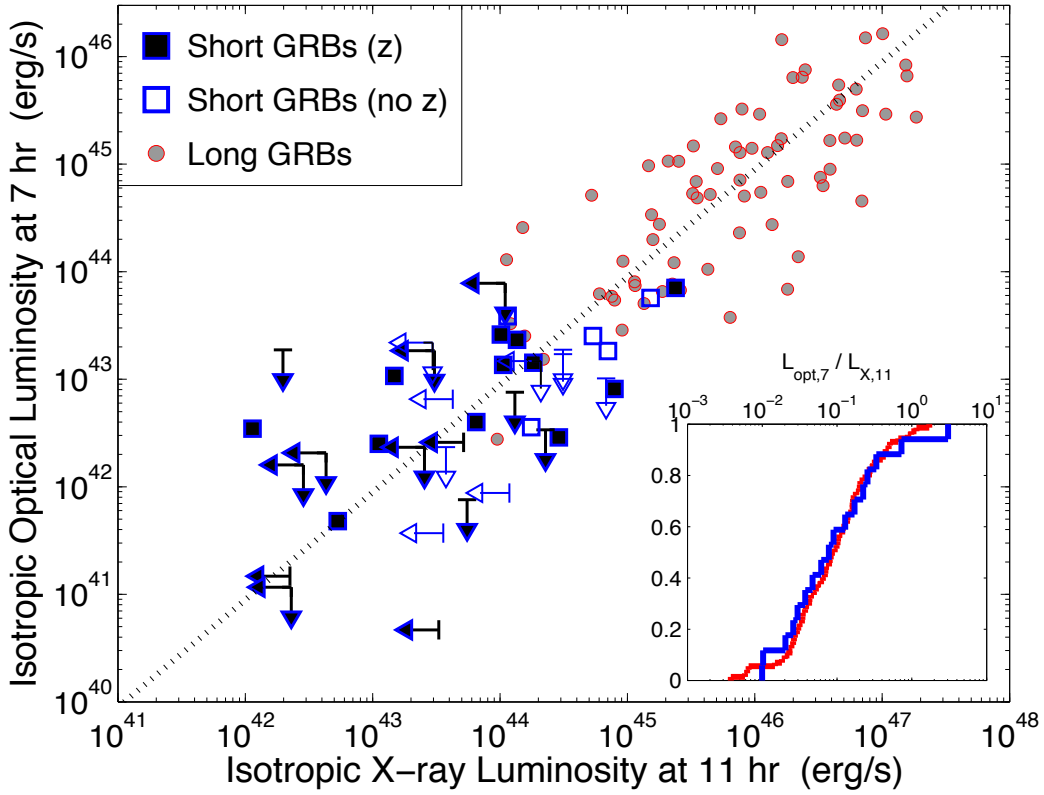

Figure 16:

Isotropic-equivalent afterglow optical luminosity at a rest-frame time of 7 hr ($L_{\rm opt,7}$) versus isotropic-equivalent afterglow X-ray luminosity at a rest-frame time of 11 hr ($L_{\rm X,11}$). Symbols are as in Figure 14. The dotted black line marks a linear correlation, expected for $\nu_X \lesssim \nu_c$. The inset shows the distribution of the ratio $L_{\rm opt,7}/L_{X,11}$, indicating that both short and long GRBs exhibit a similar ratio, and that in general $L_{\rm opt,7}/L_{X,11} \lesssim 1$, indicative of $\nu_X \lesssim \nu_c$ for short GRBs.

between the optical and X-ray bands (e.g., $\nu_c \sim 10^{16}$ Hz) the expected ratio is $L_{\rm opt,7}/L_{X,11} \approx 1$, higher than most observed values. Thus, the comparison of optical and X-ray luminosities suggests that generally ν_c is located near or above the X-ray band.

Since the ratio of optical to X-ray luminosity for $\nu_c \sim \nu_X$ and for $\nu_c \gg \nu_X$ is essentially the same, and since in the latter case both the X-ray and optical luminosity depend on density (with $F_\nu \propto n^{0.5}$), the lower values of $L_{\rm opt,7}/E_{\gamma,\rm iso}$ and $L_{X,11}/E_{\gamma,\rm iso}$ for short GRBs can be interpreted as being due to a lower density scale; this will also naturally lead to $\nu_c \gg \nu_X$ since $\nu_c \propto n^{-1}$. On the other hand, long GRBs generally have higher densities and hence $\nu_c \sim \nu_X$. To match the observed weaker optical and X-ray afterglows of short GRBs, requires a density scale that is about 50 times lower than for long GRBs, corresponding to $n \sim 0.1$ cm^{-3}.

An alternative possibility is that the systematic offset in the trends of $L_{\rm opt,7}$ and $L_{X,11}$ versus $E_{\gamma,\rm iso}$ for short and long GRBs is due to systematic differences between the γ-ray and blastwave kinetic energies. In particular, if ϵ_γ for short GRBs is systematically higher than for long GRBs, this would lead to values of $E_{\gamma,\rm iso}$ that over-predict $E_{\rm K,iso}$ and hence to lower ratios of $L_{\rm opt,7}/E_{\gamma,\rm iso}$ and $L_{X,11}/E_{\gamma,\rm iso}$ compared to those for long GRBs. Given the overall shift of the best-fit relations shown in Figures 14 and 15, this scenario

would require an efficiency that is about an order of magnitude larger in short GRBs. With a fiducial value of $\epsilon_\gamma \sim 0.5$ for long GRBs (e.g., Panaitescu & Kumar 2002), this requires $\epsilon_\gamma \sim 0.95$ for short GRBs, an unlikely scenario.

A possible variation of this scenario is that the blastwave kinetic energies of long GRBs are systematically larger relative to $E_{\gamma,\rm iso}$ due to significant energy injection into the forward shock following the prompt emission phase, which is absent in short GRBs. Indeed, the X-ray plateaus in long GRBs, spanning $\sim 10^3 - 10^4$ s, have been interpreted as evidence for significant energy injection (Nousek et al. 2006), but a smaller fraction of short GRBs exhibit such plateaus (Margutti et al. 2013). Effectively, larger energy injection in long GRBs will translate to a lower value of ϵ_γ than for short GRBs. An energy injection factor in long GRBs of about an order of magnitude will bring the relations for short and long GRBs into alignment.

8.2.2 The Energy and Density Scale Extracted from Optical Observations

Independent of the relative behavior of short and long GRB afterglows, each optical detection or upper limit can be converted to an allowed range in the phase-space of $E_{\rm K,iso}$ and n. For this purpose I use fixed fiducial values of the microphysical parameters, $\epsilon_e = 0.1$, $\epsilon_B = 0.01$, and $p = 2.4$. In addition, I restrict the range of $E_{\rm K,iso}$ for each burst to $(0.3 - 3) \times E_{\gamma,\rm iso}$ for a reasonable expected range of ϵ_γ. The resulting distribution is shown in Figure 17. For the bulk of the short GRB population, the inferred density range is $n \sim 10^{-3} - 1$ cm^{-3}, with a median for the full distribution of $\langle n \rangle \lesssim 0.15$ cm^{-3}; this is an upper limit due to the substantial fraction of optical non-detections. This result confirms our inference of a lower density scale compared to long GRBs based on the ratios of optical and X-ray luminosity to $E_{\gamma,\rm iso}$.

There are three bursts that may stand out from this distribution, with inferred densities of $\sim 50 - 10^3$ cm^{-3} (if $E_K \approx E_\gamma$ and if their microphysical parameters are as listed above). Two of these events (GRBs 070724A and 110112A) have low γ-ray fluences of $F_\gamma \approx 3 \times 10^{-8}$ erg cm^{-2}, which may indicate that the *Swift*/BAT energy band severely underestimates the value of $E_{\gamma,\rm iso}$, and hence their likely $E_{\rm K,iso}$ values. With larger energies, the required densities will be lower than the values inferred above. On the other hand, the third event (GRB 050709) does not fall in this category. Clearly, the inferred distribution of circumburst densities is affected by dispersions in the microphysical parameters and in the ratio of $E_{\gamma,\rm iso}$ to $E_{\rm K,iso}$, and may therefore be somewhat wider or narrower than inferred here. However, the median of the distribution is fairly robust. The relatively low density is not unexpected considering that most short GRB offsets are larger than 1 r_e and that nearly half of all short GRBs reside in regions with no detectable stellar light (§7).

8.3 Radio Afterglow Emission

Radio afterglow observations have been undertaken for 28 short GRBs, and have so far led to only 3 detections (GRBs 050724, 051221A, and 130603B; Berger et al. 2005b, Soderberg et al. 2006b, Fong et al. 2013); see Table 1. With the exception of a few short GRBs observed with the improved sensitivity of the JVLA starting in 2011, most upper limits are in the range of $F_\nu \sim 60 - 150$ μJy (3σ). It is clear from a comparison to the fiducial synchrotron model listed above (with $F_\nu \sim 40$ μJy at ~ 10 GHz; Equation 5) that most of the existing limits are too shallow compared to the expected flux density scale for $n \sim 0.1$ cm^{-3}. On the other hand, since in the relevant regime ($\nu_a < \nu_{\rm radio} < \nu_m$) the flux density scales as $F_\nu \propto n^{0.5}$, the non-detections generally indicate $n \lesssim$ few cm^{-3}. This result is supported by the three events with detected radio afterglows (Berger et al. 2005b, Soderberg et al. 2006a, Fong et al. 2013), and agrees with the more constraining results from the optical afterglow data. I also note that of the three bursts with potential high density based on optical observations, I find that radio observations of GRB 050709 instead indicate $n \lesssim 0.05$ cm^{-3} (see also Fox et al. 2005); the radio limits for GRBs 070724A and 110112A are not

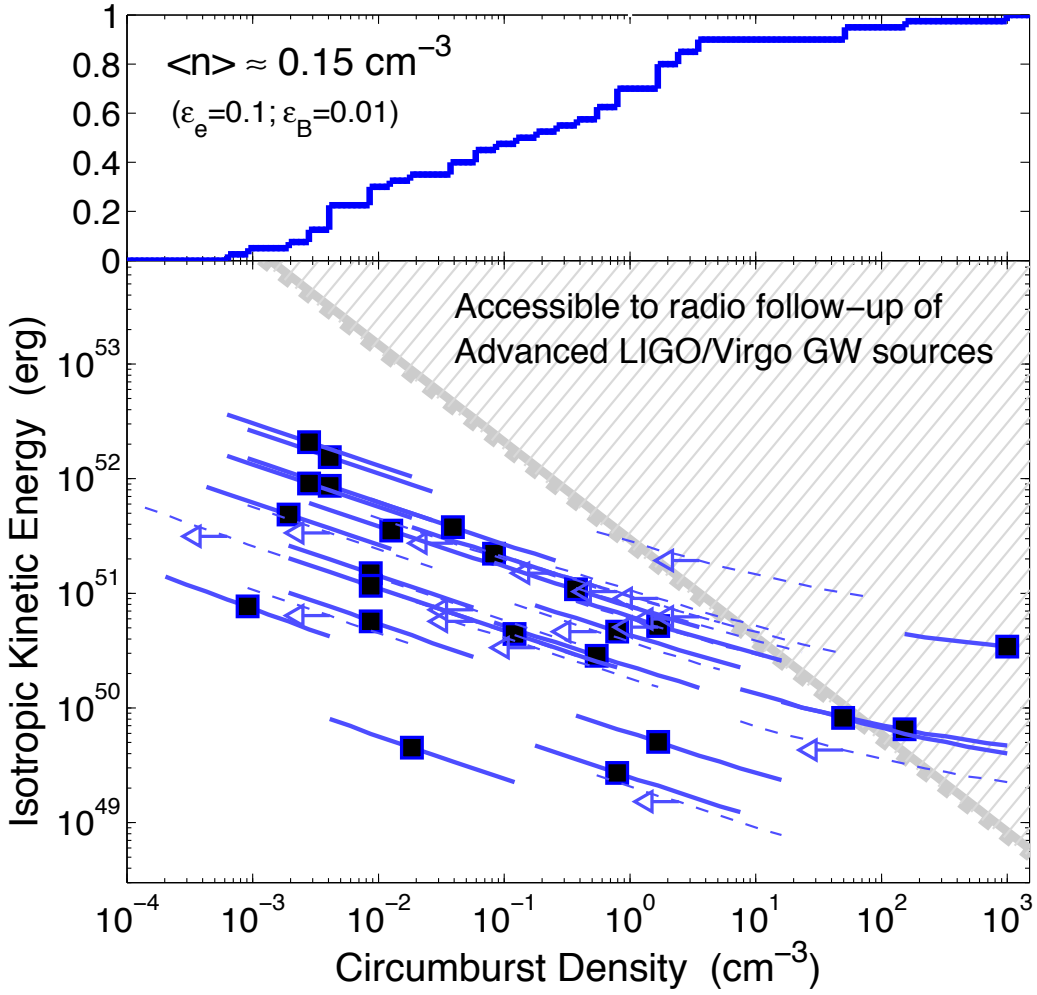

Figure 17:

Bottom: Blastwave isotropic-equivalent kinetic energy ($E_{\rm K,iso}$) versus circumburst density (n) for individual short GRBs based on their optical afterglow emission (arrows indicate optical non-detections). The lines span $E_{\rm K,iso} = (0.3-3)\times E_{\gamma,\rm iso}$. The diagonal gray lines delineate the phase-space required for the detections of radio counterparts to Advanced LIGO/Virgo gravitational wave sources (hatched gray region; based on the models in Nakar & Piran 2011). The solid line is for an off-axis short GRB afterglow with fiducial parameters (§8), while the dashed line is for an isotropic mildly-relativistic outflow. The short GRB results point to an energy-density scale that will generally prevent radio detections of Advanced LIGO/Virgo sources in searches that cover a full error region (§10). Top: Cumulative distribution of the circumburst densities (for $E_{\rm K,iso} = E_{\gamma,\rm iso}$). The median circumburst density is $\lesssim 0.15$ cm^{-3}, at least an order of magnitude lower than for long GRBs, pointing to explosions in more tenuous environments.

constraining beyond the information available from the optical detections.

8.4 Jets and Implications for the Energy Scale and Event Rates

The collimation of GRB outflows has direct implications for the true energy scale and event rate, as well as for our understanding of the energy extraction mechanism. The signature of collimation in GRB afterglows is the so-called jet break that occurs at the time (t_j) when the bulk Lorentz factor of the outflow declines to $\Gamma(t_j) \approx 1/\theta_j$ (Rhoads 1999; Sari, Piran & Halpern 1999). The break is due to a combination of an edge effect, when the entire emitting surface of the jet becomes visible, and sideways expansion of the outflow. Together, these effects lead to a change in the evolution of the synchrotron spectrum. In particular, at frequencies above the spectral peak ($\nu \gtrsim \nu_m$) the jet break is manifested as a steepening in the decline rate from roughly $F_\nu \propto t^{-1}$ to $F_\nu \propto t^{-p}$. This is relevant for the optical and X-ray bands. In the radio band, which is located below ν_m for typical jet break timescales, the evolution transitions from a mild rise to a shallow decline, subsequently followed by $F_\nu \propto t^{-p}$ when ν_m declines below the radio band. Since the jet break is due to relativistic and hydrodynamic effects, it is expected to be achromatic from radio to X-rays. The relation between the jet break time and opening angle is given by (Sari, Piran & Halpern 1999):

$$\theta_j = 0.13 \left(\frac{t_{j,d}}{1+z}\right)^{3/8} \left(\frac{n_0}{E_{52}}\right)^{1/8} \quad (6)$$

In the case of long GRBs, there is ample evidence for jet collimation based on the detection of jet breaks in the X-rays, optical, and/or radio on a wide range of timescales (Harrison et al. 1999; Bloom, Frail & Sari 2001; Frail et al. 2001; Panaitescu & Kumar 2002; Berger, Kulkarni & Frail 2003). The resulting jet opening angles are mainly in the range $\theta_j \approx 3-10^\circ$, with some events extending to about 20° (Bloom, Frail & Sari 2001; Frail et al. 2001; Berger, Kulkarni & Frail 2003). The typical beaming correction factor is therefore $f_b \equiv [1-\cos(\theta_j)] \approx 6\times10^{-3}$. This leads to a two orders of magnitude downward correction in the energy scale, with a resulting typical value of $E_\gamma \sim E_K \sim$ few $\times\, 10^{51}$ erg (Bloom, Frail & Sari 2001; Frail et al. 2001; Berger, Kulkarni & Frail 2003), albeit with a spread of about an order of magnitude (Soderberg et al. 2006b, Cenko et al. 2011). Similarly, the upward correction to the long GRB rate is $f_b^{-1} \sim 10^2$.

The information on jet breaks in short GRBs is more sparse, and with the exception of GRB 130603B (Fong et al. 2013), the claimed breaks have not been detected in multiple wave-bands that can confirm the expected achromatic behavior. The key challenge for jet break detections is the faintness of short GRB afterglows, which typically fade below detectable levels on a day timescale, translating to a weak constraint of $\theta_j \gtrsim 3^\circ$ if no break is observed (Fong et al. 2012).

Despite this observational challenge, there are a few credible detections of jet breaks so far. GRB 051221A was the first short GRB with evidence for collimation based on a break in its X-ray light curve at about 5 d, with the expected steepening to a power law index of $\alpha_X \lesssim -2$ (Burrows et al. 2006, Soderberg et al. 2006a). The inferred opening angle is $\theta_j \approx 6-8^\circ$ (Soderberg et al. 2006a), similar to the opening angles of long GRBs. GRB 111020A similarly exhibited a break in its X-ray light curve, at about 2 d, leading to an inferred opening angle of $\theta_j \approx 3-8^\circ$ (Fong et al. 2012); the larger uncertainty compared to GRB 051221A is due to the unknown redshift of this burst. Most recently, GRB 130603B exhibited a significant break in its optical light curve at about 0.45 d, accompanied by a decline in the radio band that matches the expectations of a post-jet break behavior (Fong et al. 2013). The inferred opening angle is $\theta_j \approx 4-8^\circ$ (Fong et al. 2013). A potential break was also noted in the optical light curve of GRB 090426 at about 0.4 d, with a steep decline typical of post jet break evolution (Nicuesa Guelbenzu et al. 2011), and an inferred opening angle of $\theta_j \approx 4^\circ$.

In addition to these likely breaks, there are also several meaningful lower limits on jet opening angles. X-ray observations of GRB 050724 with *Swift*/XRT and *Chandra* revealed no break to about 22 d, leading to an inferred lower limit of $\theta_j \gtrsim 20^\circ$ (Grupe et al. 2006). The optical afterglow of GRB 050709 exhibited potential steepening at about 10 d based on a single data point (Fox et al. 2005), which if attributed to a

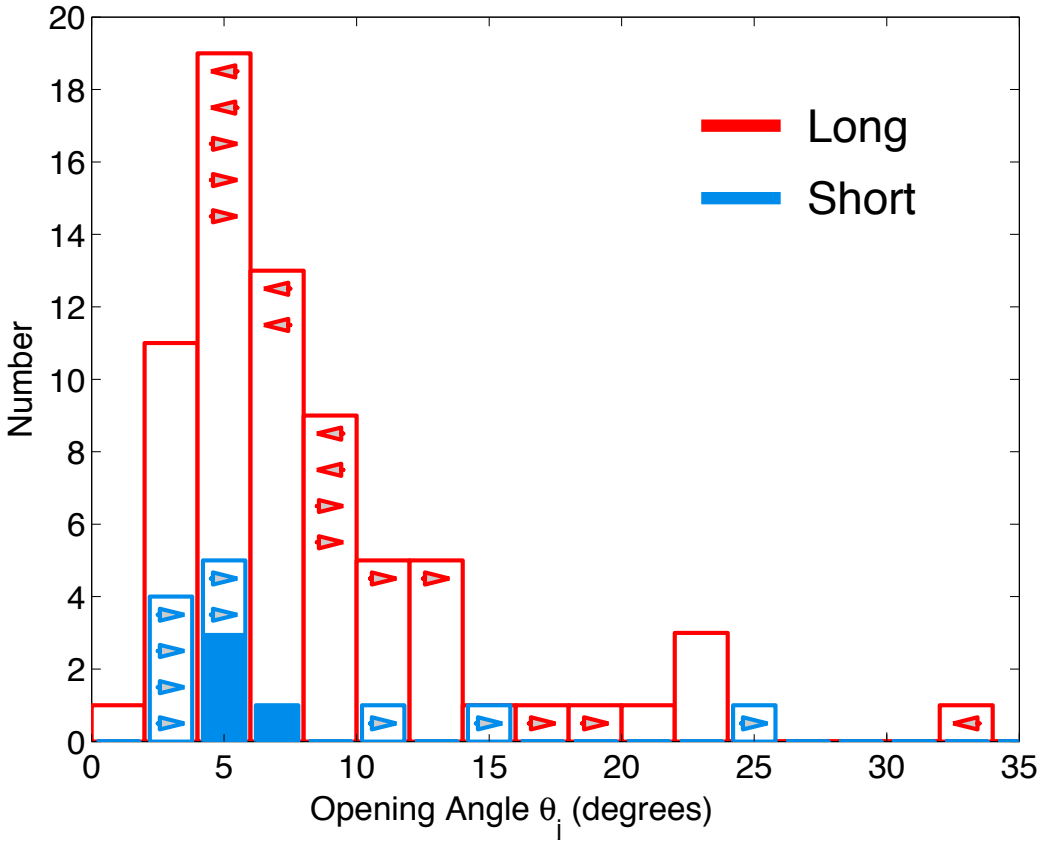

Figure 18:

Distributions of jet opening angles for short (blue) and long (red) GRBs, based on breaks in their afterglow emission. Arrows mark lower or upper limits on the opening angles. The observations are summarized in §8.4. From Fong et al. (2013) and references therein.

jet break leads to $\theta_j \approx 15°$; however, this interpretation has been disputed (Watson et al. 2006), and here I conservatively use $\theta_j \gtrsim 15°$ as a lower limit. X-ray observations of GRB 111117A with *Swift*/XRT and *Chandra* revealed no break to about 3 d, leading to an inferred lower limit of $\theta_j \gtrsim 6°$ (Margutti et al. 2012). Finally, the lack of a break in the X-ray afterglow of GRB 120804A to about 46 d, indicates an opening angle of $\theta_j \gtrsim 11°$ (Berger et al. 2013).

There are also several claimed breaks at much earlier times, $\sim 0.5 - 2$ hr, with a post-break steep decline rate that is reminiscent of jet break behavior (GRBs 061201, 090305, 090510). If these are indeed jet breaks, then the resulting opening angles are even narrower than for most long GRBs, $\theta_j \sim 1 - 2°$. However, in the case of GRB 090305 the claimed break is based on a single optical data point (Nicuesa Guelbenzu et al. 2012a), while for GRB 090510 there is no corresponding break in the optical band despite simultaneous coverage (Nicuesa Guelbenzu et al. 2012b). In addition to these putative breaks, several short GRBs exhibit no break in their X-ray light curves to $\sim$ day, leading to typical limits of $\gtrsim 3°$ (GRBs 070714B, 070724A, 071227, 081226, 101219A; Fong et al. 2012). The distribution of jet opening angles for short GRBs, along with a comparison to long GRB jets is shown in Figure 18.

Using the most robust detections and constraints described above (3 detections and 4 lower limits), I find

that the mean opening angle is $\langle\theta_j\rangle \gtrsim 10^\circ$. The resulting mean beaming factor is $f_b \gtrsim 0.015$, indicating that the correction to the observed short GRB rate is a factor of $\lesssim 70$, or a rate of up to $\sim 10^3$ Gpc^{-3} yr^{-1} (Nakar, Gal-Yam & Fox 2006; Coward et al. 2012; Fong et al. 2012, 2013). In the context of compact object mergers, this value coincides with the middle of the range based on estimates from the Galactic NS-NS binary population and from population synthesis models (Kalogera et al. 2004, Abadie et al. 2010). When converted to the rate within the expected sensitivity volume of Advanced LIGO ($\sim$ 200 Mpc), the resulting value is ~ 25 yr^{-1}. I note that if claimed values of $\theta_j \sim 1-2^\circ$ are indeed correct, then it is possible that the correction to the short GRB rate is up to $\sim 3\times10^3$, leading to an Advanced LIGO detection rate of $\sim 10^3$ yr^{-1}. Thus, in the framework of compact object binary progenitors, the discovery rate of NS-NS binaries with Advanced LIGO will provide insight on short GRB beaming.

The inferred opening angles also determine the true energy scale of short GRBs. For the 3 events with likely jet breaks, the inferred beaming-corrected γ-ray energies are $E_\gamma \approx (0.5-5)\times10^{49}$ erg. The 4 events with lower limits on the opening angles lead to a similar range for their minimum beaming-corrected γ-ray energies (with the upper bounds determined by the isotropic-equivalent values). Since the short GRB sample spans $E_{\gamma,\rm iso} \sim 10^{49}-10^{52}$ erg (Figures 14 and 15), it is likely that the beaming-corrected energies are generally $E_\gamma \lesssim 10^{50}$ erg (using the typical beaming correction of $f_b \sim 0.015$). It remains to be seen, when a larger sample of opening angles becomes available, whether the true energies span a narrow range, centered on $E_\gamma \sim 10^{49}$ erg, about two orders of magnitude lower than the energy scale of long GRBs.

8.5 Implications for the Progenitors and Energy Source

The comparison of short and long GRB afterglows, and the comparison of short GRB afterglow data to the standard synchrotron model, reveal several important trends. First, the ratios $L_{X,11}/E_{\gamma,\rm iso}$ and $L_{\rm opt,7}/E_{\gamma,\rm iso}$ are systematically lower for short GRBs, by about a factor of 7. On the other hand, the ratio $L_{\rm opt,7}/L_{X,11}$ is similar for both GRB samples. One implication of these results is that the afterglows of short and long GRBs are overall similar in their properties, and are generated by the same mechanism, namely an external shock with the circumburst environment that amplifies magnetic fields and accelerates electrons to relativistic velocities. However, short GRBs appear to explode in lower density environments. Using the optical afterglows, I find a typical density scale of $\lesssim 0.15$ cm^{-3}. This is supported by radio afterglow limits, which indicate $n \lesssim 1$ cm^{-3}, and by the few events with radio to X-ray detections (Berger et al. 2005b, Soderberg et al. 2006a, Fong et al. 2013). The relatively low circumburst densities are consistent with the larger offsets of short GRBs compared to long GRBs, and with their weak spatial correlation with the underlying distribution of stellar light in their hosts. Although it is less likely, the difference in the ratios of $L_{X,11}$ and $L_{\rm opt,7}$ to $E_{\gamma,\rm iso}$ for short and long GRBs may also reflect a systematic difference in the γ-ray efficiency, either due to a higher radiative efficiency in the prompt emission of short GRBs, or due to substantial energy injection in the early afterglow phase of long GRBs. In either case, a difference by about an order of magnitude is required to reconcile the two samples.

Beyond the relative trends, it is clear from Figures 14 and 15 that the distribution of $E_{\gamma,\rm iso}$ for short GRBs is just as broad as for long GRBs, but with systematically lower values of $\sim 10^{49}-10^{52}$ erg. The beaming-corrected energies in the several cases with likely jet opening angle measurements or meaningful lower limits are $E_\gamma \sim (0.5-5)\times10^{49}$, about two orders of magnitude lower than for long GRBs. The opening angles are generally broader than for long GRBs, with a range of $\theta_j \sim 5^\circ$ to $\gtrsim 20^\circ$ and a median of $\langle\theta_j\rangle \gtrsim 10^\circ$.

It is instructive to compare these inferences to the results of hydrodynamic and magnetohydrodynamic (MHD) simulations of compact object mergers as they pertain to estimates of the geometry, energy extraction mechanism, and the energy scale of relativistic outflows. Several researchers carried out hydrodynamic

simulations of jets launched by the neutrino-antineutrino annihilation mechanism and found jets with typical opening angles of $\theta_j \sim 5 - 20^\circ$, and total isotropic-equivalent energies of $\sim 10^{51}$ erg (or typical beaming-corrected energies of up to $\sim 10^{49}$ erg; Janka et al. 1999; Rosswog, Ramirez-Ruiz & Davies 2003; Setiawan, Ruffert & Janka 2004; Aloy, Janka & Müller 2005; Birkl et al. 2007; Dessart et al. 2009). However, only $\sim 10\%$ of this energy is available to produce the prompt emission, leading a typical true energy of $E_\gamma \sim 10^{48}$ erg. This value, and the estimated upper bound on $E_{\rm iso}$, are about an order of magnitude lower than observed in short GRBs, although the jet opening angle estimates agree with the observed values. This suggests that for at least some short GRBs, the neutrino-antineutrino annihilation mechanism is not likely to provide sufficient energy to power the observed emission.

Instead, recent general relativistic MHD simulations by Rezzolla et al. (2011) suggest the formation of a $\sim 10^{15}$ G magnetic field in both the torus (toroidal) and along the rotation axis (poloidal) following a compact object merger and the formation of a black hole. The typical opening angle of the poloidal component is $\sim 10 - 30^\circ$. If an outflow is then powered by the Blandford-Znajek mechanism (Blandford & Znajek 1977), the typical isotropic-equivalent energy scale is $\sim$ few $\times 10^{51}$ $(B/2 \times 10^{15}\,{\rm G})^2$ erg (e.g., Lee, Wijers & Brown 2000; Rosswog, Ramirez-Ruiz & Davies 2003; Shibata et al. 2011); this assumes that 10% of the available energy is channeled into the relativistic outflow, and that the typical opening angle is $\sim 10^\circ$ based on the existing observations. Thus, these simulations suggest that compact object mergers can lead to conditions that give rise to opening angles and an energy scale (via the Blandford-Znajek mechanism) that are well-matched to the observations of short GRBs.

9 "Kilonova" Emission and the Short GRB 130603B

One of the key predictions of the compact object merger model is the ejection of neutron-rich matter, either dynamically during the merger, or by winds from an accretion disk (Lattimer & Schramm 1974, Eichler et al. 1989). The typical ejecta masses and velocities inferred from merger simulations are in the range of $M_{\rm ej} \sim 10^{-3}$–few$\times 10^{-2}$ $M_\odot$ and $v_{\rm ej} \sim 0.1$–$0.3c$ (Rosswog et al. 1999, 2000; Ruffert & Janka 2001; Rosswog 2005; Etienne et al. 2008; Bauswein, Goriely & Janka 2013; Piran, Nakar & Rosswog 2013; Rosswog, Piran & Nakar 2013); the ejecta masses generally increase with larger asymmetry in the mass ratio (i.e., they are larger for NS-BH mergers than for NS-NS mergers; Hotokezaka et al. 2013; Kyutoku, Ioka & Shibata 2013; Rosswog, Piran & Nakar 2013). The resulting kinetic energy of the outflow is therefore in the range $E_K \sim 10^{49} - 3 \times 10^{51}$ erg. The ejecta will generate radio emission through interaction with the ambient medium, with the ejecta velocity and kinetic energy, as well as the ambient density, determining the peak brightness and timescale of the radio emission (see §10).

The rapid decompression of the neutron-rich matter from nuclear densities will lead to the formation of heavy radioactive elements via the *r*-process (Lattimer & Schramm 1974, Eichler et al. 1989). The radioactive decay of these elements spans a wide range of half-lives as the elements settle on the region of β stability, and provide a source of heating (Li & Paczyński 1998). Given the low ejecta mass and rapid expansion velocity, the ejecta will become optically thin on a shorter timescale and with a lower peak luminosity than supernova explosions. This has led to the terminology of "mini-SN", "macronova", or "kilonova" to describe these counterparts (Li & Paczyński 1998; Metzger et al. 2010b; Goriely, Bauswein & Janka 2011; Roberts et al. 2011; Piran, Nakar & Rosswog 2013); I use the latter term here. In addition to the dynamical properties of the ejecta, the timescale, luminosity, and characteristic spectral energy distribution of a kilonova also depend on the opacity of the *r*-process material, since the peak of the light curve is expected when the opacity becomes sufficiently low that photons can diffuse on the expansion timescale

(e.g., Arnett 1982). The diffusion timescale is given by (e.g., Metzger et al. 2010b, Barnes & Kasen 2013):

$$t_d = \frac{B\kappa M_{\rm ej}}{cR}, \tag{7}$$

where $B \approx 0.07$ is a geometric factor, κ is the opacity, and $R = vt$ is the radius of the expanding ejecta. In addition, the peak luminosity is given by the radioactive heating rate (Q) at the diffusion timescale:

$$L_p \approx \frac{Q_p}{t_d(R_p)}, \tag{8}$$

where R_p is the radius of the ejecta at the diffusion timescale. Finally, the characteristic blackbody temperature of the resulting emission is given by:

$$T_p \approx \left(\frac{L_p}{4\pi R_p^2 \sigma}\right)^{1/4} \tag{9}$$

For an opacity of $\kappa \sim 0.1$ cm^2 g^{-1} at $\sim 0.3 - 1$ μm, typical of the Fe-peak elements synthesized in SNe, the resulting peak timescale is $t_p \sim 0.3$ d, with a luminosity of $L_p \sim$ few $\times\, 10^{41}\, (f_{-6})$ erg s^{-1} (where $f \sim$ few $\times\, 10^{-6}$ is the fraction of ejecta rest-mass energy that goes into radioactive heating; Li & Paczyński 1998, Metzger et al. 2010b), and the photospheric temperature is $T_p \approx 10^4$ K, leading to a peak in the UV/optical.

However, recent investigations of the opacities due to r-process elements lead to a different conclusion. In a pioneering effort, Kasen, Badnell & Barnes (2013) and Barnes & Kasen (2013) demonstrated that the opacities of r-process matter, particularly the lanthanides, are about two orders of magnitude higher than for Fe-peak elements, with $\kappa \sim 10-100$ cm^2 g^{-1} at $\lambda \sim 0.3-3$ μm. With these opacity values, the expected peak timescale becomes longer by about an order of magnitude, $t_p \sim$ few days, the peak luminosity becomes correspondingly lower, $L_p \sim$ few $\times\, 10^{40}$ erg s^{-1}, and the characteristic temperatures shifts to $T_p \sim 3000$ K, or a peak in the near-IR. Initial calculations of the r-process opacities and the resulting light curves and spectral energy distributions are provided in several recent papers (Barnes & Kasen 2013; Bauswein, Goriely & Janka 2013; Grossman et al. 2013; Tanaka & Hotokezaka 2013).

From an observational point of view, the effect of the larger opacities is dramatic. Instead of a transient that peaks in the blue part of the optical spectrum on a timescale of $\sim$ day and with an absolute magnitude of about -15, the kilonova is expected to peak with a similar absolute magnitude in the near-IR (~ 1.5 μm) on a timescale of $\sim$ week. In the optical bands, on the other hand, the peak absolute magnitude and timescale are about -12 mag and $\sim$ day. This has significant implications for the detectability of kilonovae in blind surveys or in optical follow-up of gravitational wave sources (§10).

Optical searches for kilonova emission have been carried out in association with the short GRBs 050509B (Bloom et al. 2006), 070724A (Berger et al. 2009, Kocevski et al. 2010), 080503A (Perley et al. 2009), 080905A (Rowlinson et al. 2010), and 100206A (Perley et al. 2012), but none have yielded detections. These searches were guided by the early predictions for bright UV/optical emission with a $\sim$ day timescale, but unfortunately, they do not provide strong constraints in the context of the current opacity estimates.

The first credible search focusing on the near-IR band was carried out for GRB 130603B at $z = 0.356$ using a combination of ground-based observations at $\lesssim 2$ d and *HST* observations at about 9 and 30 d (Berger, Fong & Chornock 2013; Tanvir et al. 2013); see Figure 19. The afterglow of this burst was relatively bright at early time, but faded rapidly with $F_\nu \propto t^{-2.6}$ starting at about 0.45 d (indicative of a jet break as discussed in §8.4). Based on the decline rate and spectral energy distribution, the afterglow was predicted to have an exceedingly low flux at the time of the first *HST* observation, $m_{\rm F606W} \approx 31$ mag and $m_{\rm F160W} \approx 29.3$ mag. Instead, the *HST* observations revealed a source with $m_{\rm F160W} \approx 25.8$ mag, but with no corresponding counterpart in the optical data (to $m_{\rm F606W} \approx 27.7$ mag). The excess emission in the near-IR

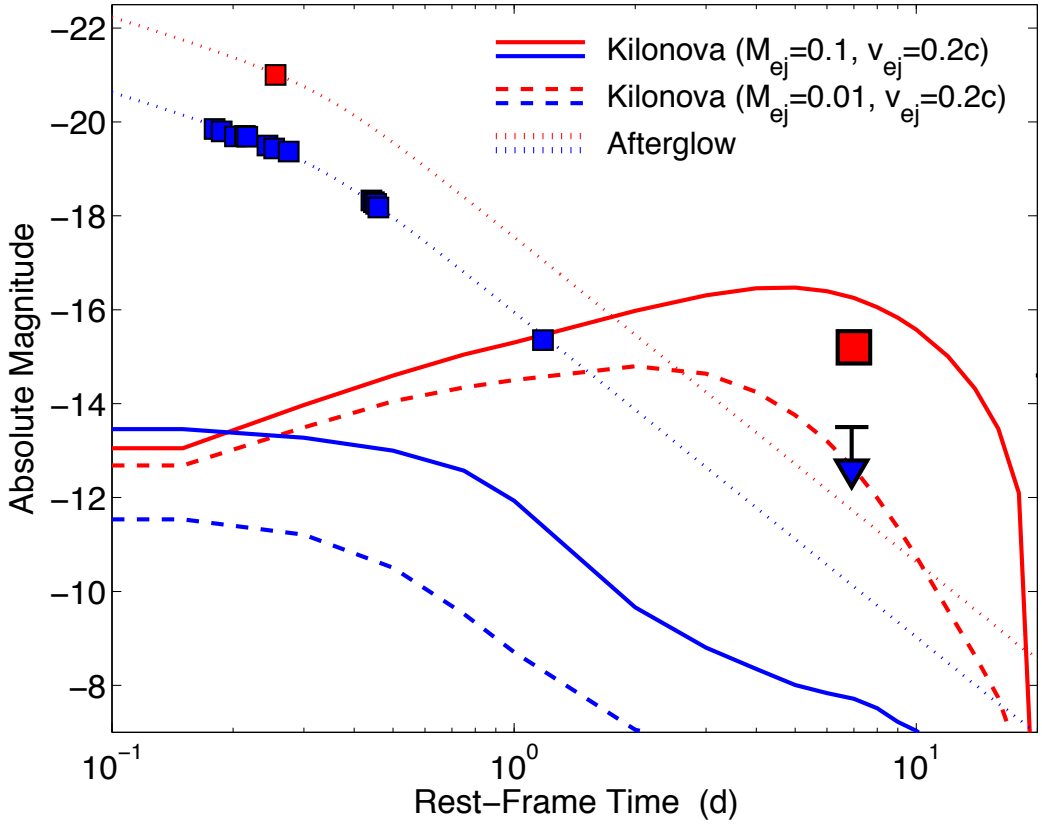

Figure 19:

Optical (blue) and near-IR (red) observations of the short GRB 130603b from ground-based telescopes ($\lesssim 2$ d) and from *HST* (Berger, Fong & Chornock 2013; Cucchiara et al. 2013; Fong et al. 2013; Tanvir et al. 2013). The dotted lines are a fit to the early afterglow evolution, which underestimates the near-IR flux detected in the *HST* observations. The excess emission can be explained as emission from an *r*-process kilonova, resulting from a compact object binary merger. Theoretical kilonova models from Barnes & Kasen (2013) that take into account the opacities of *r*-process elements are shown as dashed and solid lines for ejecta masses of 0.01 and 0.1 $M_\odot$, respectively. From Berger, Fong & Chornock (2013).

by a factor of about 25, coupled with the unusually red color, match the predictions for a kilonova in the context of *r*-process opacities. At the time of writing, this is one of the strongest lines of evidence in favor of compact object binary progenitors.

The near-IR luminosity of the likely kilonova in GRB 130603B provides a rough estimate of the mass of *r*-process ejecta produced in this event. Utilizing the *r*-process opacity models, Berger, Fong & Chornock (2013) estimate $M_{\rm ej} \approx 0.03-0.08\,M_\odot$ for ejecta velocities of $v_{\rm ej} \approx 0.1-0.3c$. Clearly, the theoretical models are preliminary, and there are variations between the calculations carried out by different groups (Barnes & Kasen 2013; Bauswein, Goriely & Janka 2013; Grossman et al. 2013; Tanaka & Hotokezaka 2013), but the results for GRB 130603B suggest that at least some short GRB progenitors may eject as much as $\sim$ few $\times 10^{-2}\,M_\odot$ of *r*-process material. Coupled with current estimates for the rate of NS-NS mergers, this indicates that compact object binary mergers may be the dominant site of *r*-process nucleosynthesis.

Detailed multi-epoch and multi-band follow-up observations of future nearby short GRBs will establish

the ubiquity of kilonova associations and determine the range of ejecta masses. In particular, near-IR spectroscopy may reveal broad absorption features that will uniquely establish a non-afterglow origin and will also provide a rough measure of the typical ejecta velocities. The key challenges for such searches are the need for short GRBs at $z \lesssim 0.3$, which occur at a rate of $\lesssim 1$ yr^{-1}; a fast-fading afterglow to avoid significant contamination; and rapid follow-up with *HST* in the optical and near-IR. A key strategy to confirm a kilonova origin for any late-time excess emission is the use of multiple near-IR and optical filters to trace the expected sharp spectral cut-off at ~ 1 μm.

10 Short GRBs as Electromagnetic Counterparts of Gravitational Wave Sources

Several lines of evidence, presented in the previous sections, point to compact object mergers as the progenitors of short GRBs. As a result, existing observations of short GRBs and their afterglows can uniquely shed light on the on- and off-axis electromagnetic (EM) signatures that will accompany gravitational wave (GW) sources detected by Advanced LIGO/Virgo. The frequency range of these GW detectors is designed to uncover the final inspiral and merger of compact object binaries (NS-NS, NS-BH, BH-BH). The expected EM counterparts of Advanced LIGO/Virgo sources, and their detectability with existing and upcoming facilities, are a topic of growing interest, which has been explored in several recent papers (e.g., Metzger & Berger 2012; Piran, Nakar & Rosswog 2013). To assess the importance and detectability of various EM counterparts it is important to note that the Advanced LIGO/Virgo volume-averaged distance for neutron star binary mergers is about 200 Mpc, while ideally-placed and oriented binaries (overhead relative to the detector network and with a face-on binary orientation) can be detected to about 450 Mpc (Abadie et al. 2010). The face-on orientation may also be ideal for the detection of an on-axis short GRB since the jet axis is expected to be oriented perpendicular to the plane of the binary's orbit. The typical localization region for the Advanced LIGO/Virgo network (3 detectors) is ~ 100 deg^2, although this may improve with future detectors in Japan and India (Fairhurst 2009). The poor localization capability presents a unique challenge for EM follow-up, and for counterpart discrimination and identification, compared for example to studies of short GRBs from *Swift*, which are localized to better than a few arcminutes radius.

Despite the obvious observational challenges, the information that can be gleaned from EM counterparts is invaluable (Kochanek & Piran 1993, Metzger & Berger 2012). In particular, the joint detection of gravitational waves and a short GRB will definitively establish the compact object merger model, and may also shed light on any differences in the short GRB population that are due to mergers of NS-NS versus NS-BH binaries. Even more broadly, EM counterparts are essential for pinpointing the exact locations of the mergers, thereby providing an association with host galaxies, measurements of a distance scale, and a relation to specific stellar populations that will shed light on the kick and merger timescale distributions. Similarly, the properties of the EM counterparts will shed light on the behavior of matter following the merger, namely accretion disks, jets, and dynamical or wind-driven outflows. A summary of potential counterparts is provided in Figure 20.

Metzger & Berger (2012) examined a wide range of putative on- and off-axis counterparts, and examined their potential impact for joint GW/EM studies in relation to four critical virtues: (i) detectability with present or upcoming telescope facilities using a reasonable allocation of resources; (ii) the potential to accompany a high fraction of GW detections; (iii) distinguishability from other astrophysical transients that may contaminate the large search areas; and (iv) allowing for a localization to arcsecond precision. Other studies of EM counterparts have also explored the issue of detectability and background contamination, generally reaching similar conclusions, although some studies employ different criteria for "detectability" (e.g., Nakar & Piran 2011; Piran, Nakar & Rosswog 2013).

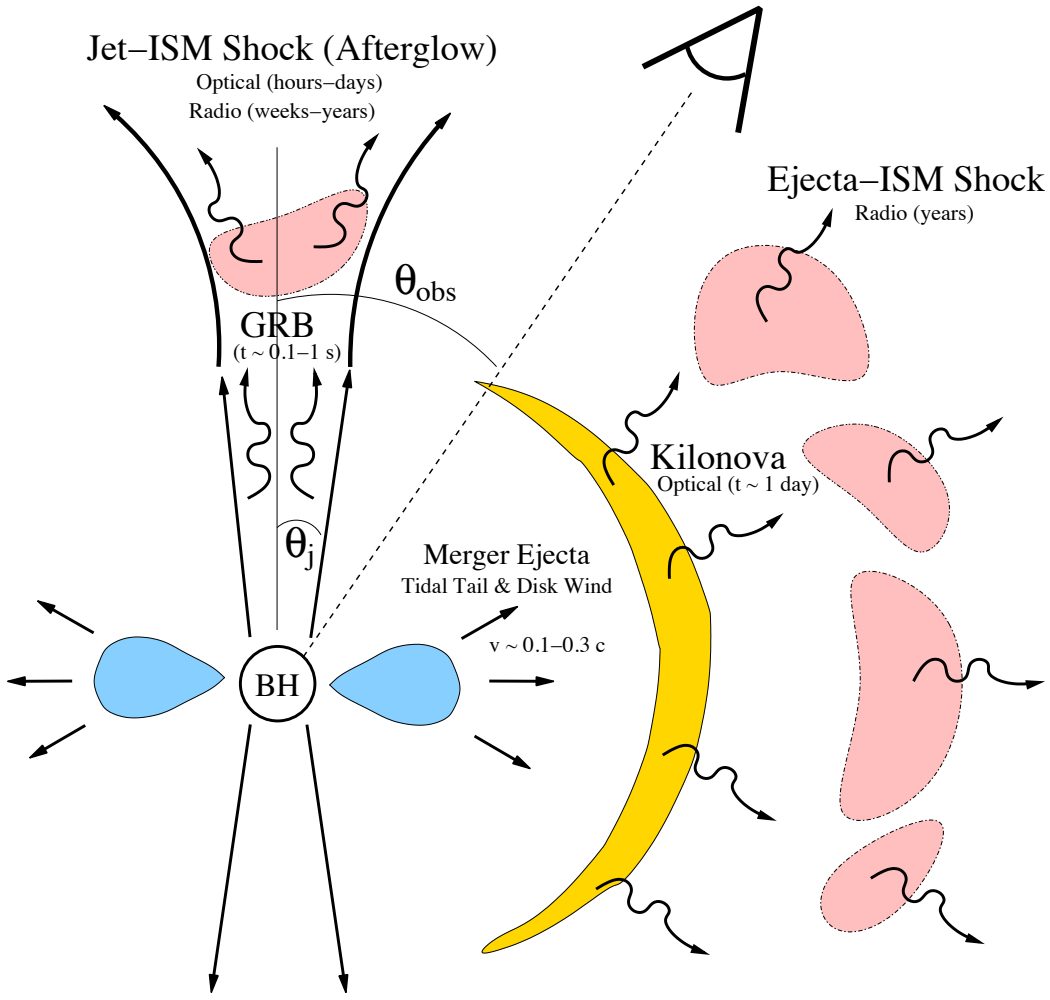

Figure 20:

Potential electromagnetic counterparts of compact object binary mergers as a function of the observer viewing angle ($\theta_{\rm obs}$). Rapid accretion of a centrifugally supported disk (blue) powers a collimated relativistic jet, which produces a short GRB. Due to relativistic beaming, the γ-ray emission is restricted to observers with $\theta_{\rm obs} \lesssim \theta_j$. Afterglow emission results from the interaction of the jet with the circumburst medium (pink). Optical afterglow emission is detectable for observers with $\theta_{\rm obs} \lesssim 2\theta_j$. Radio afterglow emission is observable from all viewing angles once the jet decelerates to mildly relativistic velocities on a timescale of months-years, and can also be produced on timescales of years from sub-relativistic ejecta. Short-lived isotropic optical/near-IR emission lasting a few days (kilonova; yellow) can also accompany the merger, powered by the radioactive decay of r-process elements synthesized in the ejecta. From Metzger & Berger (2012).

10.1 An On-Axis Short GRB Counterpart

At least some Advanced LIGO/Virgo sources are expected to be accompanied by on-axis short GRBs with detectable γ-ray emission and a bright multi-wavelength afterglow. Since existing γ-ray satellites and large ground-based telescopes are capable of detecting short GRBs and their afterglows to $z \sim 1$, such an event

at $\lesssim$ 450 Mpc ($z \lesssim 0.1$) will be exceedingly bright. In particular, using the measured X-ray and optical luminosities of even the least energetic short GRBs (with $E_{\gamma,\rm iso} \sim 10^{49}$ erg; Figures 14 and 15), I predict an X-ray flux at ~ 0.5 d of $F_X \sim 5 \times 10^{-14}$ erg s^{-1} cm^{-2} and an optical brightness of $r \sim 23$ mag. These are detectable levels assuming that the γ-ray emission can be pinpointed to an area typical of *Swift*/BAT localizations. For a short GRB with a median energy scale, the expected X-ray flux is $F_X \sim 5 \times 10^{-12}$ erg s^{-1} cm^{-2} and the optical brightness is $r \sim 20$ mag. Such a bright optical counterpart may be detectable even if the γ-ray position is as poor as the GW localization, for example typical of *Fermi*/GBM positions. However, such a large area cannot be effectively searched with *Swift*/XRT, which has a small field-of-view of only 0.25 deg^2.

The temporally coincident detection of a short GRB and a GW source will serve as the clearest smoking gun for the compact object merger model. It may also help to improve the positional accuracy of the GW source (if detected by an instrument such as *Swift*/BAT), but even a poor γ-ray localization will provide a convincing association based on the temporal coincidence. However, since the current estimate of the beaming fraction is $f_b \sim 70$ (§8.4), such joint detections will be rare. The occurrence rate can be estimated using the observed short GRB redshift distribution (Metzger & Berger 2012). In particular, there are currently no known short GRBs within the Advanced LIGO/Virgo maximum detection distance for NS-NS binaries of $z \approx 0.1$. Extrapolating the observed redshift distribution to $z \lesssim 0.1$, and correcting from the *Swift*/BAT field-of-view to roughly all-sky coverage (e.g., IPN, *Fermi*/GBM) the expected coincidence rate is ~ 0.3 yr^{-1} (Metzger & Berger 2012). Thus, while joint GW and short GRB detections will play a critical role in establishing the identity of the progenitors, and will provide particularly bright counterparts, such detections are expected to be rare.

Another profitable approach in the context of joint γ-ray and GW detections is to carry out a systematic search for GW emission in temporal coincidence with short GRBs (Abadie et al. 2012a; Metzger & Berger 2012; Kelley, Mandel & Ramirez-Ruiz 2013). The key advantage is that a search around a narrow time window, and with a position reconstruction that is consistent with the short GRB location, will allow for a reduced significance threshold. Such a search was carried out during LIGO Science Run 6 and Virgo Science Runs 2 and 3 (Abadie et al. 2012a), but unsurprisingly it did not yield any detections since the short GRB sample extends much beyond the reach of these initial detectors (Figure 4). On the other hand, the improved sensitivity of Advanced LIGO/Virgo may reach the nearest short GRBs.

10.2 An Off-Axis Optical Afterglow Counterpart

A coincident optical afterglow is more likely to be detected than a γ-ray counterpart since even with an initial off-axis viewing angle the jet will eventually decelerate and spread into the observer's line of sight. However, larger off-axis viewing angles result in reduced peak brightness, due to the longer timescale for the jet to spread into the line of sight. Using the existing sample of short GRB optical afterglows it is possible to predict their appearance for off-axis observers. Metzger & Berger (2012) utilized the off-axis afterglow models of van Eerten, Zhang & MacFadyen (2010) with the parameters appropriate for on-axis short GRB afterglows (§8) and found that for an off-axis angle that is twice the jet opening angle ($\theta_{\rm obs} = 2\theta_j$) the peak brightness of the afterglows at a typical distance of 200 Mpc is expected to be $\sim 23 - 25$ mag with a peak time of $\sim 1 - 10$ d, barely within the reach of the largest wide-field optical telescopes. At even larger off-axis angles the optical afterglow is essentially undetectable ($\sim 27 - 29$ mag for $\theta_{\rm obs} = 4\theta_j$).

The fraction of GW events that will be oriented within an angle of $2\theta_j$ is $f_{\rm opt} \approx 6.8\langle\theta_j\rangle^2 \sim 0.1$ (Metzger & Berger 2012), where the pre-factor of 6.8 takes into account the nearly face-on orientation of the binary, which leads to a larger detection volume than for random orientations. Thus, a few GW sources per year may be accompanied by off-axis optical afterglow emission with a peak brightness of $\sim 23 - 25$ mag and

a peak timescale of $\sim 1 - 10$ days. Finding such counterparts will require deep and rapid searches with wide-field optical telescopes, but this is within the reach of existing and upcoming facilities.

10.3 An Off-Axis Radio Afterglow Counterpart

The underlying reason for the faintness of optical afterglows at large off-axis viewing angles is that by the time the jet spreads into the observer's line of sight (weeks to months to years after the event) the outflow becomes only mildly relativistic and the peak of the synchrotron spectrum is shifted to the radio GHz band. In principle, this means that radio afterglow emission can serve as an ideal counterpart for all GW sources due to its detectability from any off-axis angle (Nakar & Piran 2011). In reality, the detectability of such radio emission depends on the kinetic energy of the blastwave and the ambient density. In addition to the initially collimated and relativistic outflow, radio emission will also be produced by any non-relativistic isotropic outflow as it interacts with the ambient medium and decelerates (Nakar & Piran 2011). In the latter scenario the initial velocity of the outflow is another critical parameter that determines the detectability of the radio emission. Such outflows are expected in compact object mergers from tidally unbound debris or from accretion disk winds (Rosswog et al. 1999, 2000; Ruffert & Janka 2001; Rosswog 2005; Etienne et al. 2008; Bauswein, Goriely & Janka 2013; Piran, Nakar & Rosswog 2013; Rosswog, Piran & Nakar 2013).

For the case of an initially collimated and relativistic outflow it is again useful to consider the observed properties of short GRB afterglows to investigate the expected brightness and detectability of an off-axis radio afterglow. The timescale for the blastwave to decelerate, isotropize, and reach peak brightness is $t_{\rm dec} \approx 30\,{\rm d}\,E_{K,49}^{1/3}\,n_0^{-1/3}\,\beta_0^{-5/3}$, where $E_{K,49}$ is the kinetic energy in units of 10^{49} erg and β_0 is the blastwave velocity in units of the speed of light; for an initially collimated and relativistic jet $\beta_0 \approx 1$ (Nakar & Piran 2011). Thus, for the typical energy and density scales inferred for short GRBs ($E_{K,49} \sim$ few and $n \sim 0.1$ cm^{-3}; §8), the resulting peak time is $t_{\rm dec} \sim 100$ d. The expected peak brightness (occurring at $t = t_{\rm dec}$) is $F_{\nu,{\rm p}} \approx 0.15\,{\rm mJy}\,E_{K,49}\,n_0^{0.8}\,\epsilon_{B,-2}^{0.8}\,\epsilon_{e,-1}^{1.2}\,\beta_0^2\,\nu_{\rm GHz}^{-0.6}$ (Nakar & Piran 2011), where I have scaled to a distance of 200 Mpc and to the fiducial values of $\epsilon_e = 0.1$ and $\epsilon_B = 0.01$ used in §8 to infer the short GRB afterglow properties. For the typical energy and density of short GRBs, this leads to $F_{\nu,{\rm p}} \sim 0.1$ mJy.

For dynamical or wind-driven ejecta the typical mass scale is ~ 0.01 M$_\odot$ with a velocity of $\beta \sim 0.2$, corresponding to $E_{K,49} \approx 40$ (Rosswog, Piran & Nakar 2013). Since the density of ~ 0.1 cm^{-3} inferred from short GRB observations is still relevant for this case, this indicates $t_{\rm dec} \approx 2$ years and $F_{\nu,{\rm p}} \approx 0.03$ mJy. For the most extreme outflow parameters indicated by numerical simulations (~ 0.1 M$_\odot$ and $\beta \sim 0.3$), the peak brightness is $F_{\nu,{\rm p}} \approx 1.5$ mJy, but it will only occur on a timescale of $t_{\rm dec} \approx 10$ years. It is important to note that $t_{\rm dec}$ represents not only the timescale to reach peak brightness, but also the typical timescale for the source to display significant brightness variability. From the point of view of a counterpart search, a source that does not vary significantly on a decade timescale, about a decade following a GW trigger is unlikely to be identified as an associated transient with any level of confidence.

The key question, therefore, is whether a radio transient with a typical peak brightness of $\sim 0.03 - 0.1$ mJy and a peak/variability timescale of $\sim$ year can be detected and identified in a ~ 100 deg^2 region with existing and upcoming facilities. To assess this question, I note that for the JVLA, with a 0.45 deg^2 field-of-view at 1 GHz, full coverage of such an area requires at least 200 individual pointings. With a synthesized beam of about 5″ diameter, there are about 10^8 independent beams within this region, indicating that the minimum required significance level for a detection is 6σ (making the unrealistically optimistic assumption that the noise in a 100 deg^2 region is purely Gaussian, with no systematic effects). To detect such a source as a transient requires at least a factor of two change in brightness, which means that the observations need to reach a typical 1σ noise level of $\sim 3 - 10$ μJy. With the JVLA this requires a few hours of integration per pointing, or about a month of continuous observing per epoch. This unrealistic follow-up scenario is

further exacerbated by the fact that at 1 GHz source confusion leads to a sensitivity floor of $\sim 0.03-0.1$ mJy (depending on the JVLA configuration), which is comparable to the level of the expected signal. Thus, it is unlikely that radio emission will be detectable with JVLA follow-up of a typical Advanced LIGO/Virgo error region.

The Australian Square Kilometre Array Pathfinder (ASKAP) wide-field interferometer is expected to image $\sim 10^2$ deg^2 in only a few pointings, and is therefore better matched to typical GW error regions. However, ASKAP's limited angular resolution of about 10″ will lead to source confusion at the level of the anticipated signal, $\sim 0.05-0.1$ mJy (Johnston et al. 2008). Finally, lower frequency instruments such as the Low-Frequency Array (LOFAR) and the Murchison Widefield Array (MWA) have sufficiently wide fields to instantaneously cover a full GW error region, but they are even more severely hampered by source confusion due to their lower angular resolution and the increased background at lower radio frequencies ($\sim 0.1-0.3$ GHz). Moreover, at the these frequencies the typical timescale for the outflow to reach peak brightness will be years to decades, instead of months at GHz frequencies.

I therefore conclude that while radio counterparts are in principle detectable from all viewing angles, existing facilities are not well-matched to the faintness of the anticipated signals. It is possible that in the long term multi-detector GW networks will localize some events to $\lesssim 10$ deg^2 (Fairhurst 2009), making radio searches more feasible. In addition, since the radio signal is delayed compared to counterparts at other wave-bands, a more profitable approach may be to use radio observations to follow up candidate counterparts from γ-ray, X-ray, or optical/near-IR searches, potentially as a way of distinguishing a true counterpart from unrelated sources (e.g., supernovae, AGN).

10.4 A Kilonova Counterpart

As I discussed in §9, NS-NS and NS-BH mergers are also expected to be accompanied by isotropic optical/near-IR emission produced by the radioactive decay of *r*-process elements in a dynamical or accretion disk wind driven outflow (Rosswog et al. 1999, 2000; Ruffert & Janka 2001; Rosswog 2005; Etienne et al. 2008; Bauswein, Goriely & Janka 2013; Piran, Nakar & Rosswog 2013; Rosswog, Piran & Nakar 2013). To date, the primary insight on the expected properties of such counterparts comes from numerical simulations coupled with *r*-process opacity calculations (Barnes & Kasen 2013; Bauswein, Goriely & Janka 2013; Grossman et al. 2013; Tanaka & Hotokezaka 2013), and from the near-IR counterpart associated with the short GRB 130603B (§9; Berger, Fong & Chornock 2013; Tanvir et al. 2013). In this context, the peak of the kilonova spectral energy distribution is expected at $\sim 1.5-3$ μm (the near-IR HK bands) with an apparent brightness of $\sim 21.5-24$ AB mag, and a timescale of $\sim$ week. In the optical izy bands ($0.7-1$ μm) the peak brightness is $\sim 22-24$ AB mag and the timescale is $\sim 1-3$ d (e.g., Barnes & Kasen 2013).

While the kilonova spectral energy distribution is expected to peak in the near-IR, deep wide-field searches in this band are not currently feasible. For example, ESO's Visible and Infrared Survey Telescope for Astronomy (VISTA) has an instantaneous field-of-view of about 0.6 deg^2, requiring about 170 pointings to cover a typical GW error region. This limits the exposure time per pointing to ~ 100 s for a single-night visit. The 5σ point-source sensitivity in such an exposure time is $H \approx 20.5$ AB mag, about a magnitude too shallow even for a bright kilonova. A better chance to detect the near-IR emission from a kilonova counterpart may be presented by a future space-based observatory, for example WFIRST. The current design reference document (Spergel et al. 2013) indicates an instantaneous field-of-view of about 0.3 deg^2, requiring several hundred pointings to cover a typical GW error region. However, the point-source sensitivity in a 1 min exposure is expected to be $H \approx 25$ AB mag (5σ), allowing for the detection of a wide range of kilonovae.

A more profitable approach, especially prior to the launch of a facility such as WFIRST, is to use wide-field optical telescopes in the reddest bands accessible to CCD detectors (izy). In this context, there are several existing and upcoming facilities capable of mounting sensitive follow-up campaigns (Pan-STARRS, Blanco/DECam, Subaru/HSC, LSST). To detect the faint and fast kilonova signal with sufficient significance requires at least nightly coverage of the full GW error region. For example, Pan-STARRS has a field-of-view of 7 deg^2 and can therefore cover a typical error region with about 15 min per pointing, achieving a 5σ point source sensitivity of $iz \approx 23.5$ AB mag. Similarly, with the DECam field-of-view of 3 deg^2 a typical GW error region can be covered to a depth of $iz \approx 24.5$ AB mag (5σ) in a single night. A similar depth can be reached with Subaru/HSC which has a larger aperture, but a smaller field of view. Finally, LSST will be able to provide rapid and efficient coverage to $iz \approx 24.5$ AB mag (5σ) in ~ 0.5 hr, or alternatively to $iz \approx 26$ AB mag in a single night. These sensitivities are sufficient to detect kilonovae over a broad range of expected ejecta masses, provided that a systematic campaign lasting several days is undertaken. Equally important, non-detections with such searches will yield meaningful upper bounds on the ejecta properties.

Unlike in γ-rays, and to some extent even in the radio band, optical searches with the required area and depth to robustly detect a kilonova will undoubtedly yield a wide range of unrelated variable and transient sources. To robustly identify or rule out a kilonova will therefore require the ability to reject background and foreground contaminants. One possibility is to restrict the search area to regions around galaxies within the expected Advanced LIGO/Virgo range of 200 Mpc (Nuttall & Sutton 2010, LIGO Scientific Collaboration et al. 2012). To achieve this goal requires all-sky spectroscopic information for galaxies down to at least ~ 0.1 L*, which represent the hosts of short GRBs (Figure 8; Berger 2009). Such spectroscopic information can be obtained from a narrow-band Hα imaging survey, or using an HI emission line radio survey.

The potential of such surveys was investigated by Metzger, Kaplan & Berger (2013) using information from existing galaxy surveys, as well as guidance from the distribution of short GRB host galaxy properties (e.g., stellar masses, star formation rates). The basic finding is that realistic Hα and HI surveys can uncover about 80 – 90% of the star formation within 200 Mpc, but only $\sim$ 30 – 50% of the stellar mass. The high incompleteness for stellar mass is due to the fact that about half of the stellar mass in the local universe is contained in elliptical galaxies which produce weak or no Hα emission and contain little neutral hydrogen gas. The level of completeness with respect to the population of short GRB hosts is about 50% for both methods (Metzger, Kaplan & Berger 2013). Thus, using galaxy catalogs to reduce the search area to locations around galaxies within 200 Mpc may result in a factor of 2 – 3 loss in the counterpart identification rate. On the other hand, this approach may reduce the background and foreground contamination dramatically (Nuttall & Sutton 2010, LIGO Scientific Collaboration et al. 2012). For NS-BH mergers, which can be detected to much larger distances, this method is likely to be inefficient.

The mitigation of contaminating sources may also benefit from color information. In the existing kilonova models, the spectral energy distribution is unusually red compared to most known transients. Therefore, the combined use of iz band photometry could substantially reduce the contamination from AGN flares, supernovae, supernova shock breakouts, or Galactic stellar flares which generally peak in the optical/UV (Metzger & Berger 2012). Finally, the shorter duration of kilonova events, though still $\sim$ 1 – 3 days, can help to distinguish these sources from foreground stellar flares (generally $\sim$ hour durations) and background supernovae (generally $\sim$ weeks durations). Clearly, the challenge of background/foreground rejection should be investigated using observations that match the anticipated signal in depth, timescale, and color. These parameters are not currently covered by on-going time-domain surveys such as Pan-STARRS, PTF, or DES.

10.5 Speculative Counterparts

In addition to potential EM counterparts that are motivated by existing short GRB observations, other speculative counterparts have been theorized in recent years. The validity of these theoretical models, and the nature of any resulting EM radiation are difficult to assess without observational evidence, while the proposed energy scale for some counterparts is likely too low to be detectable with existing facilities. Zrake & MacFadyen (2013) argue that compact object mergers lead to the amplification of $\sim 10^{16}$ G magnetic fields on the merger timescale, and speculate that if even $\sim 0.1\%$ of the available energy is channeled into γ-rays, the resulting isotropic signal will be detectable with *Swift*/BAT. Palenzuela et al. (2013) consider the interaction of the NS magnetospheres and show that it can power EM emission with $\sim 10^{40} - 10^{43}$ erg s^{-1} prior to the merger. However, the nature of the resulting radiation (e.g., radio, γ-rays) is unclear. Several researchers considered the formation of a massive millisecond magnetar as a merger remnant, which could power an isotropic counterpart with an optical/near-IR luminosity approaching those of supernovae and a typical timescale of hours to days, as well as bright X-ray emission on a timescale of hours (Gao et al. 2013; Yu, Zhang & Gao 2013; Zhang 2013) . Lehner et al. (2012) consider the collapse of a massive, rapidly-rotating magnetar remnant to a black hole and find that the detached magnetosphere can power a bright EM counterpart. Kyutoku, Ioka & Shibata (2012) suggest that the shock produced by the merger may accelerate the outer layer of the neutron star to relativistic velocities, with an energy of $\sim 10^{47}$ erg, which may produce an isotropic radio to X-ray afterglow through interaction with the ambient medium. Another proposed energy source for EM radiation is the failure or cracking of the neutron star crust prior to the merger, with a potential energy release of up to $\sim 10^{47}$ erg, although the nature of any resulting radiation is unclear (Penner et al. 2012, Tsang et al. 2012).

11 The Progenitors of Short GRBs and Future Directions

The discovery of short GRB afterglows in 2005 was a watershed event that led to the first identifications of host galaxies, to a determination of the distance scale, and to a delineation of the burst properties. In the span of less than a decade, intense follow-up efforts aimed at studying the afterglow emission and the host galaxy population have led to several key findings that I summarized and explored in this review:

- Short GRBs span a wide range of redshifts, at least $z \sim 0.1 - 1.5$. The redshift distribution appears to be affected by the sensitivity threshold of *Swift*/BAT, as evidenced by the similar redshift distributions in early- and late-type hosts, despite the anticipated longer time delay in the former. The redshift distribution indicates typical progenitor delay times of $\lesssim$ few Gyr.
- Short GRBs at $z \lesssim 0.5$, for which sensitive SN searches have been carried out lack associations with Type Ic SNe similar to those that accompany long GRBs. Nearly all of these limits are for short GRBs in star-forming galaxies, indicating that such environments are not indicative of an association with massive stars.
- Short GRBs occur in both early- and late-type galaxies, with the former accounting for about 20% of the sample. The sub-dominant fraction of early-type hosts indicates that the short GRB rate is influenced by both stellar mass and star formation activity. The inferred delay time distribution based on the host demographics is roughly $P(\tau) \propto \tau^{-1}$.
- The distribution of host galaxy stellar masses follows the expectation from the field galaxy mass function for early-type hosts, but is lower than expected for late-type hosts. This indicates that star formation activity results in an elevated short GRB rate per unit stellar mass. Combined with the broad distribution of host galaxy stellar population ages, the inferred delay time distribution roughly follows $P(\tau) \propto \tau^{-1}$.

- The host galaxies of short GRBs follow the general properties and trends of the field galaxy population (in terms of stellar masses, star formation rates, specific star formation rates, metallicities), but have systematically higher luminosities, larger stellar masses, older stellar population ages, higher metallicities, and lower star formation rates and specific star formation rates than the hosts of long GRBs.
- Short GRBs have systematically larger radial offsets from their host galaxies than long GRBs, but match the predicted offset distribution of compact object binaries from population synthesis models that include natal kicks. About 10% of short GRBs have offsets of $\gtrsim 20$ kpc, extending beyond the typical visible extent of their host galaxies. These bursts appear host-less in deep optical/near-IR imaging from *HST*, but exhibit nearby galaxies with a low probability of chance coincidence. The short GRB offsets normalized by host galaxy size are similarly larger than those of long GRBs, core-collapse SNe, and Type Ia SNe, with only 20% located at $\lesssim 1\ r_e$, and about 20% located at $\gtrsim 5\ r_e$. These results are indicative of natal kicks, or an origin in globular clusters, both of which point to compact object binary mergers. The inferred kick velocities are $\sim 20 - 140$ km s^{-1}, in reasonable agreement with Galactic NS-NS binaries and population synthesis models.
- Short GRBs exhibit a weak spatial correlation with the underlying distribution of UV and optical light in their host galaxies, with $\sim 50\%$ of all bursts located in the faintest regions of their hosts, often with no detectable underlying stellar light despite deep imaging with *HST*. This distribution is distinct from the strong correlation of long GRBs and core-collapse SNe with UV light, and the correlation of Type Ia SNe with optical light. This is indicative of natal kicks that displace the progenitors from their birth-sites to their evental explosion sites.
- The afterglows of short GRBs are systematically less luminous than those of long GRBs. This is partly a result of the lower isotropic-equivalent energy scale of short GRBs, but also reflects a lower density scale by about an order of magnitude. The distribution of optical afterglow luminosities indicates a typical density scale of ~ 0.1 cm^{-3}, supported by radio limits that require a density scale of $\lesssim 1$ cm^{-3}.
- Short GRBs exhibit evidence for collimation based on breaks in their X-ray, optical, and radio light curves that closely match the expectations for jet breaks. The inferred opening angles span $\sim 5^\circ$ to $\gtrsim 20^\circ$, with a resulting mean beaming factor of about 70. This leads to a beaming-corrected energy scale of $\sim (0.5 - 5) \times 10^{49}$ erg, and an event rate of $\sim 10^3$ Gpc^{-3} yr^{-1}. The inferred rate within the Advanced LIGO sensitivity volume is ~ 25 yr^{-1}.
- There is evidence for a kilonova association from late near-IR excess emission in the short GRB 130603B, with an inferred r-process ejecta mass of ~ 0.05 M$_\odot$. If confirmed with future kilonova detections, this result provides strong evidence for compact object binary progenitors, indicates that compact object mergers are the dominant site for r-process nucleosynthesis, and demonstrates that Advanced LIGO/Virgo gravitational wave sources will be accompanied by detectable optical/near-IR emission.
- In the context of compact object binary progenitors, short GRBs provide unique insight on the expected electromagnetic counterparts of Advanced LIGO/Virgo gravitational wave sources, both on- and off-axis. Coincident detections of gravitational waves and on-axis short GRBs are expected to be rare, ~ 0.3 yr^{-1}. Off-axis optical afterglow emission is expected to be detectable for $\sim 10\%$ of gravitational wave sources. Radio emission from an off-axis jet or from an isotropic mildly-relativistic outflow is in principle detectable for all viewing angles, but the predicted fluxes are too low to be detected with existing or upcoming facilities. Finally, kilonova emission can be detected within the Advanced LIGO/Virgo volume using large wide-field optical telescopes in the reddest optical bands.

Within the range of proposed progenitor systems for short GRBs, the binary compact object merger scenario provides the best agreement with the broad range of observations. A dominant channel of young

magnetars conflicts with the occurrence of short GRBs in early-type galaxies, with the large offsets, and with the lack of spatial correlation with host UV light. A dominant channel of delayed magnetars, formed through white dwarf accretion-induced collapse or white dwarf binary mergers, can explain the host demographics, but does not naturally lead to the observed offset distribution or to the weak spatial correlation with optical light. Finally, models in which short GRBs are produced by massive stars in a similar fashion to long GRBs are ruled out by the lack of SN associations, the occurrence of short GRBs in early-type galaxies, the clear differences in the host galaxy population, the lack of spatial association with UV light, and the large differences in energy and circumburst density scales. It is indeed quite remarkable that the underlying theoretical motivations that led to the compact object binary merger model prior to the identification of short GRBs as a distinct class (e.g., Eichler et al. 1989; Narayan, Paczynski & Piran 1992) have been borne out by the extensive observational effort over the past decade.

At the same time, there are clear challenges for the compact object binary merger model, which may require a more careful assessment of the physical conditions during the merger, or perhaps a minor contribution from a distinct progenitor channel. For example, the $\sim$ 100-sec extended emission observed in about 15% of short GRBs does not naturally fit in the basic merger framework, although several theoretical explanations exist for this emission component (MacFadyen, Ramirez-Ruiz & Zhang 2005; Rosswog 2007; Metzger, Quataert & Thompson 2008; Metzger et al. 2010a; Bucciantini et al. 2012). Similarly, there are potential clues in the commonalities and differences between the prompt emission properties of long and short GRBs (with and without extended emission) that may shed light on the nature of the progenitors and/or the engine. In addition, it remains to be seen if NS-BH mergers contribute to the short GRB population, and if so, what observational signatures distinguish them from NS-NS binary mergers. The answer may have to await gravitational wave detections that can shed light on the relative fraction of occurrence of NS-NS and NS-BH binaries.

Continued studies of short GRBs from *Swift*, *Fermi*, and future γ-ray missions remain a top priority. The existing sample already provides deep insight into the nature of the progenitors and the explosion properties, but larger samples, combined with individual high-quality events (e.g., GRB 130603B) are essential for addressing some of the open questions listed above. An operational γ-ray satellite (preferably with all-sky coverage) in the Advanced LIGO/Virgo era is also critical for establishing a direct connection between compact object mergers and short GRBs.

Acknowledgements: I thank my primary collaborators in the study of short GRBs: Wen-fai Fong, Ryan Chornock, Raffaella Margutti, Brian Metzger, Ashley Zauderer, and Derek Fox. I also acknowledge helpful discussions and occasional collaborations with Alicia Soderberg, Ramesh Narayan, Josh Grindlay, Christopher Fryer, Enrico Ramirez-Ruiz, Eliot Quataert, Lars Bildsten, Daniel Kasen, Camille Leibler, S. Bradley Cenko, Ehud Nakar, Re'em Sari, Nial Tanvir, Andrew Levan, Krzysztof Belczynski, Duncan Brown, Luis Lehner, Daniel Holz, Alessandra Bounano, David Kaplan, Neil Gehrels, Jochen Greiner, Ryan Foley, Dale Frail, Avishay Gal-Yam, Antonino Cucchiara, Shrinivas Kulkarni, and Paul Price. I also thank the participants of the "Chirps, Mergers and Explosions: The Final Moments of Coalescing Compact Binaries" workshop at the Kavli Institute for Theoretical Physics, Santa Barbara for stimulating discussions about short GRBs and gravitational wave astrophysics. Finally, I acknowledge support for some of this work from the National Science Foundation under Grant AST-1107973, and from several NASA *Swift* and *Fermi* grants.

Literature Cited

1. Abadie J, Abbott BP, Abbott R, Abbott TD, Abernathy M, et al. 2012a. *ApJ* 760:12
2. Abadie J, Abbott BP, Abbott R, Abernathy M, Accadia T, et al. 2010. *Classical and Quantum Gravity* 27:173001
3. Abadie J, Abbott BP, Abbott TD, Abbott R, Abernathy M, et al. 2012b. *ApJ* 755:2
4. Abbott B, Abbott R, Adhikari R, Agresti J, Ajith P, et al. 2008. *ApJ* 681:1419–1430
5. Abdo AA, Ackermann M, Ajello M, Asano K, Atwood WB, et al. 2009. *Nature* 462:331–334
6. Abdo AA, Ackermann M, Ajello M, Asano K, Atwood WB, et al. 2010. *ApJ* 712:558–564
7. Abramovici A, Althouse WE, Drever RWP, Gursel Y, Kawamura S, et al. 1992. *Science* 256:325–333
8. Accadia T, Acernese F, Antonucci F, Astone P, Ballardin G, et al. 2011. *Classical and Quantum Gravity* 28:114002
9. Ackermann M, Asano K, Atwood WB, Axelsson M, Baldini L, et al. 2010. *ApJ* 716:1178–1190
10. Aloy MA, Janka HT, Müller E. 2005. *A&A* 436:273–311
11. Amati L, Frontera F, Tavani M, in't Zand JJM, Antonelli A, et al. 2002. *A&A* 390:81–89
12. Antonelli LA, D'Avanzo P, Perna R, Amati L, Covino S, et al. 2009. *A&A* 507:L45–L48
13. Antoniadis J, Freire PCC, Wex N, Tauris TM, Lynch RS, et al. 2013. *Science* 340:448
14. Arnett WD. 1982. *ApJ* 253:785–797
15. Asano K, Guiriec S, Mészáros P. 2009. *ApJ* 705:L191–L194
16. Band D, Matteson J, Ford L, Schaefer B, Palmer D, et al. 1993. *ApJ* 413:281–292
17. Baring MG, Harding AK. 1997. *ApJ* 491:663
18. Barnes J, Kasen D. 2013. *ApJ* 775:18-26
19. Barthelmy SD, Chincarini G, Burrows DN, Gehrels N, Covino S, et al. 2005. *Nature* 438:994–996
20. Battaglia G, Helmi A, Morrison H, Harding P, Olszewski EW, et al. 2005. *MNRAS* 364:433–442
21. Bauswein A, Goriely S, Janka HT. 2013. *ApJ* 773:78
22. Beckwith SVW, Stiavelli M, Koekemoer AM, Caldwell JAR, Ferguson HC, et al. 2006. *AJ* 132:1729–1755
23. Belczynski K, Holz DE, Fryer CL, Berger E, Hartmann DH, O'Shea B. 2010. *ApJ* 708:117–126
24. Belczynski K, Perna R, Bulik T, Kalogera V, Ivanova N, Lamb DQ. 2006. *ApJ* 648:1110–1116
25. Bell EF, McIntosh DH, Katz N, Weinberg MD. 2003. *ApJS* 149:289–312
26. Berger E. 2007. *ApJ* 670:1254–1259
27. Berger E. 2009. *ApJ* 690:231–237
28. Berger E. 2010. *ApJ* 722:1946–1961
29. Berger E. 2011. *New Astronomy Reviews* 55:1–22
30. Berger E, Cenko SB, Fox DB, Cucchiara A. 2009. *ApJ* 704:877–882
31. Berger E, Chornock R, Holmes TR, Foley RJ, Cucchiara A, et al. 2011. *ApJ* 743:204
32. Berger E, Fong W, Chornock R. 2013. *ApJ* 774:L23–L27
33. Berger E, Fox DB, Price PA, Nakar E, Gal-Yam A, et al. 2007a. *ApJ* 664:1000–1010
34. Berger E, Kulkarni SR, Fox DB, Soderberg AM, Harrison FA, et al. 2005a. *ApJ* 634:501–508
35. Berger E, Kulkarni SR, Frail DA. 2003. *ApJ* 590:379–385
36. Berger E, Price PA, Cenko SB, Gal-Yam A, Soderberg AM, et al. 2005b. *Nature* 438:988–990
37. Berger E, Shin MS, Mulchaey JS, Jeltema TE. 2007b. *ApJ* 660:496–503
38. Berger E, Zauderer BA, Levan A, Margutti R, Laskar T, et al. 2013. *ApJ* 765:121
39. Bhattacharya D, van den Heuvel EPJ. 1991. *Physics Reports* 203:1–124
40. Birkl R, Aloy MA, Janka HT, Müller E. 2007. *A&A* 463:51–67
41. Blandford RD, Znajek RL. 1977. *MNRAS* 179:433–456
42. Bloom JS, Butler NR, Perley DA. 2008. In *American Institute of Physics Conference Series*, eds. M Galassi, D Palmer, E Fenimore, vol. 1000 of *American Institute of Physics Conference Series*
43. Bloom JS, Djorgovski SG, Kulkarni SR, Frail DA. 1998. *ApJ* 507:L25–L28
44. Bloom JS, Frail DA, Sari R. 2001. *AJ* 121:2879–2888
45. Bloom JS, Kulkarni SR, Djorgovski SG. 2002. *AJ* 123:1111–1148
46. Bloom JS, Kulkarni SR, Djorgovski SG, Eichelberger AC, Côté P, et al. 1999. *Nature* 401:453–456
47. Bloom JS, Kulkarni SR, Price PA, Reichart D, Galama TJ, et al. 2002. *ApJ* 572:L45–L49
48. Bloom JS, Perley DA, Chen HW, Butler N, Prochaska JX, et al. 2007. *ApJ* 654:878–884
49. Bloom JS, Prochaska JX, Pooley D, Blake CH, Foley RJ, et al. 2006. *ApJ* 638:354–368

50. Bloom JS, Sigurdsson S, Pols OR. 1999. *MNRAS* 305:763–769
51. Brodie JP, Strader J. 2006. *ARA&A* 44:193–267
52. Bromberg O, Nakar E, Piran T, Sari R. 2013. *ApJ* 764:179
53. Bucciantini N, Metzger BD, Thompson TA, Quataert E. 2012. *MNRAS* 419:1537–1545
54. Burgay M, D'Amico N, Possenti A, Manchester RN, Lyne AG, et al. 2003. *Nature* 426:531–533
55. Burrows DN, Grupe D, Capalbi M, Panaitescu A, Patel SK, et al. 2006. *ApJ* 653:468–473
56. Burrows DN, Romano P, Falcone A, Kobayashi S, Zhang B, et al. 2005. *Science* 309:1833–1835
57. Campana S, Tagliaferri G, Lazzati D, Chincarini G, Covino S, et al. 2006. *A&A* 454:113–117
58. Caputi KI, Lagache G, Yan L, Dole H, Bavouzet N, et al. 2007. *ApJ* 660:97–116
59. Caputi KI, McLure RJ, Dunlop JS, Cirasuolo M, Schael AM. 2006. *MNRAS* 366:609–623
60. Castro-Tirado AJ, de Ugarte Postigo A, Gorosabel J, Fathkullin T, Sokolov V, et al. 2005. *A&A* 439:L15–L18
61. Cenko SB, Frail DA, Harrison FA, Haislip JB, Reichart DE, et al. 2011. *ApJ* 732:29
62. Champion DJ, Lorimer DR, McLaughlin MA, Cordes JM, Arzoumanian Z, et al. 2004. *MNRAS* 350:L61–L65
63. Chandra P, Frail DA. 2012. *ApJ* 746:156
64. Chevalier RA, Li ZY. 2000. *ApJ* 536:195–212
65. Chincarini G, Mao J, Margutti R, Bernardini MG, Guidorzi C, et al. 2010. *MNRAS* 406:2113–2148
66. Chincarini G, Moretti A, Romano P, Falcone AD, Morris D, et al. 2007. *ApJ* 671:1903–1920
67. Christensen L, Hjorth J, Gorosabel J. 2004. *A&A* 425:913–926
68. Church RP, Levan AJ, Davies MB, Tanvir N. 2011. *MNRAS* 413:2004–2014
69. Connaughton V. 2002. *ApJ* 567:1028–1036
70. Costa E, Frontera F, Heise J, Feroci M, in't Zand J, et al. 1997. *Nature* 387:783–785
71. Coward DM, Howell EJ, Piran T, Stratta G, Branchesi M, et al. 2012. *MNRAS* 425:2668–2673
72. Cucchiara A, Levan AJ, Fox DB, Tanvir NR, Ukwatta TN, et al. 2011. *ApJ* 736:7
73. Cucchiara A, Prochaska JX, Perley DA, Cenko SB, Werk J, et al. 2013. *ArXiv*:1306.2028
74. Dahle H, Sarazin CL, Lopez LA, Kouveliotou C, Patel SK, et al. 2013. *ApJ* 772:23
75. D'Avanzo P, Malesani D, Covino S, Piranomonte S, Grazian A, et al. 2009. *A&A* 498:711–721
76. de Ugarte Postigo A, Castro-Tirado AJ, Guziy S, Gorosabel J, Jóhannesson G, et al. 2006. *ApJ* 648:L83–L87
77. de Ugarte Postigo A, Thoene CC, Rowlinson A, Garcia-Benito R, Levan AJ, et al. 2013. *ArXiv*:1308.2984
78. Della Valle M, Chincarini G, Panagia N, Tagliaferri G, Malesani D, et al. 2006. *Nature* 444:1050–1052
79. Demorest PB, Pennucci T, Ransom SM, Roberts MSE, Hessels JWT. 2010. *Nature* 467:1081–1083
80. Dessart L, Ott CD, Burrows A, Rosswog S, Livne E. 2009. *ApJ* 690:1681–1705
81. Dezalay JP, Barat C, Talon R, Syunyaev R, Terekhov O, Kuznetsov A. 1992. In *American Institute of Physics Conference Series*, eds. WS Paciesas, GJ Fishman, vol. 265 of *American Institute of Physics Conference Series*
82. Dhawan V, Mirabel IF, Ribó M, Rodrigues I. 2007. *ApJ* 668:430–434
83. Djorgovski SG, Kulkarni SR, Bloom JS, Goodrich R, Frail DA, et al. 1998. *ApJ* 508:L17–L20
84. Drout MR, Soderberg AM, Gal-Yam A, Cenko SB, Fox DB, et al. 2011. *ApJ* 741:97
85. Duncan RC, Thompson C. 1992. *ApJ* 392:L9–L13
86. Eichler D, Livio M, Piran T, Schramm DN. 1989. *Nature* 340:126–128
87. Eke VR, Baugh CM, Cole S, Frenk CS, King HM, Peacock JA. 2005. *MNRAS* 362:1233–1246
88. Etienne ZB, Faber JA, Liu YT, Shapiro SL, Taniguchi K, Baumgarte TW. 2008. *Phys. Rev. D* 77:084002
89. Fairhurst S. 2009. *New Journal of Physics* 11:123006
90. Falcone AD, Morris D, Racusin J, Chincarini G, Moretti A, et al. 2007. *ApJ* 671:1921–1938
91. Fenimore EE, Epstein RI, Ho C. 1993. *A&AS* 97:59–62
92. Filippenko AV. 1997. *ARA&A* 35:309–355
93. Fishman GJ, Meegan CA. 1995. *ARA&A* 33:415–458
94. Fong W, Berger E, Chornock R, Margutti R, Levan AJ, et al. 2013. *ApJ* 769:56
95. Fong W, Berger E, Chornock R, Tanvir NR, Levan AJ, et al. 2011. *ApJ* 730:26
96. Fong W, Berger E, Fox DB. 2010. *ApJ* 708:9–25
97. Fong W, Berger E, Margutti R, Zauderer BA, Troja E, et al. 2012. *ApJ* 756:189
98. Fong W, Berger E, Metzger BD, Margutti R, Chornock R, et al. 2013. *arXiv*: 1309.7479

99. Fong Wf, Berger E. 2013. *ApJ* 776:18
100. Fox DB, Frail DA, Price PA, Kulkarni SR, Berger E, et al. 2005. *Nature* 437:845–850
101. Frail DA, Kulkarni SR, Nicastro L, Feroci M, Taylor GB. 1997. *Nature* 389:261–263
102. Frail DA, Kulkarni SR, Sari R, Djorgovski SG, Bloom JS, et al. 2001. *ApJ* 562:L55–L58
103. Frederiks DD, Aptekar RL, Golenetskii SV, Il'Inskii VN, Mazets EP, et al. 2004. In *Gamma-Ray Bursts in the Afterglow Era*, eds. M Feroci, F Frontera, N Masetti, L Piro, vol. 312 of *Astronomical Society of the Pacific Conference Series*
104. Fruchter AS, Levan AJ, Strolger L, Vreeswijk PM, Thorsett SE, et al. 2006. *Nature* 441:463–468
105. Fryer C, Burrows A, Benz W. 1998. *ApJ* 496:333
106. Fryer C, Kalogera V. 1997. *ApJ* 489:244
107. Fryer CL, Woosley SE, Hartmann DH. 1999. *ApJ* 526:152–177
108. Fukugita M, Hogan CJ, Peebles PJE. 1998. *ApJ* 503:518–530
109. Fynbo JPU, Watson D, Thöne CC, Sollerman J, Bloom JS, et al. 2006. *Nature* 444:1047–1049
110. Gal-Yam A, Fox DB, Price PA, Ofek EO, Davis MR, et al. 2006. *Nature* 444:1053–1055
111. Gal-Yam A, Nakar E, Ofek EO, Cenko SB, Kulkarni SR, et al. 2008. *ApJ* 686:408–416
112. Galama TJ, Vreeswijk PM, van Paradijs J, Kouveliotou C, Augusteijn T, et al. 1998. *Nature* 395:670–672
113. Galbany L, Miquel R, Östman L, Brown PJ, Cinabro D, et al. 2012. *ApJ* 755:125
114. Gao H, Ding X, Wu XF, Zhang B, Dai ZG. 2013. *ApJ* 771:86
115. Gehrels N, Barthelmy SD, Burrows DN, Cannizzo JK, Chincarini G, et al. 2008. *ApJ* 689:1161–1172
116. Gehrels N, Chincarini G, Giommi P, Mason KO, Nousek JA, et al. 2004. *ApJ* 611:1005–1020
117. Gehrels N, Norris JP, Barthelmy SD, Granot J, Kaneko Y, et al. 2006. *Nature* 444:1044–1046
118. Gehrels N, Ramirez-Ruiz E, Fox DB. 2009. *ARA&A* 47:567–617
119. Gehrels N, Sarazin CL, O'Brien PT, Zhang B, Barbier L, et al. 2005. *Nature* 437:851–854
120. Ghirlanda G, Ghisellini G, Celotti A. 2004. *A&A* 422:L55–L58
121. Ghirlanda G, Ghisellini G, Nava L. 2010. *A&A* 510:L7
122. Ghirlanda G, Ghisellini G, Nava L. 2011. *MNRAS* 418:L109–L113
123. Ghirlanda G, Magliocchetti M, Ghisellini G, Guzzo L. 2006. *MNRAS* 368:L20–L24
124. Ghirlanda G, Nava L, Ghisellini G, Celotti A, Firmani C. 2009. *A&A* 496:585–595
125. Giannios D. 2006. *A&A* 455:L5–L8
126. Goodman J. 1986. *ApJ* 308:L47–L50
127. Goriely S, Bauswein A, Janka HT. 2011. *ApJ* 738:L32
128. Granot J, Sari R. 2002. *ApJ* 568:820–829
129. Grindlay J, Portegies Zwart S, McMillan S. 2006. *Nature Physics* 2:116–119
130. Grossman D, Korobkin O, Rosswog S, Piran T. 2013. *ArXiv*:1307.2943
131. Grupe D, Burrows DN, Patel SK, Kouveliotou C, Zhang B, et al. 2006. *ApJ* 653:462–467
132. Guetta D, Piran T. 2005. *A&A* 435:421–426
133. Hakkila J, Preece RD. 2011. *ApJ* 740:104
134. Hansen BMS, Lyutikov M. 2001. *MNRAS* 322:695–701
135. Harris WE. 1991. *ARA&A* 29:543–579
136. Harrison FA, Bloom JS, Frail DA, Sari R, Kulkarni SR, et al. 1999. *ApJ* 523:L121–L124
137. Harry GM, LIGO Scientific Collaboration. 2010. *Classical and Quantum Gravity* 27:084006
138. Hjorth J, Bloom JS. 2012. *The Gamma-Ray Burst - Supernova Connection*. 169–190
139. Hjorth J, Sollerman J, Gorosabel J, Granot J, Klose S, et al. 2005a. *ApJ* 630:L117–L120
140. Hjorth J, Sollerman J, Møller P, Fynbo JPU, Woosley SE, et al. 2003. *Nature* 423:847–850
141. Hjorth J, Watson D, Fynbo JPU, Price PA, Jensen BL, et al. 2005b. *Nature* 437:859–861
142. Hogg DW, Pahre MA, McCarthy JK, Cohen JG, Blandford R, et al. 1997. *MNRAS* 288:404–410
143. Hotokezaka K, Kiuchi K, Kyutoku K, Okawa H, Sekiguchi Yi, et al. 2013. *Phys. Rev. D* 87:024001
144. Hulse RA, Taylor JH. 1975. *ApJ* 195:L51–L53
145. Hurley K, Berger E, Castro-Tirado A, Castro Cerón JM, Cline T, et al. 2002. *ApJ* 567:447–453
146. Hurley K, Rowlinson A, Bellm E, Perley D, Mitrofanov IG, et al. 2010. *MNRAS* 403:342–352
147. Ilbert O, Salvato M, Le Floc'h E, Aussel H, Capak P, et al. 2010. *ApJ* 709:644–663
148. Jakobsson P, Levan A, Fynbo JPU, Priddey R, Hjorth J, et al. 2006. *A&A* 447:897–903
149. Janka HT, Eberl T, Ruffert M, Fryer CL. 1999. *ApJ* 527:L39–L42
150. Johnston S, Taylor R, Bailes M, Bartel N, Baugh C, et al. 2008. *Experimental Astronomy* 22:151–273

151. Kalogera V, Kim C, Lorimer DR, Burgay M, D'Amico N, et al. 2004. *ApJ* 601:L179–L182
152. Kaneko Y, Preece RD, Briggs MS, Paciesas WS, Meegan CA, Band DL. 2006. *ApJS* 166:298–340
153. Kann DA, Klose S, Zhang B, Covino S, Butler NR, et al. 2011. *ApJ* 734:96
154. Kasen D, Badnell NR, Barnes J. 2013. *ApJ* 774:25
155. Kehoe R, Akerlof C, Balsano R, Barthelmy S, Bloch J, et al. 2001. *ApJ* 554:L159–L162
156. Kelley LZ, Mandel I, Ramirez-Ruiz E. 2013. *Phys. Rev. D* 87:123004
157. Kelly PL, Kirshner RP. 2012. *ApJ* 759:107
158. Kelly PL, Kirshner RP, Pahre M. 2008. *ApJ* 687:1201–1207
159. Klebesadel RW, Strong IB, Olson RA. 1973. *ApJ* 182:L85
160. Kobulnicky HA, Kewley LJ. 2004. *ApJ* 617:240–261
161. Kocevski D, Thöne CC, Ramirez-Ruiz E, Bloom JS, Granot J, et al. 2010. *MNRAS* 404:963–974
162. Kochanek CS, Piran T. 1993. *ApJ* 417:L17
163. Kouveliotou C, Dieters S, Strohmayer T, van Paradijs J, Fishman GJ, et al. 1998. *Nature* 393:235–237
164. Kouveliotou C, Meegan CA, Fishman GJ, Bhat NP, Briggs MS, et al. 1993. *ApJ* 413:L101–L104
165. Kouveliotou C, Norris JP, Cline TL, Dennis BR, Desai UD, et al. 1987. *ApJ* 322:L21–L25
166. Krolik JH, Pier EA. 1991. *ApJ* 373:277–284
167. Kulkarni SR, Djorgovski SG, Odewahn SC, Bloom JS, Gal RR, et al. 1999. *Nature* 398:389–394
168. Kumar P, Barniol Duran R. 2010. *MNRAS* 409:226–236
169. Kyutoku K, Ioka K, Shibata M. 2012. *ArXiv*:1209.5747
170. Kyutoku K, Ioka K, Shibata M. 2013. *ArXiv*:1305.6309
171. Lamb DQ. 1995. *PASP* 107:1152
172. Laros JG, Fenimore EE, Klebesadel RW, Atteia JL, Boer M, et al. 1987. *ApJ* 320:L111–L115
173. Lattimer JM, Mackie F, Ravenhall DG, Schramm DN. 1977. *ApJ* 213:225–233
174. Lattimer JM, Schramm DN. 1974. *ApJ* 192:L145–L147
175. Lattimer JM, Schramm DN. 1976. *ApJ* 210:549–567
176. Lazzati D. 2005. *MNRAS* 357:722–731
177. Lazzati D, Begelman MC. 2005. *ApJ* 629:903–907
178. Lazzati D, Morsony BJ, Begelman MC. 2010. *ApJ* 717:239–244
179. Lazzati D, Ramirez-Ruiz E, Ghisellini G. 2001. *A&A* 379:L39–L43
180. Le Floc'h E, Papovich C, Dole H, Bell EF, Lagache G, et al. 2005. *ApJ* 632:169–190
181. Lee HK, Wijers RAMJ, Brown GE. 2000. *Physics Reports* 325:83–114
182. Lee WH, Ramirez-Ruiz E. 2007. *New Journal of Physics* 9:17
183. Lee WH, Ramirez-Ruiz E, López-Cámara D. 2009. *ApJ* 699:L93–L96
184. Lee WH, Ramirez-Ruiz E, van de Ven G. 2010. *ApJ* 720:953–975
185. Lehner L, Palenzuela C, Liebling SL, Thompson C, Hanna C. 2012. *Phys. Rev. D* 86:104035
186. Leibler CN, Berger E. 2010. *ApJ* 725:1202–1214
187. Levan AJ, Tanvir NR, Fruchter AS, Rol E, Fynbo JPU, et al. 2006a. *ApJ* 648:L9–L12
188. Levan AJ, Wynn GA, Chapman R, Davies MB, King AR, et al. 2006b. *MNRAS* 368:L1–L5
189. Levesque EM, Bloom JS, Butler NR, Perley DA, Cenko SB, et al. 2010a. *MNRAS* 401:963–972
190. Levesque EM, Kewley LJ, Berger E, Zahid HJ. 2010b. *AJ* 140:1557–1566
191. Li L, Paczyński B. 1998. *ApJ* 507:L59–L62
192. Li W, Chornock R, Leaman J, Filippenko AV, Poznanski D, et al. 2011. *MNRAS* 412:1473–1507
193. LIGO Scientific Collaboration, Virgo Collaboration, Abadie J, Abbott BP, Abbott R, et al. 2012. *A&A* 539:A124
194. Lü HJ, Liang EW, Zhang BB, Zhang B. 2010. *ApJ* 725:1965–1970
195. MacFadyen AI, Ramirez-Ruiz E, Zhang W. 2005. *astro-ph*/0510192
196. MacFadyen AI, Woosley SE. 1999. *ApJ* 524:262–289
197. Malesani D, Covino S, D'Avanzo P, D'Elia V, Fugazza D, et al. 2007. *A&A* 473:77–84
198. Mannucci F, Cresci G, Maiolino R, Marconi A, Gnerucci A. 2010. *MNRAS* 408:2115–2127
199. Mannucci F, Della Valle M, Panagia N. 2006. *MNRAS* 370:773–783
200. Mannucci F, Della Valle M, Panagia N, Cappellaro E, Cresci G, et al. 2005. *A&A* 433:807–814
201. Maoz D, Badenes C. 2010. *MNRAS* 407:1314–1327
202. Maoz D, Mannucci F, Brandt TD. 2012. *MNRAS* 426:3282–3294
203. Maoz D, Mannucci F, Li W, Filippenko AV, Della Valle M, Panagia N. 2011. *MNRAS* 412:1508–1521

204. Margutti R, Berger E, Fong W, Zauderer BA, Cenko SB, et al. 2012. *ApJ* 756:63
205. Margutti R, Chincarini G, Granot J, Guidorzi C, Berger E, et al. 2011. *MNRAS* 417:2144–2160
206. Margutti R, Guidorzi C, Chincarini G, Bernardini MG, Genet F, et al. 2010. *MNRAS* 406:2149–2167
207. Margutti R, Zaninoni E, Bernardini MG, Chincarini G, Pasotti F, et al. 2013. *MNRAS* 428:729–742
208. McGlynn S, Foley S, McBreen S, Hanlon L, O'Connor R, et al. 2008. *A&A* 486:405–410
209. Meegan CA, Fishman GJ, Wilson RB, Horack JM, Brock MN, et al. 1992. *Nature* 355:143–145
210. Mészáros P. 2002. *ARA&A* 40:137–169
211. Meszaros P, Rees MJ. 1993. *ApJ* 418:L59
212. Meszaros P, Rees MJ. 1997. *ApJ* 476:232
213. Metzger BD, Arcones A, Quataert E, Martínez-Pinedo G. 2010a. *MNRAS* 402:2771–2777
214. Metzger BD, Berger E. 2012. *ApJ* 746:48
215. Metzger BD, Kaplan DL, Berger E. 2013. *ApJ* 764:149
216. Metzger BD, Martínez-Pinedo G, Darbha S, Quataert E, Arcones A, et al. 2010b. *MNRAS* 406:2650–2662
217. Metzger BD, Quataert E, Thompson TA. 2008. *MNRAS* 385:1455–1460
218. Metzger MR, Djorgovski SG, Kulkarni SR, Steidel CC, Adelberger KL, et al. 1997. *Nature* 387:878–880
219. Modjaz M, Kewley L, Kirshner RP, Stanek KZ, Challis P, et al. 2008. *AJ* 135:1136–1150
220. Nakar E. 2007. *Physics Reports* 442:166–236
221. Nakar E, Gal-Yam A, Fox DB. 2006. *ApJ* 650:281–290
222. Nakar E, Piran T. 2002. *MNRAS* 330:920–926
223. Nakar E, Piran T. 2011. *Nature* 478:82–84
224. Narayan R, Paczynski B, Piran T. 1992. *ApJ* 395:L83–L86
225. Nicuesa Guelbenzu A, Klose S, Greiner J, Kann DA, Krühler T, et al. 2012a. *A&A* 548:A101
226. Nicuesa Guelbenzu A, Klose S, Krühler T, Greiner J, Rossi A, et al. 2012b. *A&A* 538:L7
227. Nicuesa Guelbenzu A, Klose S, Rossi A, Kann DA, Krühler T, et al. 2011. *A&A* 531:L6
228. Norris JP, Bonnell JT. 2006. *ApJ* 643:266–275
229. Norris JP, Cline TL, Desai UD, Teegarden BJ. 1984. *Nature* 308:434
230. Norris JP, Gehrels N, Scargle JD. 2010. *ApJ* 717:411–419
231. Norris JP, Gehrels N, Scargle JD. 2011. *ApJ* 735:23
232. Norris JP, Hertz P, Wood KS, Kouveliotou C. 1991. *ApJ* 366:240–252
233. Nousek JA, Kouveliotou C, Grupe D, Page KL, Granot J, et al. 2006. *ApJ* 642:389–400
234. Nuttall LK, Sutton PJ. 2010. *Phys. Rev. D* 82:102002
235. Nysewander M, Fruchter AS, Pe'er A. 2009. *ApJ* 701:824–836
236. Ofek EO, Cenko SB, Gal-Yam A, Fox DB, Nakar E, et al. 2007. *ApJ* 662:1129–1135
237. Ofek EO, Muno M, Quimby R, Kulkarni SR, Stiele H, et al. 2008. *ApJ* 681:1464–1469
238. O'Shaughnessy R, Belczynski K, Kalogera V. 2008. *ApJ* 675:566–585
239. Paciesas WS, Briggs MS, Preece RD, Mallozzi RS. 2003. In *Gamma-Ray Burst and Afterglow Astronomy 2001: A Workshop Celebrating the First Year of the HETE Mission*, eds. GR Ricker, RK Vanderspek, vol. 662 of *American Institute of Physics Conference Series*
240. Paczynski B. 1986. *ApJ* 308:L43–L46
241. Paczynski B. 1995. *PASP* 107:1167
242. Paczynski B, Rhoads JE. 1993. *ApJ* 418:L5
243. Palenzuela C, Lehner L, Ponce M, Liebling SL, Anderson M, et al. 2013. *Physical Review Letters* 111:061105
244. Panaitescu A, Kumar P. 2002. *ApJ* 571:779–789
245. Panaitescu A, Kumar P, Narayan R. 2001. *ApJ* 561:L171–L174
246. Pedersen K, Elíasdóttir Á, Hjorth J, Starling R, Cerón JMC, et al. 2005. *ApJ* 634:L17–L20
247. Penner AJ, Andersson N, Jones DI, Samuelsson L, Hawke I. 2012. *ApJ* 749:L36
248. Perley DA, Metzger BD, Granot J, Butler NR, Sakamoto T, et al. 2009. *ApJ* 696:1871–1885
249. Perley DA, Modjaz M, Morgan AN, Cenko SB, Bloom JS, et al. 2012. *ApJ* 758:122
250. Perna R, Armitage PJ, Zhang B. 2006. *ApJ* 636:L29–L32
251. Perna R, Belczynski K. 2002. *ApJ* 570:252–263
252. Pian E, Mazzali PA, Masetti N, Ferrero P, Klose S, et al. 2006. *Nature* 442:1011–1013
253. Piran T. 1992. *ApJ* 389:L45–L48
254. Piran T. 2004. *Reviews of Modern Physics* 76:1143–1210

255. Piran T, Nakar E, Rosswog S. 2013. *MNRAS* 430:2121–2136
256. Piranomonte S, D'Avanzo P, Covino S, Antonelli LA, Beardmore AP, et al. 2008. *A&A* 491:183–188
257. Prieto JL, Stanek KZ, Beacom JF. 2008. *ApJ* 673:999–1008
258. Prochaska JX, Bloom JS, Chen HW, Foley RJ, Perley DA, et al. 2006. *ApJ* 642:989–994
259. Proga D, Zhang B. 2006. *MNRAS* 370:L61–L65
260. Qin B, Wu XP, Chu MC, Fang LZ, Hu JY. 1998. *ApJ* 494:L57
261. Qin YP, Chen ZF. 2013. *MNRAS* 430:163–173
262. Rees MJ, Meszaros P. 1992. *MNRAS* 258:41P–43P
263. Rezzolla L, Giacomazzo B, Baiotti L, Granot J, Kouveliotou C, Aloy MA. 2011. *ApJ* 732:L6
264. Rhoads JE. 1999. *ApJ* 525:737–749
265. Ricker GR, Atteia JL, Crew GB, Doty JP, Fenimore EE, et al. 2003. In *Gamma-Ray Burst and Afterglow Astronomy 2001: A Workshop Celebrating the First Year of the HETE Mission*, eds. GR Ricker, RK Vanderspek, vol. 662 of *American Institute of Physics Conference Series*
266. Roberts LF, Kasen D, Lee WH, Ramirez-Ruiz E. 2011. *ApJ* 736:L21
267. Rosswog S. 2005. *ApJ* 634:1202–1213
268. Rosswog S. 2007. *MNRAS* 376:L48–L51
269. Rosswog S, Davies MB, Thielemann FK, Piran T. 2000. *A&A* 360:171–184
270. Rosswog S, Liebendörfer M, Thielemann FK, Davies MB, Benz W, Piran T. 1999. *A&A* 341:499–526
271. Rosswog S, Piran T, Nakar E. 2013. *MNRAS* 430:2585–2604
272. Rosswog S, Ramirez-Ruiz E, Davies MB. 2003. *MNRAS* 345:1077–1090
273. Rosswog S, Ramirez-Ruiz, E. 2003. *MNRAS* 336:L7–L11
274. Rowlinson A, O'Brien PT, Metzger BD, Tanvir NR, Levan AJ. 2013. *MNRAS* 430:1061–1087
275. Rowlinson A, Wiersema K, Levan AJ, Tanvir NR, O'Brien PT, et al. 2010. *MNRAS* 408:383–391
276. Ruderman M. 1975. In *Seventh Texas Symposium on Relativistic Astrophysics*, eds. PG Bergman, EJ Fenyves, L Motz, vol. 262 of *Annals of the New York Academy of Sciences*
277. Ruffert M, Janka HT. 2001. *A&A* 380:544–577
278. Salvaterra R, Devecchi B, Colpi M, D'Avanzo P. 2010. *MNRAS* 406:1248–1252
279. Sari R, Piran T, Halpern JP. 1999. *ApJ* 519:L17–L20
280. Sari R, Piran T, Narayan R. 1998. *ApJ* 497:L17
281. Savaglio S, Glazebrook K, Le Borgne D. 2009. *ApJ* 691:182–211
282. Schmidt M. 2001. *ApJ* 559:L79–L82
283. Schmidt M, Higdon JC, Hueter G. 1988. *ApJ* 329:L85–L87
284. Setiawan S, Ruffert M, Janka HT. 2004. *MNRAS* 352:753–758
285. Shemi A, Piran T. 1990. *ApJ* 365:L55–L58
286. Shibata M, Suwa Y, Kiuchi K, Ioka K. 2011. *ApJ* 734:L36
287. Shin MS, Berger E. 2007. *ApJ* 660:1146–1150
288. Soderberg AM, Berger E, Kasliwal M, Frail DA, Price PA, et al. 2006a. *ApJ* 650:261–271
289. Soderberg AM, Kulkarni SR, Nakar E, Berger E, Cameron PB, et al. 2006b. *Nature* 442:1014–1017
290. Spergel D, Gehrels N, Breckinridge J, Donahue M, Dressler A, et al. 2013. *ArXiv*:1305.5425
291. Stanek KZ, Garnavich PM, Kaluzny J, Pych W, Thompson I. 1999. *ApJ* 522:L39–L42
292. Stanek KZ, Gnedin OY, Beacom JF, Gould AP, Johnson JA, et al. 2006. *Acta Astronomica* 56:333–345
293. Stanek KZ, Matheson T, Garnavich PM, Martini P, Berlind P, et al. 2003. *ApJ* 591:L17–L20
294. Stone N, Loeb A, Berger E. 2013. *Phys. Rev. D* 87:084053
295. Stratta G, D'Avanzo P, Piranomonte S, Cutini S, Preger B, et al. 2007. *A&A* 474:827–835
296. Sullivan M, Le Borgne D, Pritchet CJ, Hodsman A, Neill JD, et al. 2006. *ApJ* 648:868–883
297. Svensson KM, Levan AJ, Tanvir NR, Fruchter AS, Strolger LG. 2010. *MNRAS* 405:57–76
298. Tanaka M, Hotokezaka K. 2013. *ArXiv*:1306.3742
299. Tanvir NR, Levan AJ, Fruchter AS, Hjorth J, Hounsell RA, et al. 2013. *Nature* 500:547–549
300. Taylor GB, Frail DA, Berger E, Kulkarni SR. 2004. *ApJ* 609:L1–L4
301. Thöne CC, Fynbo JPU, Östlin G, Milvang-Jensen B, Wiersema K, et al. 2008. *ApJ* 676:1151–1161
302. Tremonti CA, Heckman TM, Kauffmann G, Brinchmann J, Charlot S, et al. 2004. *ApJ* 613:898–913
303. Troja E, King AR, O'Brien PT, Lyons N, Cusumano G. 2008. *MNRAS* 385:L10–L14
304. Troja E, Rosswog S, Gehrels N. 2010. *ApJ* 723:1711–1717
305. Tsang D, Read JS, Hinderer T, Piro AL, Bondarescu R. 2012. *Physical Review Letters* 108:011102

306. Tsutsui R, Yonetoku D, Nakamura T, Takahashi K, Morihara Y. 2013. *MNRAS* 431:1398–1404
307. van den Bergh S. 1983. *Ap&SS* 97:385–388
308. van den Bergh S. 1990. *PASP* 102:1318–1320
309. van den Bergh S, Tammann GA. 1991. *ARA&A* 29:363–407
310. van Eerten H, Zhang W, MacFadyen A. 2010. *ApJ* 722:235–247
311. van Paradijs J, Groot PJ, Galama T, Kouveliotou C, Strom RG, et al. 1997. *Nature* 386:686–689
312. van Paradijs J, Kouveliotou C, Wijers RAMJ. 2000. *ARA&A* 38:379–425
313. Villasenor JS, Lamb DQ, Ricker GR, Atteia JL, Kawai N, et al. 2005. *Nature* 437:855–858
314. Wainwright C, Berger E, Penprase BE. 2007. *ApJ* 657:367–377
315. Wang C, Lai D, Han JL. 2006. *ApJ* 639:1007–1017
316. Wang X, Wang L, Filippenko AV, Zhang T, Zhao X. 2013. *Science* 340:170–173
317. Watson D, Hjorth J, Jakobsson P, Xu D, Fynbo JPU, et al. 2006. *A&A* 454:L123–L126
318. Waxman E, Kulkarni SR, Frail DA. 1998. *ApJ* 497:288
319. Wong TW, Willems B, Kalogera V. 2010. *ApJ* 721:1689–1701
320. Woosley SE, Bloom JS. 2006. *ARA&A* 44:507–556
321. Xue XX, Rix HW, Zhao G, Re Fiorentin P, Naab T, et al. 2008. *ApJ* 684:1143–1158
322. Yonetoku D, Murakami T, Nakamura T, Yamazaki R, Inoue AK, Ioka K. 2004. *ApJ* 609:935–951
323. Yost SA, Harrison FA, Sari R, Frail DA. 2003. *ApJ* 597:459–473
324. Yu YW, Zhang B, Gao H. 2013. *ArXiv*:1308.0876
325. Zhang B. 2013. *ApJ* 763:L22
326. Zhang B, Zhang BB, Liang EW, Gehrels N, Burrows DN, Mészáros P. 2007. *ApJ* 655:L25–L28
327. Zhang B, Zhang BB, Virgili FJ, Liang EW, Kann DA, et al. 2009. *ApJ* 703:1696–1724
328. Zheng Z, Ramirez-Ruiz E. 2007. *ApJ* 665:1220–1226
329. Zrake J, MacFadyen AI. 2013. *ApJ* 769:L29

Table 1: Prompt Emission and Afterglow Properties of Short GRBs

GRB	Satellite	T_{90} (s)	F_γ (erg cm^{-2})	z	$F_{\rm X,11}$ (erg cm^{-2} s^{-1})	$t_{\rm opt}$ (hr)	$F_{\nu,\rm opt}$ (μJy)	$t_{\rm radio}$ (hr)	$F_{\nu,\rm radio}$ (μJy)
050202	*Swift*	0.27	3.0×10^{-8}	...	...[a]	...	...	...	...
050509B	*Swift*	0.04	2.3×10^{-8}	0.225	$< 1.95 \times 10^{-14}$	2.1	< 0.8	...	...
050709	HETE-2	0.07	4.0×10^{-7}	0.161	1.92×10^{-14}	34.0	2.3	1.57	< 65
050724	*Swift*	3.0/EE	6.3×10^{-7}	0.257	9.55×10^{-14}	12.0	8.4	1.69	465
050813	*Swift*	0.6	1.2×10^{-7}	...	$< 2.12 \times 10^{-14}$	12.8	< 1.9	1.64	< 55
050906	*Swift*	0.26	6.0×10^{-9}	...	...[b]	...	...	...	...
050925	*Swift*	0.07	7.6×10^{-8}	...	...[b]	...	...	...	...
051210	*Swift*	1.3	8.3×10^{-8}	1.3	$< 2.70 \times 10^{-14}$	19.2	< 1.6	...	...
051105A	*Swift*	0.09	2.2×10^{-8}	...	...[b]	...	...	...	...
051221A	*Swift*	1.4	1.2×10^{-6}	0.546	1.08×10^{-12}	3.1	5.8	0.91	173
060121	HETE-2	2.0	4.7×10^{-6}	...	1.09×10^{-12}	7.4	8.8	...	...
060313	*Swift*	0.7	1.1×10^{-6}	...	3.85×10^{-13}	2.8	10.8	2.12	< 110
060502B	*Swift*	0.09	4.0×10^{-8}	0.287	$< 1.47 \times 10^{-14}$	16.8	< 0.7	...	...
060801	*Swift*	0.5	8.1×10^{-8}	1.130	$< 9.80 \times 10^{-15}$	12.4	< 0.8	0.49	< 105
061006	*Swift*	0.4/EE	1.4×10^{-6}	0.438	2.27×10^{-13}	14.9	2.9	...	...
061201	*Swift*	0.8	3.3×10^{-7}	0.111	1.92×10^{-13}	8.6	2.9	...	...
061210	*Swift*	0.2/EE	3.0×10^{-7}	0.409	1.36×10^{-13}	2.1	< 1.4	1.90	< 102
061217	*Swift*	0.2	4.6×10^{-8}	0.827	...	2.8	< 2.0	...	...
070209	*Swift*	0.09	2.2×10^{-8}	...	...[b]	...	...	...	...
070406	*Swift*	1.20	3.6×10^{-8}	...	...[a]	...	...	...	...
070429B	*Swift*	0.5	6.3×10^{-8}	0.902	1.13×10^{-13}	4.8	< 0.6	...	...
070707	INTEGRAL	1.1	1.4×10^{-6}	...	5.04×10^{-13}	11.0	1.9	...	...
070714B	*Swift*	2.0	7.2×10^{-7}	0.923	6.30×10^{-14}	23.6	0.7	15.5	< 139
070724A	*Swift*	0.4	3.0×10^{-8}	0.457	1.28×10^{-13}	3.3	3.8	1.06	< 250
070729	*Swift*	0.9	1.0×10^{-7}	0.8	$< 4.71 \times 10^{-14}$	0	< 0	...	...
070809	*Swift*	1.3	1.0×10^{-7}	0.473	5.30×10^{-13}	11.2	0.7	...	...
070810B	*Swift*	0.08	1.2×10^{-8}	...	...[b]	...	...	...	...
070923	*Swift*	0.05	5.0×10^{-8}	...	...[a]	...	...	...	...
071112B	*Swift*	0.30	4.8×10^{-8}	...	$< 2.00 \times 10^{-13}$	...	...	...	...
071227	*Swift*	1.8	2.2×10^{-7}	0.381	3.20×10^{-14}	7.0	1.6	...	...
080121	*Swift*	0.7	3.0×10^{-8}	...	...[a]	...	...	...	...
080426	*Swift*	1.7	3.7×10^{-7}	...	2.24×10^{-13}	7.5	< 2.6	...	...
080503	*Swift*	0.3/EE	6.1×10^{-8}	...	$< 3.05 \times 10^{-14}$	25.9	0.3	3.05	< 55
080702A	*Swift*	0.5	3.6×10^{-8}	...	$< 1.06 \times 10^{-13}$	...	...	0.83	< 155
080905A	*Swift*	1.0	1.4×10^{-7}	0.122	$< 6.70 \times 10^{-14}$	8.5	0.8	...	...
080919	*Swift*	0.6	7.2×10^{-8}	...	$< 2.12 \times 10^{-14}$	...[d]	...	...	...
081024	*Swift*	1.8	1.2×10^{-7}	...	$< 4.56 \times 10^{-14}$	...[d]	...	...	...
081226A	*Swift*	0.4	9.9×10^{-8}	...	$< 2.57 \times 10^{-14}$	0.37	1.3	...	...
090305	*Swift*	0.4	7.5×10^{-8}	...	$< 8.50 \times 10^{-14}$	0.56	2.0	...	...
090417A	*Swift*	0.07	1.9×10^{-8}	...	...[a]	...	...	...	...
090426	*Swift*	1.2	1.8×10^{-7}	2.609	2.63×10^{-13}	0.35	14.7	...	...
090510	*Swift*	0.3	3.4×10^{-7}	0.903	5.04×10^{-14}	9.0	2.3	1.46	< 145
090515	*Swift*	0.04	2.1×10^{-8}	0.403	$< 8.43 \times 10^{-14}$	1.9	0.1	0.87	< 60
090621B	*Swift*	0.14	7.0×10^{-8}	...	2.70×10^{-14}	0.9	< 3.3	0.61	< 54
090715	*Swift*	0.5/EE	9.7×10^{-7}	...	...[a]	...	...	...	...
090815C	*Swift*	0.6	4.4×10^{-8}	...	$< 7.00 \times 10^{-14}$	...	...	...	...
090916	*Swift*	0.3/EE	9.5×10^{-7}	...	$< 3.00 \times 10^{-14}$	...	...	...	...
091109B	*Swift*	0.3	1.9×10^{-7}	...	1.26×10^{-13}	6.0	0.7	...	...
100117A	*Swift*	0.3	9.3×10^{-8}	0.915	$< 2.50 \times 10^{-14}$	8.4	0.2	...	...
100206A	*Swift*	0.1	1.4×10^{-7}	0.408	$< 1.07 \times 10^{-14}$	15.7	< 0.5	...	...
100625A	*Swift*	0.3/EE	2.3×10^{-7}	0.453	3.95×10^{-15}	12.7	< 4.4	...	...
100628A	*Swift*	0.04	2.5×10^{-8}	...	...[b]	...	...	...	...
100702A	*Swift*	0.16/EE	1.2×10^{-7}	...	$< 6.63 \times 10^{-14}$	...[d]	...	...	...
101129A	*Swift*	0.35	9.0×10^{-8}	...	...[a]	...	...	...	...
101219A	*Swift*	0.6	4.6×10^{-7}	0.718	$< 2.00 \times 10^{-14}$	1.0	< 3.2	...	...
101224A	*Swift*	0.2	5.8×10^{-7}	...	...[c]	...	...	...	...
110112A	*Swift*	0.5	3.0×10^{-8}	...	8.22×10^{-14}	15.4	2.8	1.90	< 75
110420B	*Swift*	0.08	5.3×10^{-8}	...	$< 1.40 \times 10^{-13}$	...	...	0.46	< 45
111020A	*Swift*	0.4	6.5×10^{-8}	...	4.87×10^{-13}	17.7	< 0.6	0.7	< 39

Continued on next page

Table 1 – Continued from previous page

GRB	Satellite	T_{90} (s)	F_γ (erg cm^{-2})	z	$F_{\rm X,11}$ (erg cm^{-2} s^{-1})	$t_{\rm opt}$ (hr)	$F_{\nu,\rm opt}$ (μJy)	$t_{\rm radio}$ (hr)	$F_{\nu,\rm radio}$ (μJy)
111117A	*Swift*	0.5	1.4×10^{-7}	1.3	3.21×10^{-14}	13.2	< 0.2	0.50	< 18
111121A	*Swift*	0.45/EE	2.2×10^{-6}	...	4.80×10^{-13}	...[d]	...	0.80	< 78
111126A	*Swift*	0.8	7.0×10^{-8}	...	...[a]	...	...	...	...
120229A	*Swift*	0.22	4.1×10^{-8}	...	...[a]	...	...	...	...
120305A	*Swift*	0.10	2.0×10^{-7}	...	2.40×10^{-14}	...	...	2.25	< 18
120403A	*Swift*	1.25	1.0×10^{-7}	...	...[a]	...	...	...	...
120521A	*Swift*	0.45	7.8×10^{-8}	...	$< 1.50 \times 10^{-13}$	17.7	< 0.9	...	...
120630A	*Swift*	0.6	6.1×10^{-8}	...	...[c]	...	...	...	...
120804A	*Swift*	0.81	8.8×10^{-7}	1.3	5.86×10^{-13}	5.5	5.4	1.95	< 18
121226A	*Swift*	1.0	1.4×10^{-7}	...	2.24×10^{-13}	11.1	< 1.9	...	...
130603B	*Swift*	0.18	6.3×10^{-7}	0.356	6.00×10^{-13}	8.2	8.6	0.37	119

Table 1: Prompt emission and afterglow properties of the short GRB sample spanning January 2005 to January 2013, with the addition of GRB 130603B. The columns are: (i) GRB name; (ii) discovery satellite; (iii) duration (EE: extended emission); (iv) fluence in the 15 – 150 keV band for *Swift* events; (v) redshift; (vi) observed X-ray flux at 11 hr post-burst; (vii) time of first optical detection; (viii) flux density in the optical r-band; (ix) time of radio observation for non-detections, or of peak radio brightness for detections; and (x) radio flux density (at 5 or 8.5 GHz).

[a] No rapid *Swift*/XRT follow-up due to observing constraints.

[b] No *Swift*/XRT detection despite rapid follow-up.

[c] No *Swift*/XRT observations at $\gtrsim 10^3$ s.

[d] Sight-line with significant Milky Way extinction.

Table 2: Properties of Short GRB Host Galaxies

GRB	z	Type	L_B (L^*)	SFR ($M_\odot$ yr^{-1})	τ_* (Gyr)	log(M_*) ($M_\odot$)	12+log(O/H)
Sub-arcsecond Localizations							
050709	0.161	L	0.1	0.15	0.26	8.8	8.5
050724A	0.257	E	1.0	< 0.1	0.94	10.8	...
051221A	0.546	L	0.3	0.95	0.17	9.4	8.8
060121	< 4.1	?	...	...	...	...	...
060313	< 1.7	?	...	...	...	...	...
061006	0.438	L	0.1	0.24	0.24	9.0	8.6
061201	0.111	H/L	0.1	0.14	...	...	...
070429B	0.902	L	0.6	1.1	0.46	10.4	...
070707	< 3.6	?	...	...	...	...	...
070714B	0.922	L	0.1	0.44	0.22	9.4	...
070724A	0.457	L	1.4	2.5	0.30	10.1	8.9
070809	0.473	H/E	1.9	< 0.1	3.10	11.4	...
071227	0.381	L	1.2	0.6	0.49	10.4	8.5
080503	< 4.2	H/?	...	...	...	...	...
080905A	0.122	L	...	...	...	...	8.7
081226A	< 4.1	?	...	...	...	...	...
090305	< 4.1	H/?	...	...	...	...	...
090426A	2.609	L	...	...	...	...	...
090510	0.903	L	0.3	0.3	0.14	9.7	...
090515	0.403	H/E	1.0	0.1	4.35	11.2	...
091109B	< 4.4	?	...	...	...	...	...
100117A	0.915	E	0.5	< 0.2	0.79	10.3	...
110112A	< 5.3	H/?	...	...	...	...	...
111020A	...	?	...	...	...	...	...
111117A	1.2	L	0.6	6.0	0.09	9.6	...
120804A	1.3	L	0.8	8.0	0.13	10.8	...
130603B	0.356	L	1.0	1.7	...	9.7	8.7
Swift/XRT Positions Only							
050509B	0.225	E	5.0	< 0.15	3.18	11.6	...
050813	...	E	...	...	...	...	...
051210	> 1.4	?	...	...	...	...	...
060502B	0.287	E	1.6	0.8	1.3	11.8	...
060801	1.130	L	0.6	6.1	0.03	9.1	...
061210	0.409	L	0.9	1.2	0.38	9.6	8.8
061217	0.827	L	0.4	2.5	0.03	9.1	...
070729	0.8	E	1.0	< 1.5	0.98	10.6	...
080123	0.495	L	1.2	...	0.31	10.1	...
100206A	0.407	L	1.0	30	0.10	10.8	9.2
100625A	0.452	E	0.2	0.3	0.79	10.3	...
101219A	0.718	L	1.3	16	0.03	9.2	...

Table 2: Properties of short GRB host galaxies. The columns are: (i) GRB name; (ii) redshift; (iii) galaxy type (E: early-type; L: late-type; ?: unknown; H: host-less); (iv) optical B-band luminosity normalized by L_B^* at the appropriate redshift; (v) star formation rate; (vi) dominant stellar population age; (vii) logarithm of the stellar mass; and (viii) metallicity. Data are from Berger (2009), Leibler & Berger (2010), Berger (2010), Fong et al. (2013) and references therein.